Pergamon

Progress in Nuclear Energy, Vol. 29, No. 2, pp. 63–127, 1995
Elsevier Science Ltd
Printed in Great Britain
0149-1970/95 $29.00

0149-1970(94)00016-6

RADIATION EFFECTS IN NUCLEAR WASTE FORMS FOR HIGH-LEVEL RADIOACTIVE WASTE

R. C. Ewing,* W. J. Weber† and F. W. Clinard, Jr‡

*University of New Mexico, Albuquerque, NM 87131, U.S.A.
†Pacific Northwest Laboratory, P.O. Box 999, Richland, WA 99352, U.S.A.
‡Los Alamos National Laboratory, Los Alamos, NM 87545, U.S.A.

(*Received* 12 *July* 1994)

Abstract—High-level nuclear waste in the United States comprises large volumes (tens of millions of cubic meters), high total activities (billions of Curies) and highly diverse and complex compositions. The principal sources of nuclear waste are: (i) spent nuclear fuel from commercial and research nuclear reactors; (ii) liquid waste produced during the reprocessing of commercial spent nuclear fuel; (iii) waste generated by the nuclear weapons and naval propulsion programs. The latter category now includes over 100 metric tons of plutonium and many hundreds of tons of highly enriched uranium from the dismantling of nuclear weapons.

Most of these wastes will require chemical treatment, processing and solidification into waste forms for permanent disposal. The long-term effects of radiation on waste form solids is a critical concern in the performance assessment of the long-term containment strategy. In the case of spent nuclear fuel, the radiation dose due to the in-reactor neutron irradiation is already substantial, and additional damage accumulation during disposal is not anticipated to be significant; thus, this is not a subject addressed in this review paper. In contrast, the post-disposal radiation damage to waste form glasses and crystalline ceramics is significant. The cumulative α-decay doses which are projected for nuclear waste glasses reach values of 10^{16} α-decays g^{-1} in 100 yr. Similarly, crystalline waste forms, such as Synroc will reach values of $> 10^{18}$ α-decay events g^{-1} in 1000 yr for a 20 wt% waste loading. These doses are well within the range for which important changes in the physical and chemical properties may occur, e.g. the transition from the crystalline-to-aperiodic state in ceramics.

This paper provides a comprehensive review of radiation effects (due to γ-, β- and α-decay events, as well as from actinide doping experiments and particle irradiations) on nuclear waste form glasses and crystalline ceramics, particularly Synroc phases, zircon, apatite, monazite and titanite. The paper also includes recommendations for future research needs.

1. INTRODUCTION

High-level nuclear waste (HLW) in the United States has three major sources: (i) spent nuclear fuel from commercial and research nuclear reactors; (ii) liquid waste produced at West Valley, New York, in the 1960s during the reprocessing of commercial spent nuclear fuel; (iii) waste generated by the nuclear weapons and naval propulsion programs. Much of the defense waste is stored in tanks at Hanford and Savannah River sites in Washington and South Carolina, respectively. The volumes are substantial. At the Hanford site alone the total inventory of low- and high-level waste includes 11,000,000 m^3 of fluids and 6900 metric tons of nuclear materials, which includes 4100 metric tons of uranium and 15 metric tons of Cs and Sr in capsules. The total activity of the waste at the Hanford site is estimated to be 446,000,000 Curies (Illman, 1993). For all of the principal DOE sites (Hanford, Savannah River, Idaho Chemical Processing Plant and the West Valley Demonstration Project) the combined total volume of high-level waste through 1988) is 385,000 m^3, and the total activity is 1,200,000,000 Curies (Office of Technology Assessment, 1991). Although the defense wastes account for 95% of the volume of the current total United States HLW inventory, they account for only 9% of the total radioactivity. The majority of the radioactivity is contained in commercial spent nuclear fuel (Weber, 1991a). Except in the case of direct disposal of spent fuel, which is the current U.S. policy, these wastes must be treated and solidified prior to permanent disposal. Finally, under the first and second Strategic Arms Reduction Treaties (START I and II) and unilateral pledges made by the United States and the former Soviet Union and Russia, many thousands of nuclear weapons will be dismantled during the next decade. This will generate over 100 metric tons of plutonium and many hundreds of tons of highly enriched uranium that will require disposal (National Academy of Sciences Report, 1994).

To the extent that these radioactive wastes must be treated and solidified prior to final disposition, the effect of radiation on waste form solids is a critical concern. One of the most important applications of the study of radiation effects in ceramics (vitreous and crystalline) during the past decade has been the effect of radiation on nuclear waste forms, e.g. borosilicate glasses, single and polyphase crystalline ceramics, and the UO_2 in spent nuclear fuel (Weber and Roberts, 1983; Matzke, 1988a,b; Ewing *et al.*, 1988; Weber, 1991a). In the case of spent fuel, the radiation dose due to the in-reactor neutron irradiation is already substantial, and additional damage accumulation during disposal is not anticipated to be significant. In contrast, the post-disposal radiation damage to waste form glasses and crystalline ceramics is significant. The cumulative α-decay doses per gram which are projected for the nuclear waste glasses to be used for the West Valley Demonstration Project (WVDP) and the Savannah River Plant (SRP) reach values of 10^{17} α-decay events g^{-1} in 1000 yr (Weber, 1991a). Similarly, crystalline waste forms, e.g. the titanate assemblage, Synroc, would reach values of $>10^{18}$ α-decay events g^{-1} in 1000 yr for a 20 wt% waste loading. For this Synroc composition, the total accumulated dose at the end of 10,000 yr is nearly equivalent to 0.5 displacements per atom. This dose is well within the range for which important changes in physical and chemical properties, most notably the transition from the crystalline-to-aperiodic (amorphous or metamict) state can occur.

Although present performance assessments of radionuclide containment rely primarily on the geologic repository, the physical and chemical durability of the waste form can contribute greatly to successful isolation of nuclear waste (Ewing, 1992a). Thus, the effect of radiation on physical properties and chemical durability are of importance. The changes in chemical and physical properties occur over relatively long periods of storage, 10^4–10^6 yr, and at temperatures which range from 100 to 450°C depending on waste loading, age of the waste, depth of burial, and the repository-specific geothermal gradient. Thus, one challenge is to simulate effectively radiation damage at relatively low fluxes over long periods of time. In this regard, studies of naturally occurring U- and Th-bearing phases that are structurally and chemically analogous to waste form phases have provided important data and reference points for long-term effects (Ewing *et al.*, 1988).

The essential issues addressed and summarized in this review are the following:

(1) What are the changes in physical properties (e.g. volume, fracture toughness and hardness), chemical properties (e.g. thermodynamic stability and leach rate) and stored energy as a function of radiation dose, temperature and time?
(2) How can the changes in physical and chemical properties to relevant radiation doses be simulated in accelerated experiments (for a waste form age of 10^4–10^6 yr)?

We begin with a brief history of the development of nuclear waste forms and a summary of their types.

1.1. *History*

The early history of the development of nuclear waste forms is summarized by Lutze (1988). These efforts, mainly in the 1950s, focused on the incorporation of radioactive waste into glasses of widely varying compositions. The first radioactive wastes were incorporated into a nepheline syenite (a silica-deficient igneous rock) glass at Chalk River, Canada. The processing temperature of the nepheline syenite glass (1350°C) was much higher than that of the now widely adopted borosilicate glasses (1100–1150°C). Major programs during the 1960s in the United States, Canada, Germany, France, Italy, Japan, the United Kingdom and the Soviet Union were directed at developing glass compositions that had lower melting points in order to reduce loss of radionuclides by volatilization, incorporated waste without phase separation, resulted in glasses which were durable, and for which vitrification was a feasible large scale industrial process. Borosilicate glass is now the waste glass composition of choice for most nations. Industrial use of the vitrification process has been in progress since 1978.

During the period from 1977 to 1982, there was a tremendous diversity in the types of nuclear waste forms which were under development (Lutze and Ewing, 1988). In the United States, much of this work ended with the decision to use borosilicate glass as the waste form for U.S. defense waste at Savannah River (Hench *et al.*, 1984). Synroc, a titanate ceramic waste form, was selected as the alternative U.S. waste form, but further development in the United States ended with the absence of funded programs. A major research and development program for the development of Synroc continued in Australia, culminating in the construction of a 'cold' Synroc pilot-scale processing plant. Basic research on the properties of Synroc were continued at the Australian National University by the late Professor Ted Ringwood and his colleagues (see Ringwood, 1985 and Ringwood *et al.*, 1988) and at the Australian Nuclear Science and Technology Organization, with collaborative work at the Japanese Atomic Energy Research Institute and AERE Harwell

in the United Kingdom. Synroc is perhaps the most thoroughly studied ceramic alternative to borosilicate glass.

Investigations into the properties and performance of other ceramic waste forms have revived during the past 10 yr for application to special waste stream compositions. At Lawrence Livermore National Laboratory, a Mixed Waste Management Facility is being developed in order to demonstrate an alternative to incineration (Oversby *et al.*, 1994). The waste form under study is a derivative of a Synroc composition originally developed for the immobilization of reprocessed residues at Savannah River, and typical phases include zirconolite, perovskite, spinel, nepheline and rutile. Although the radioactivity is low, this does illustrate the ubiquity of a rather limited set of phases, many of which are discussed in this paper. At the Idaho National Engineering Laboratory, an iron-enriched basalt waste form is under development, and the addition of ZrO_2 and TiO_2 has produced zirconolite as an actinide host in a silicate ceramic, i.e. a basalt (Reimann and Kong, 1994). At Argonne National Laboratory glassy slags have been developed for mixed wastes with high metal contents (Feng *et al.*, 1994). The glassy slag may have crystalline components which are as high as 80 vol.% in a vitreous matrix. Spent fuel–a metal clad, ceramic oxide—has become the major high level waste form under consideration in the U.S., as well as in Canada, Sweden and Switzerland, since these countries have decided against reprocessing [see summary of recent work in Ewing (1992b)].

1.2. *Principles of nuclide isolation in solid waste forms*

Borosilicate glass is, at present, the waste form of choice for most countries that have defense waste or have reprocessed high-level waste (e.g. France, Great Britain and the United States) and for most waste compositions. The selection of borosilicate glass is based mainly on an anticipated ease of processing (glass frit and the waste are mixed, melted at relatively low temperatures, and poured into canisters), the fact that the technology is well demonstrated for actual (radioactive) waste, and finally the assumption that the glass as an aperiodic solid will easily accommodate wide variations in waste stream compositions which are extremely complex (29–30 component systems), as well as not being susceptible to radiation-induced transformations (it is already aperiodic). Ceramic waste forms, with the exception of Synroc, have never been developed to a degree that the processing technology can be evaluated or demonstrated with actual waste. The basis for comparison and evaluation has been bench scale samples and usually samples that are not radioactive. Despite the lack of data on waste forms that have incorporated actual waste, the knowledge of radiation effects in ceramic waste forms is much further advanced than that of radiation effects in glass waste forms.

In contrast to glass forms in which the radionuclides are in principle homogeneously distributed throughout the waste solid, ceramic waste forms may incorporate radionuclides in two ways:

(1) Radionuclides may occupy specific atomic positions in the periodic structures of constituent crystalline phases, that is as a dilute solid solution. The coordination polyhedra in each phase impose specific size, charge and bonding constraints on the nuclides that can be incorporated into the structure. This means that ideal waste form phases usually have relatively complex structure types with a number of different coordination polyhedra of various sizes and shapes and with multiple substitutional schemes to allow for charge balance with radionuclide substitutions. Extensive nuclide substitution can result in cation and anion vacancies, interstitial defects, and changes in structure type. The formation of polytypes and twinning on a fine scale is common. The point defects can themselves become sites for the radionuclides. Except in unusual situations (e.g. monazite, $CePO_4$), the complexity of the waste composition results in the formation of a polyphase assemblage (e.g. Synroc consists of phases such as zirconolite, $CaZrTi_2O_7$; perovskite, $CaTiO_3$; and 'hollandite', $BaAl_2Ti_6O_{16}$), with unequal partitioning of radionuclides between the phases. In Synroc, actinides partition preferentially into zirconolite and perovskite. The polyphase assemblages are sensitive to waste stream compositions, and minor phases form, including glass segregated along grain boundaries. Ideally, all waste stream elements, radioactive and non-radioactive, are important components in the phases formed. In some rare cases, a single phase (e.g. monazite or sodium zirconium phosphate) can incorporate nearly all of the radionuclides into a single structure.

(2) Radioactive phases, perhaps resulting from simply drying the waste sludges, can be encapsulated in non-radioactive phases. The most common approach has been to encapsulate individual grains of radioactive phases in TiO_2 or Al_2O_3, mainly because of their extremely low solubilities. This approach requires major modifications to the waste stream composition and special processing considerations to keep temperatures low enough to avoid volatilization of radionuclides. A similar approach may be taken

with low temperature assemblages (e.g. mixing with concrete), but in this case there is the possibility of reaction between the encapsulating phase and the radioactive phases. Both the above types of waste forms are specifically formulated for the incorporation or encapsulation of radionuclides.

Spent fuel—a metal-clad, UO_2 ceramic—results from the use of reactor fuel that is designed without consideration of its waste form properties; but in order to avoid reprocessing, spent fuel has become an important potential waste form. The properties of spent fuel as a waste form are determined primarily by the irradiation history of the UO_2 in the reactor and the disposal conditions (e.g. nearly insoluble under reducing conditions and easily corroded under oxidizing conditions). Radionuclides are distributed through the fuel matrix as interstitial defects, as exsolved/precipitated phases, along grain boundaries, or in voids and cracks of the fuel–cladding gap. There is an extensive literature on neutron damage effects in UO_2 (Nakae *et al.*, 1979) and α-particle damage (Weber, 1981), as well as radiation damage in naturally occurring UO_{2+x} (Janeczek and Ewing, 1991). A summary of the work on spent fuel is beyond the scope of this review; thus, radiation effects in UO_2 as a nuclear waste form will not be discussed.

1.3. *Types of nuclear waste forms*

The following sections give brief summaries of the characteristics of the different waste forms. A careful description of the characteristics of a waste form is essential in anticipating potential radiation effects. As an example, the waste loading ultimately determines the radiation dose and the thermal history of the waste form (i.e. the decay of fission products is responsible for the thermal pulse in the early history of the waste form). The final damage state will be a function of the balance between accumulated damage and the kinetics of annealing of the individual phases. For polyphase waste forms, which include both glass and ceramics, the partitioning of actinides and fission products into separate phases can have dramatic differential effects, such as the selective amorphization of phases, while others retain their crystallinity. Anisotropic expansion of phases that experience different radiation doses of different types of radiation may lead to microfractures and disaggregation of the waste form. Despite the complexity of crystalline, polyphase ceramics, certain structure types are common to a wide variety of waste forms and waste stream compositions. This summary focuses on the present knowledge of radiation effects in the most common phases, e.g. pyrochlore, zirconolite, hollandite, perovskite, zircon, apatite and monazite. Extended discussions of the properties of the waste forms and additional details on radiation effects can be found in Lutze and Ewing (1988).

1.3.1. *Glass.* Glass waste forms can be of a wide variety of compositions, including silicate glasses, borosilicate glasses and phosphate glasses [summarized by Lutze (1988)]. In principle, radionuclides are evenly dispersed throughout the glass, although noble metal precipitates and, in some cases, crystalline oxide precipitates enriched in radionuclides may be present. Waste loadings (defense and commercial) are typically in the range of 10–30 wt%.

1.3.2. *Synroc. Synroc* is a titanium based, polyphase ceramic developed at the Australian National University and the Australian Nuclear Science and Technology Organization. The primary phases are: zirconolite ($CaZrTi_2O_7$), hollandite-like phase ($Ba_{1.2}(Al, Ti)_8O_{16}$), perovskite ($CaTiO_3$), and titanium oxides (e.g. TiO_2). Other phases, such as pyrochlore ($A_{1-m}B_2O_6(O, OH, F)_{1-n}pH_2O$; A = Ca, REE, U, Th, Pu, etc.; B = Ti, Nb, Ta) may be abundant depending on the waste stream composition. Minor phases also include titanates and aluminates, as well as noble metals. Processing conditions are sufficiently reducing to form Ru-rich and PdTe-rich phases. The principal components can each accommodate a range of radionuclides. Hollandite can retain fission products such as Cs, Rb, Ba; zirconolite, U, Zr, Np, Pu; perovskite, Sr and transuranics such as Np and Pu, The variable compositions of the waste are accepted over relatively wide ranges by simple and complex atomic substitutions within the structure of individual phases and by changing the relative proportions of the principal phases. Certain elements (e.g. Na_2O greater than 2 wt% together with SiO_2 and Al_2O_3) can lead to the formation of more soluble silicate phases (e.g. nepheline, $NaAlSiO_4$). Still, waste loadings up to 20 wt% can be made without deleterious effects on the properties of the waste form.

1.3.3. *Tailored ceramics.* Tailored ceramics were developed mainly at the Rockwell International Science Center (Harker, 1988). Another silicate and oxide based ceramic, *supercalcine*, was developed at the Pennsylvania State University (McCarthy, 1977; McCarthy *et al.*, 1979). These crystalline, ceramic waste forms are also polyphase assemblages, not different in principle from Synroc, but perhaps

broader in conceptual design with a wider variety of 'high-integrity mineral-like crystalline phases' (McCarthy *et al.*, 1979). The strategy again is to modify the waste stream composition so as to form specific, stable, crystalline phase assemblages. A broader range of phases (oxides, silicates and phosphates) are considered for radionuclide immobilization. Actinides are incorporated into fluorite (CaF_2), zirconolite, pyrochlore, perovskite ($CaTiO_3$), monazite ($CePO_4$), apatite ($Ca_5(PO_4)_3F$), and zircon ($ZrSiO_4$); Sr into magnetoplumbite ($Pb(Fe, Mn)_{12}O_{19}$), perovskite and hollandite; Cs into nepheline, perovskite, magnetoplumbite, hollandite; Tc into reduced metal alloys. Residual glass with fission products can occur along grain boundaries. Non-radioactive phases may be prominent, such as spinel ($MgAl_2O_4$), corundum (Al_2O_3) or rutile (TiO_2). As an example, a ceramic waste form tailored for the Savannah River defense waste consisted of magnetoplumbite, spinel, nepheline, uraninite (UO_{2+x}, and higher oxides) and corundum, and a ceramic waste form tailored for high-level Barnwell waste consisted of pyrochlore, perovskite, monazite, fluorite and a Ru alloy. In general, the silicate based assemblages are less stable than the titanates in the presence of water. Waste loadings are comparable to that in Synroc but the higher density of Synroc (4.35 g cc^{-1}) versus a typical tailored ceramic (4.05 g cc^{-1}) means that a slightly greater amount of waste can be incorporated in Synroc for a weight-equivalent waste loading.

1.3.4. *TiO_2–ceramic.* The TiO_2–ceramic matrix waste form was developed at the Kernforschungszentrum Karlsruhe (Adehelm *et al.*, 1988) and encapsulates the waste in a rutile (TiO_2) matrix. Waste loadings of simulated waste oxides of up to 12 wt% were attained in the laboratory scale experiments. The final product has a low leach rate as compared to borosilicate glass, because of the low solubility of TiO_2.

1.3.5. *Glass ceramics.* Glass ceramics have been developed at the Hahn-Meitner Institut in Berlin and at the Whiteshell Nuclear Research Establishment in Canada (Hayward, 1988). The Canadian glass ceramic consists of discrete crystals of sphene (the proper mineral name is 'titanite'), $CaTiSiO_5$, within a matrix of aluminosilicate glass. The sphene structure is capable of accepting a wide range of nuclides. Actinide elements, as well as fission products such as Sr, can substitute for the Ca. Larger cations, such as Cs, do not fit into the sphene structure and remain in the glass phase. The aluminosilicate glass matrix that remains after sphene crystallization is rather durable and can be produced in the glass-ceramic at lower temperatures than those required to produce the glass alone. Leach rates under comparable conditions are lower than for borosilicate glass. In the Canadian repository (granitic), sphene, instead of perovskite, is the thermodynamically stable phase. Optimal waste loadings are approximately 15 wt%. A number of other glass ceramic compositions have been studied in less detail. These include: (1) celsian glass-ceramics which yield, as individual phases, celsian ($BaAl_2Si_2O_8$), perovskite ($CaTiO_3$), diopside ($CaMgSi_2O_6$), or eucryptite ($LiAlSi_2O_6$); (2) fresnoite glass-ceramics which form fresnoite ($Ba_2TiSi_2O_8$), priderite ($(K,Ba)(Ti, Fe)_8O_{16}$), pyrochlore ($A_{1-m}B_2O6(O, OH, F)_{1-n}$ pH_2O) and scheelite ($CaWO_4$); (3) basalt glass-ceramics which form augite ($(Ca, Mg, Fe)_2Si_2O_6$) and the spinel trevorite ($NiFe_2O_4$); (4) iron-enriched basalt glass-ceramics which form spinel (enriched in Fe_3O_4), plagioclase ($CaAl_2Si_2O_8$), augite ($(Ca, Mg, Fe)_2Si_2O_6$), fluorapatite ($Ca_5(PO_4)_3F$) and zircon ($ZrSiO_4$). Other glass-ceramic compositions have been studied mainly in the hope of improving the leach resistance of the borosilicate glasses. Perhaps the most important feature of the glass-ceramics is that the processing technology is not very different from the demonstrated technology for the borosilicate glass. The only difference is the final heat treatment required, and depending on the specific glass-ceramic used (e.g. the sphene glass-ceramic), there is a resulting increase in chemical durability.

1.3.6. *Monazite.* Monazite developed at Oak Ridge National Laboratory is unique in that it essentially consists of a single phase, monazite ($CePO_4$) (Boatner and Sales, 1988). This composition can be synthesized for the full range of lanthanide orthophosphates. Depending on the lanthanide composition and the temperature, at least three structure types are possible. A low temperature hexagonal phase forms for compositions in the first half of the lanthanide series (from La to Dy). The hexagonal phase is metastable and will not form once the structure is transformed to the monoclinic monazite structure (Beall *et al.*, 1981; Mullica *et al.*, 1985). The heavier lanthanides (Er to Y) have a high temperature tetragonal structure isostructural with zircon ($ZrSiO_4$) (Mullica *et al.*, 1990). Actinides are incorporated into the lanthanide site. Important divalent fission products, Sr and Ba, are also accommodated in the monazite structure in order to provide charge balance for tetravalent actinides. As with many of the other ceramic waste forms, there is an important

improvement in chemical durability (factor of 20 in the leach rate for selected elements) as compared to that of borosilicate glass under comparable conditions. In contrast to other waste form phases, the lanthanide orthophosphates have a negative temperature coefficient of solubility; thus, one may expect the chemical durability in the presence of solutions to increase with increasing temperature. These compounds also have a high thermal stability with melting points in excess of 2000°C. Typical waste loadings for simulated U.S. defense waste are 20 wt% (monazite waste form density is in the range of 4.0–5.0 g cc^{-1}).

1.3.7. *Cementitious waste forms.* Cementitious waste forms are mainly considered for low-level waste (Jiang *et al.*, 1993; Quillin *et al.*, 1994). Although concrete has been used for low-level waste, FUETAP (Formed Under Elevated Temperature and Pressure) concrete was developed at Oak Ridge National Laboratory and the Pennsylvania State University (McDaniel and Delzer, 1988) and is unique in that it uses the inherent heat of the high-level waste (as well as external heat sources) to accelerate curing to drive off up to 98% of the unbound water and form a hard, dense product of improved (compared to normal concrete) physical properties. The identification and characterization of the specific phases formed and the determination of the fate of radionuclides in FUETAP have not been completed. Typical waste loadings are of the order of 15–25 wt% (density is approximately 2 g cm^{-3}). Leach rates are comparable to those of borosilicate glass. In addition to radiation damage of specific phases in cementitious materials, there is the additional possibility of radiolysis of cement-pore water and potential pressurization of waste canisters due to an accumulation of the radiolytically produced gases. Solid-state radiolysis of hydrated phases may also affect their long-term stability.

1.3.8. *Spent fuel.* Spent fuel (Johnson and Shoesmith, 1988) was first considered as a possible waste form in the early 1970s due to delays and cancellations of fuel reprocessing programs. The continued, depressed prices for uranium and lower projected nuclear power generating capacity have made the disposal of spent fuel a likely possibility. Typical fuel consists of UO_2 pellets. Stacks of the pellets are clad in Zircaloy-2 or -4. Individual pellets are pure UO_2, with 95% of theoretical maximum density and with a uniform grain size that is typically 2–4 μm. The irradiated fuel is chemically and structurally different from the unirradiated fuel. Actinides and lanthanides, as well as some fission products, form solid solutions with the UO_2. In some cases new compounds form. Cs and I react and form CsI, and some Cs is thought to form cesium uranates or cesium molybdates. The elevated temperatures (up to 1700°C) during irradiation promote grain growth with the resulting segregation of fission products that are incompatible with the UO_2 structure. Cracking and void formation are common, and volatile species (Xe, Kr, Cs and I) can accumulate. Noble metal inclusions (up to 10 μm) are also found. Despite the apparent complexity of spent fuel as a waste form, its direct disposal in a repository eliminates the need for reprocessing. The chemical durability is difficult to assess because it is dependent on the irradiation history and on the oxidation potential of the repository. Under reducing conditions UO_2 is very insoluble, but under slightly oxidizing conditions matrix corrosion proceeds by oxidative dissolution. Redox conditions may be influenced by α- and γ-radiolysis of the solution in contact with the spent fuel. Under the 'extended-dry' repository concept (e.g. at Yucca Mountain), oxidation to U_3O_8, accompanied by a volume increase and cladding rupture, is a concern. If air enters the waste packages at elevated temperatures, the subsequent entry of water could result in relatively high leach rates for the spent fuel.

1.3.9. *'Novel' ceramic waste forms.* 'Novel' ceramic waste forms include consideration of some additional, unusual phases. Most of this work has been completed at the Pennsylvania State University (Ewing, 1988). One such phase is sodium zirconium phosphate, $NaZr_2(PO_4)_3$ (NZP). The structure consists of an open three-dimensional framework with three distinct atomic sties, which can accommodate a wide range of radionuclides. At high simulated waste loadings (20 wt%), an additional phase, monazite, forms. NZP can also be mixed with concrete formulations to act as a host for Cs, resulting in a CsZP. Its main advantages lie in its potential for low-temperature processing and as a specific additive to concrete formulations. A similar waste form ceramic is the low-temperature hydroxylated ceramic. This consists of hydrated sheet silicates (clays) and framework silicates (zeolites) that in most cases form at low temperatures. Historically, clay phases were among the first to be suggested for the immobilization of nuclear waste (Hatch, 1953). The principal advantage of both of these low-temperature waste forms is that they are the common, thermodynamically stable phases at the earth's near surface, the environment of most repositories.

1.3.10. *Multi-barrier waste forms.* Multi-barrier waste forms are unique combinations of the previously discussed waste forms and some special processing technologies. Multi-barrier waste forms consist of a series of glass or ceramic barriers. This is the 'Russian doll' concept proposed by Roy (1979). Phases are either encapsulated in other more durable phases or the particles are coated with another phase. The coatings are applied to enhance chemical durability, mechanical strength or thermal stability. The coatings may be conventional ceramics (Al_2O_3, TiO_2 or SiO_2), carbon products (PyC, Cr_7C_3 or SiC), glass (borosilicate or aluminosilicate) or metals (Ni, Si or Fe). A common difficulty is the proper attachment of coatings to substrate particles without cracking or flaking of the layer. Differential expansion of phases due to radiation damage may exacerbate the cracking of the thin films.

1.4. *Radiation sources and doses*

The chief sources of radiation in high-level nuclear waste forms are the β-decay of fission products (e.g. ^{137}Cs and ^{90}Sr) and the α-decay of actinide elements (e.g. U, Np, Pu, Am and Cm). There are minor contributions to the damage process from spontaneous fission events of the actinides, and α-neutron reactions are additional sources of fission fragments and neutrons, but the production rates are low. Therefore, these latter events are not considered in this paper. β-decay is the primary source of radiation during the first 500 yr of storage, as it originates from the shorter-lived fission products (e.g. the half-life of ^{137}Cs is 30.2 yr and the half-life of ^{90}Sr is 28.1 yr). The β-decay of fission products is responsible for heat generation and the elevated temperatures early in the history of waste form storage. The α-decay damage becomes dominant as a radiation damage source after approximately 1000 yr (e.g. the half life of ^{239}Pu is 2.411×10^4 yr).

The β- and α-decay events can cause radiation damage through three processes in the waste form: (1) elastic collisions between nuclear particles (e.g. β-particles, α-particles and α-recoil nuclei) and the atoms in the host matrix which cause atomic displacements and the creation of isolated Frenkel defect pairs (combined interstitials and vacancies) or intense collision cascades; (2) ionization effects associated with the γ-rays, β-particles and α-particles; (3) the transmutation of radioactive parent nuclei into different elements. Of these three effects, the most important are processes that cause atomic displacements, as these are responsible for the atomic-scale rearrangement of the structure and hence lead to the greatest changes in physical and chemical properties. Each α-decay event results in approximately 1500 atomic displacements, while a β-decay event results in only 0.15–0.10 displacements. There is no compelling evidence that ionization events result in important structural changes in most oxide ceramics (Weber *et al.*, 1981, 1982, 1984; Weber and Roberts, 1983); however, more recent work by DeNatale and Howitt (1985, 1987) and summarized by Weber (1991a) has shown that complex borosilicate glasses can decompose by an ionization-driven radiolytic process that produces bubbles which contain molecular oxygen. Although systematic studies are lacking, the bubble formation, glass decomposition, and even changes in chemical durability may correlate with the ionizing component of energy deposition. These phenomena will be discussed in Section 4.

The cumulative doses for the waste forms can be substantial. Table 1 summarizes the anticipated cumulative doses for α, β and γ radiations for waste glasses that will be generated at the Savannah River Plant in South Carolina. If one converts these values to atomic displacements per gram or absorbed dose, the glass waste form with a 25 wt% waste loading will reach values in excess of 10^{20} atomic displacements g^{-1} ($=0.0025$ displacements per atom, dpa) or 7×10^{10} rads in only 1000 yr (Figs 1 and 2). Also included in Figs 1 and 2 are the cumulative doses generated within non-U.S. commercial waste glasses, which are several orders of magnitude higher than those for defense waste. Figure 3 shows the accumulated α-decay event

Table 1. Cumulative decay events and doses projected for SRP nuclear waste glasses (Weber, 1991a)

Time (years)	Alpha decays (per gram)	Beta decays (per gram)	Alpha dose (rad)	Beta/gamma dose (rad)
1	2×10^{14}	5×10^{16}	2×10^{7}	6×10^{8}
10	2×10^{15}	5×10^{17}	2×10^{8}	6×10^{9}
10^2	2×10^{16}	2×10^{18}	2×10^{9}	3×10^{10}
10^3	1×10^{17}	5×10^{18}	9×10^{9}	6×10^{10}
10^4	3×10^{17}	5×10^{18}	3×10^{10}	8×10^{10}
10^5	5×10^{17}	5×10^{18}	4×10^{10}	1×10^{11}
10^6	1×10^{18}	5×10^{18}	8×10^{10}	1×10^{11}

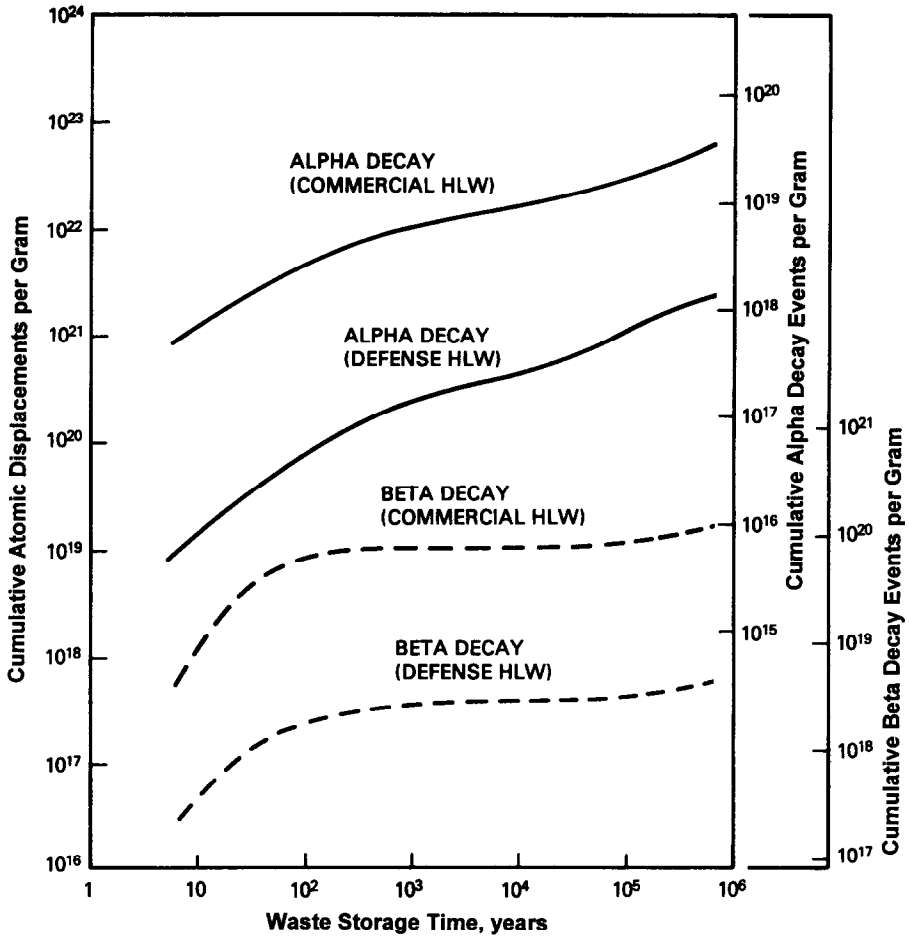

Fig. 1. Cumulative atomic displacements and decay events per gram in ceramic or glass nuclear waste forms. Basis: Commercial HLW-3.3% enriched UO_2 fuel, burn-up of 33,000 MWD/MTHM, cooled 5 yr before reprocessing and solidification, 25 wt% waste loading; Defense HLW-Savannah River Plant Waste, 25 wt% waste loading (see Table 1). After Weber *et al.* (1982).

dose in Synroc for 20 and 10 wt% waste loadings. Note, that for a 20 wt% waste loading, the accumulated dose after 10^4 yr is 4×10^{18} α-decay events g^{-1} (=0.32 dpa). This is well within the range of doses in which one may expect amorphization of actinide-bearing phases. Phases such as zircon can become aperiodic (or metamict) at doses as low as 0.3 dpa.

2. RADIATION DAMAGE PROCESSES

When solids are subjected to irradiation, any or all of three responses are possible: heating, localized displacement of the constituent ions, and disordering or other global rearrangements of those ions. Further, the irradiating particles themselves can in some cases have a significant effect on the evolution of the damage microstructure, through their deposition in the structure. In this section we discuss how damage effects vary with type of radiation (which in nuclear waste principally encompasses α, α-recoil, β and γ radiation), and how damage mechanisms can vary with the type of waste form.

2.1. *Heating*

When energy from any type of radiation is absorbed in a solid, an increase in temperature will result. The magnitude of the temperature increase depends on the rate of energy absorption, physical properties of the solid (e.g. its specific heat), and the extent of thermal conductance to the surroundings. In the case of nuclear waste, significant heating is possible: it can be shown that commercial nuclear waste forms containing typical waste loadings will, when placed in a

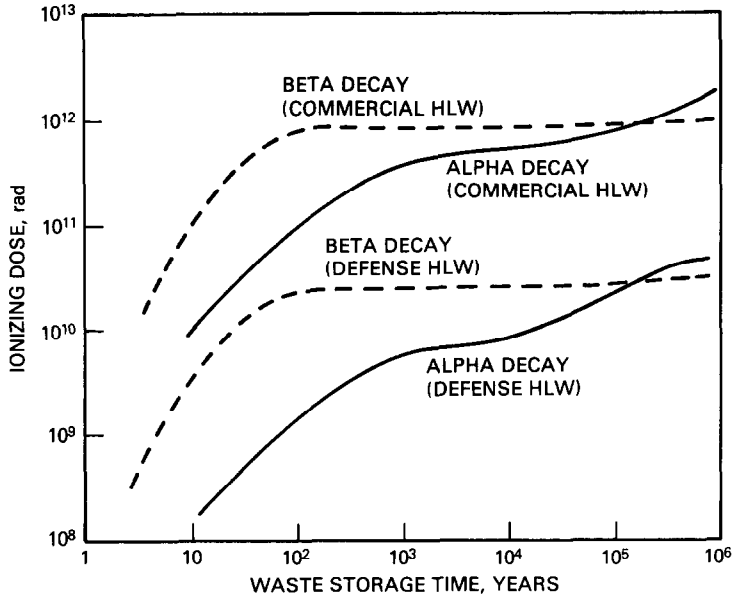

Fig. 2. Ionizing radiation dose in commercial and defense high level forms (see basis for calculations in Fig. 1). After Weber and Roberts (1983).

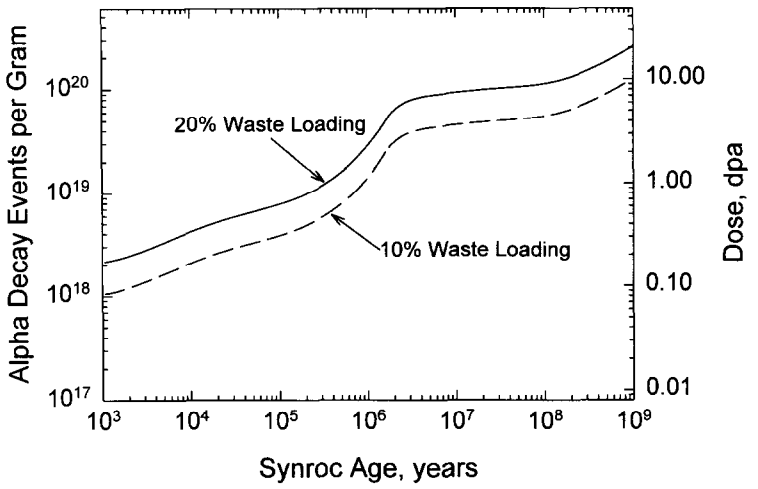

Fig. 3. The α-decay dose for Synroc (10 and 20 wt.% loading of HLW). The α-decay damage is expressed as α-decay events g^{-1} and displacements per atom (dpa) and correlated to an equivalent Synroc 'age'. After Ringwood *et al.* (1988).

repository, generate enough self-heat from decay of fission products to result in an initial storage temperature as high as 600°C. Even 100 yr after emplacement, the temperature may still be as high as 300°C. Temperature increases of this magnitude can profoundly affect the response of nuclear waste forms to self-irradiation damage.

2.2. *α- and α-recoil irradiation*

Self-damage in nuclear forms results primarily from decay of α-emitting actinide isotopes. The α-particle (helium ion) has an energy of 4.5–5.5 MeV; whereas, the recoil nucleus has an energy of 70–100 keV; thus the α-particle carries 98% of the energy of the decay event. In estimating the consequences of irradiation of

a solid by light and heavy particles of varying energies, it is important to estimate whether a given particle will deposit its energy primarily by displacive (elastic) or by ionization (inelastic) processes. This is determined by the relative velocity of the bombarding particle and that of the orbital electrons of the target ion. If the particle velocity is below that of the orbital electrons, the likelihood of electronic excitation is small and most of the energy will be transferred to the nucleus of the ion. However, if the particle velocity is higher than that of the orbital electrons excitation will dominate. As a rough rule, inelastic processes are important if the energy of the bombarding particle, expressed in keV, is greater than its atomic weight. Thus an α-particle of atomic weight 4 and energy 5 MeV will predominantly deposit its energy by ionization, while an α-recoil ion of mass 240 and energy 100 keV will lose most of its energy in elastic collisions. Reeve and Woolfrey (1980) have estimated that the α-particle accounts for only 6% of the displacive energy from an α-decay event. This energy is deposited over a range of 10–20 μm, with most of the damage occurring near the end of the path of the helium ion.

In the case of irradiation with a light but energetic ionizing particle, such as a 5 MeV α-particle, several sequential atomic collisions usually occur before the particle comes to rest. Each of these events displaces a small number of ions, so that the overall effect is a damage event spread widely throughout the solid in small clusters. As a consequence, recombination of vacancies and interstitials can easily occur and this process is enhanced by the prevalence of nearby undamaged material.

In most solids the only structural consequence of electronic excitation is heating. However, in those materials subject to damage by radiolysis, breaking of atomic bonds and displacement of atoms can result. For example, crystalline SiO_2 can be transformed to the disordered or metamict state by electrons whose energy is too low to directly displace atoms (Hobbs and Pascucci, 1980). With respect to nuclear waste, it has been observed that borosilicate waste glasses can decompose by absorption of ionizing energy with the resultant production of molecular oxygen (DeNatale and Howitt, 1987).

The more massive but lower energy (approximately 100 keV) α-recoil particle has been shown by Reeve and Woolfrey (1980) to account for 94% of the total displacement energy resulting from an α-decay event (Van Konynenburg and Guinan (1983) calculated a value of 89% for Synroc phases). Such a particle travels only a short distance in a solid, of the order of 10 nm. Thus the displacement event consists of a large number of disordered atoms in a compact microvolume. In this case most disordered atoms are surrounded by other disordered atoms, leading to an increased probability of damage retention.

When an α-particle stops in a solid, it becomes a helium atom; if present in sufficient numbers and at high enough temperatures to allow mobility, these gas atoms can result in the formation of gas bubbles (Clinard *et al.*, 1970). In some cases these aggregates affect mechanical properties, especially if located at grain boundaries.

2.3. β-*irradiation*

In nuclear waste, decay of fission products produces high-energy electrons (β-particles). Because of their low mass, these electrons usually induce only single displacement events (Frenkel pairs); most of the energy of these particles is dissipated by ionization processes, through Coulombic interactions. However, for those waste forms in which radiolytic damage is significant, ionization effects from β-particles could represent a major source of damage. Additionally, β-decay will be the principal source of heating in waste forms during the first 500 yr of waste storage, and therefore plays an important role in determining the temperature (and thus damage response) of the waste form.

Calculations have been completed by Weber *et al.* (1982) to determine the cumulative number of non-radiolytic atomic displacements in commercial and defense high-level waste that will result from the two most effective sources of displacement damage, namely α-decay and β-decay. The results, shown in Figs 1 and 2, demonstrate that α-decay is dominant and that irradiation fluxes (and therefore heating effects) are greatest early in the storage cycle.

2.4. γ-*irradiation*

Ionizing radiation such as γ-rays can, through ionization processes, cause displacement damage or even amorphization if the solid is sensitive to radiolysis. Another source of damage related to γ-irradiation is the energetic electrons that result from interaction of high-energy electromagnetic radiation with solids. However, the inefficiency of production of these electrons and their inefficiency in producing displacement damage means that this is not a significant source of radiation-induced changes in nuclear waste materials. Total ionizing dose as a function of the age of the waste form is illustrated in Fig. 2.

3. RADIATION SIMULATION TECHNIQUES

3.1. *Actinide-doping of waste forms and component phases*

Alpha-decay events associated with the decay of actinides and their daughter products are responsible for the atomic-scale structural damage that will occur in radioactive waste forms. The α-decay event consists of two, separate, simultaneous processes: (1) An α-particle (5 MeV) with a range of 10,000–20,000 nm dissipates most of its energy by ionization; however, at low velocities near the end of its track, it displaces 100–200 atoms creating Frenkel defect pairs. (2) The α-recoil atom (0.1 MeV) with a range of 10 nm produces 1000–2000 atomic displacements creating 'tracks' of disordered material. These two damaged areas are separated by thousands of unit cell distances and, as is illustrated in later sections of this review, will have different effects on the atomic structure of the solid, particularly for crystalline materials (see particularly the work by Weber (1981) on UO_2). The long-term effects of α-decay events can be simulated by incorporating highly-active, short-lived actinides, such as ^{238}Pu (half-life of 87.7 yr) or ^{244}Cm (half-life of 18.1 yr) into the waste form phase in concentrations great enough that the total α-decay dose reaches values of 10^{18}–10^{19} α-decay events g^{-1} in reasonable amounts of time (this may still require several years). This is the accepted test procedure drafted by the International Standards Organization and is the basis for the MCC-6 method for the preparation and characterization of actinide-doped waste forms (Weber and Turcotte, 1982). This test effectively simulates the simultaneous α- and α-recoil effects to doses that one expects over long periods of time (10^3–10^6 yr for waste forms and 10^8 yr for natural phases), but at much accelerated dose rates. However, as illustrated by the study of zircon (Section 5.2.5), actinide-doping experiments, with a high dose rate, do accurately simulate radiation effects at very much lower dose rates over geologic time. This is also supported by the comparisons presented by Van Konynenburg and Guinan (1983).

3.2. *Actinides in minerals as natural analogues*

Naturally occurring phases (=minerals) contain ^{238}U, ^{235}U and ^{232}Th and their daughter products. Concentrations may be as high as 30 wt% UO_2 in pyrochlores, which, depending on the age of the sample, may reach doses of 10^{20} α-decay events g^{-1}. Other phases, such as zircon, contain trace amounts of uranium (up to 5000 ppm), but with ages that are up to 10^9 yr, the doses may reach 10^{19} α-decay events g^{-1}. In many cases, these doses are sufficient to cause a radiation-induced periodic-to-aperiodic transition, that is the metamict state. Metamict minerals are one class of amorphous materials that have long been recognized to have resulted from radiation damage (Ewing, 1994), and their properties have been summarized by Pabst (1952), Ewing (1975) and Ewing *et al.* (1987). Minerals that are isostructural with crystalline phases in ceramic waste forms can therefore serve as natural analogues in the investigation of radiation damage effects (Ewing and Haaker, 1980; Ewing *et al.*, 1988). Minerals have the advantage of representing long-term radiation effects, over hundreds of millions of years, which are the result of very low dose rates. The dose rates of the actinide-doping experiments described above and the dose rates experienced by minerals span a range of nine orders of magnitude.

Unfortunately, there are no natural glasses which contain enough uranium and thorium that they can serve as natural analogues for radiation effects in waste form glasses. There is, however, one instance in which a Th-doped glass, 17 yr in age, has been studied (Eyal and Ewing, 1993).

3.3. *Neutron irradiations*

Neutron irradiations can be utilized in three ways (Weber and Roberts, 1983). Fast neutrons dissipate their energy by elastic collisions resulting in numerous atomic displacements, and the samples become moderately radioactive. This provides a fair simulation of α-recoil damage, but there is no simulation of the effect of helium build-up due to an absence of α-particles. Additionally, the only phases in polyphase waste forms that will experience α-recoil damage are those which contain actinides. All phases will experience α-particle, β-particle and γ-irradiation. Neutron irradiations damage all of the phases in the waste form, and therefore, will not simulate the phase selective α-decay damage experienced in actual waste forms. Neutron irradiations have been used to simulate damage in Synroc phases (Reeve and Woolfrey, 1980; Reeve *et al.*, 1981). Using another approach (Malow and Andersen, 1979), boron-containing glasses (e.g. the borosilicate glass) or boron-doped waste forms can be irradiated in a thermal neutron flux, and because of the high $^{10}B(n, \alpha)^7Li$ cross-section, an α-particle ($E = 1.78$ MeV) is generated. With this technique, high rates of He formation are possible, but this does not simulate the α-recoil damage of the α-decay event. Finally, thermal neutron capture by selected nuclides (e.g. ^{235}U) can lead to nuclear fission, which results in the formation of extensive zones of atomic displacements, i.e. fission

tracks (Antonini *et al.*, 1979). This is not a good simulation of α-decay damage (Weber, 1981), and the number of fission events in nuclear waste forms is so low as to make the process an unimportant damage mechanism.

3.4. *Charged-particle irradiations*

Charged-particle irradiations using electrons (Hobbs and Pascucci, 1980), protons, α-particles (Weber, 1981, 1982, 1985) or heavy ions (Weber *et al.*, 1994) have been used to study radiation damage effects. Significant doses can be reached in short periods of time (e.g. minutes), but analysis of the results is difficult because the damaged areas are thin surface layers of restricted lateral extent. The high surface area can act as a sink for migrating defects, and the dose required for amorphization may be greater than that for bulk irradiations. Implanted layers can also change the characteristics of the target material (e.g. an increase in the apparent leach rate) as a result of compositional changes that are enhanced in thin layers. Still, the α-particle irradiation is a good simulation of α-particle damage, and heavy-ion implantation (Pb^{2+}) provides a good simulation of α-recoil damage (Headley *et al.*, 1982). In fact, the two techniques used together can be used to unravel the relative contributions of α-particle and α-recoil damage to the changes in the properties of the solid. All of these techniques have been used to study α-decay damage effects in nuclear waste glasses, nuclear waste ceramics and component phases.

Most recently, Weber *et al.* (1994) have completed a detailed study of the radiation-induced crystalline-to-amorphous transition in zircon in which they made a comparison between damage caused by α-decay events (^{238}Pu-doped synthetic zircon and U-bearing natural zircons) and ion-beam irradiated zircon (0.8 MeV Ne^{+}, 1.5 MeV Ar^{+}, 1.5 MeV Kr^{+}, 0.7 MeV Kr^{+}, 1.5 MeV Xe^{+}). The results demonstrated that the amorphization dose under the high dose rates of the ion irradiation (10^{-4}–10^{-3} dpa s^{-1}) for heavy-ion irradiations is nearly identical to that of Pu-doped zircon (3×10^{-9} dpa s^{-1}), which suggests that the amorphization process is largely independent of the damage source or the dose rate for heavy particles (α-recoil particles or heavy ions) at constant temperature. This suggests that heavy ion beam irradiations can be used to simulate α-decay event damage in individual phases in nuclear waste forms. Irradiations with light ions (e.g. α-particles) can be used to simulate α-particle damage in phases that do not contain nuclides which decay by α-emission.

3.5. *γ-irradiations*

Gamma-irradiations are easily completed on waste forms using ^{60}Co or ^{137}Cs sources. The advantage of this type of irradiation is that γ-rays are so penetrating that waste forms can be irradiated in sealed containers. Dose rates on the order of 2.5×10^{6} R h^{-1} are easily achieved. However, structural damage from γ-irradiation is minimal except in those waste forms that are subject to damage by radiolysis (Hobbs and Pascussi, 1980). In terms of waste form corrosion, the most important effect of γ-radiation is the radiolytic decomposition of species such as nitrogen and carbon dioxide which are present in air or dissolved in the water, leading to the formation of nitric and carboxylic acids. The oxidation dissolution of UO_2 can result from γ-radiolysis of water in contact with spent fuel (Sunder *et al.*, 1992).

4. RADIATION EFFECTS IN GLASS WASTE FORMS

The effects of radiation in nuclear waste glasses are complex, and the fundamental understanding of the radiation damage processes and results is limited. The high-radiation environment provided by the α- and β-decay of radionuclides in nuclear waste can affect radionuclide release to the biosphere through radiation-induced physical and chemical changes in the nuclear waste glass at both the atomic and macroscopic levels. Several comprehensive reviews (Burns *et al.*, 1982a,b; Weber and Roberts, 1983; Day *et al.*, 1985; Weber, 1988, 1991a; Wronkiewicz, 1993) of radiation effects in nuclear waste glasses provide excellent technical assessments, and many unresolved scientific and engineering issues regarding radiation effects were summarized by Matzke (1988a,b) following a 1987 workshop.

4.1. *Volume changes*

Radiation effects from α-decay in actinide-doped simulated nuclear waste glasses can result in either expansion or compaction of the glass structure. The macroscopic volume changes, $\Delta V/V_0$, are usually determined by density measurements and generally follow an exponential dependence on dose, D, of the form:

$$\Delta V/V_0 = A[1 - \exp(-BD)], \quad (1)$$

where A is the volume change at saturation and B is the amount of glass damaged per unit dose. The volume changes normally saturate within the range of ±1.2% at a dose equivalent to about 10^{18} α-decays g^{-1} (10^{11} rad), as illustrated in Fig. 4 for several actinide-doped nuclear waste glasses studied at the Pacific

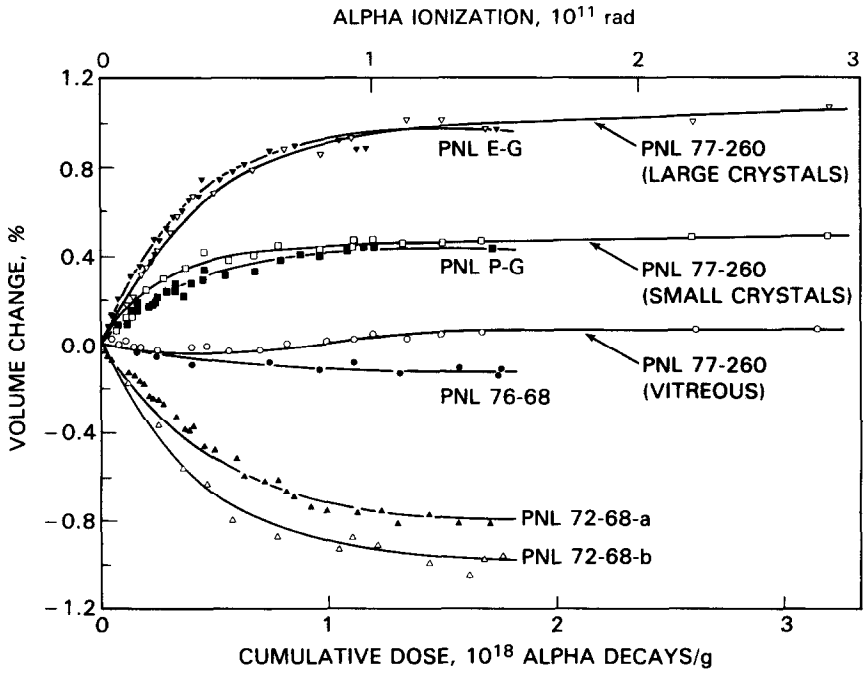

Fig. 4. Volume changes versus dose in ^{244}Cm-doped simulated Pacific Northwest Laboratory waste glasses. After Weber and Roberts (1983).

Northwest Laboratory in the U.S. (Weber and Roberts, 1983; Weber, 1988). Similar behavior has been observed in a collaborative study on actinide-doped simulated waste glasses by the Centre de Marcoule, the Hahn-Meitner Institut, and the Atomic Energy Reserch Establishment (Day *et al.*, 1985), as shown in Fig. 5. Several proposed glass compositions for Savannah River Plant waste have also been studied (Bibler and Kelley, 1978; Bibler, 1982; Weber, 1988), and the volume expansions (Fig. 6) are larger than for other waste glasses studied to date. In a more recent study of an actinide-doped waste glass by Inagaki *et al.* (1992), the volume expansion determined by density measurements at a dose of approximately 5.5×10^{18} α-decays g^{-1} ranged from 0.4 to 0.6%, which they found to be in excellent agreement with the volume change (0.51%) determined from the measured size and concentration of irradiation-induced bubbles. These results show a strong correlation between bubble formation and macroscopic volume change in nuclear waste glass and also support the hypothesis suggested by Weber (1988, 1991a) that the volume expansions observed in earlier studies (Figs 4–6) may partly be due to the formation of bubbles. Banba *et al.* (1994) have also observed a volume expansion of 0.75% after 1.5×10^{18} α-decay events g^{-1} in an actinide-doped waste glass from the Tokai Reprocessing Plant. The bubbles may be of trapped He from the α-decay event or oxygen from radiolytic decomposition of the glass. The increases in volume of neutron-irradiated nuclear waste glasses (Antonini *et al.*, 1980; Sato *et al.*, 1988) are also within the bounds observed for the actinide-doped glasses. Volume changes have not been measured in any of the ion-irradiation studies. In the simulated waste glasses that have been studied, there is a general tendency for swelling in glasses with low alkali/silicon ratios and for compaction in glasses with high alkali/silicon ratios (see shaded area of Fig. 7).

Gamma-irradiation studies in the U.S. on two simulated nuclear waste glasses have reported only slight (<0.1%) volume changes (Bibler, 1982; Weber, 1988). Shelby (1980), however, reported up to 1% compaction in commercial borosilicate glasses after γ-irradiation to 10^{10} rad, which is comparable to the compaction observed in some actinide-doped glasses (Fig. 4). Sato *et al.* (1984) have reported swelling of 0.2% in a simulated nuclear waste glass after γ-irradiation; Manara *et al.* (1984) and Sato *et al.* (1984) also observed swelling of up to 50% (from oxygen bubble formation) after electron-irradiation. Based on these results, it is impossible to determine conclusively whether the volume changes observed in α-decay studies are due to atomic displacements or ionization

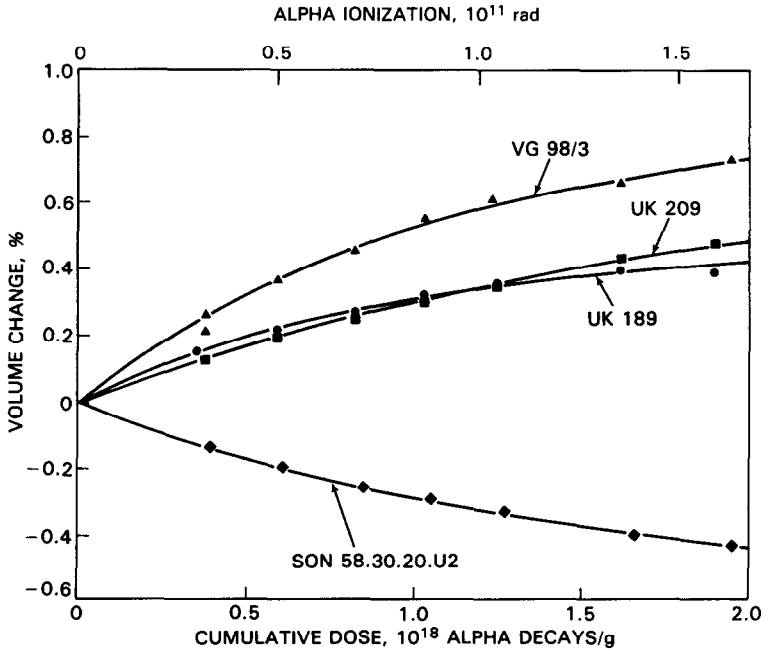

Fig. 5. Volume changes versus dose in ^{238}Pu-doped simulated European nuclear waste glasses. After Day *et al.* (1985).

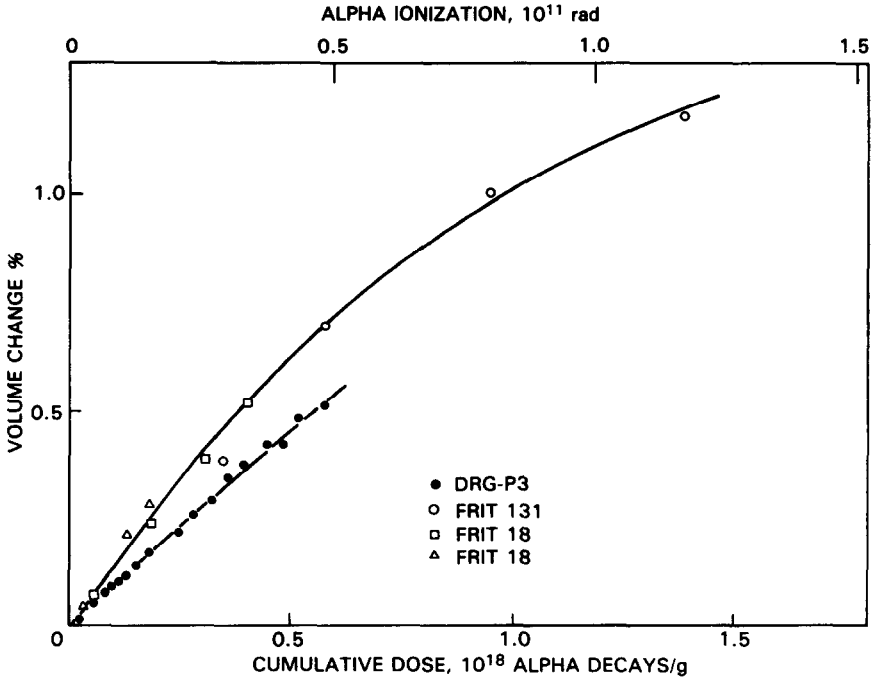

Fig. 6. Volume changes versus dose in ^{244}Cm and ^{238}Pu-doped simulated Savannah River Plant HLW glass compositions. After Weber (1988).

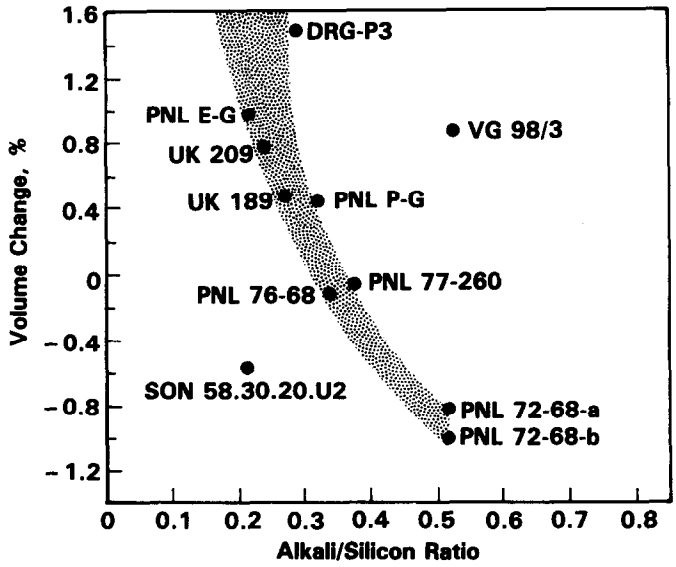

Fig. 7. Saturation volume change versus alkali/silicon ratio in simulated nuclear waste glasses. After Weber (1991a).

damage. However, the ion-irradiation studies of Arnold (1985, 1988) have strongly indicated that ionization processes are the dominant mechanism for producing volume changes in borosilicate waste glasses. Consequently, the volume changes in actual waste glasses, if due to ionization damage, could saturate within 10,000 yr for U.S. defense glasses and within several hundred years for commercial waste glasses in other countries. While the magnitude of the above volume changes does not pose any problems for the safe storage of nuclear waste, they indicate changes in microstructure that may affect the integrity of nuclear waste glasses and radionuclide release rates (which are proportional to the surface area in contact with solutions). Furthermore, differential volume changes as a result of temperature dependencies, which have not been investigated, and compositional inhomogeneities may result in microcracking, residual stresses, additional loss of integrity, and enhanced radionuclide release.

4.2. *Stored energy*

The interactions of radiation with nuclear waste glasses can result in the storage of latent energy associated with the changes in structure and bonding that is released as heat at elevated temperatures. Studies on actinide-doped simulated nuclear waste glasses at the Pacific Northwest Laboratory (Roberts *et al.*, 1976; Weber and Roberts, 1983), AERE-Harwell (Hall *et al.*, 1976), and under a collaborative European Communities program (Malow *et al.*, 1980) indicate that α-decay can result in stored energy that is generally less than 150 J g^{-1} and saturates at a dose of 0.1–0.3 $\times 10^{18}$ α-decays g^{-1} (10^{10} rad). This is illustrated in Fig. 8, where the total stored energy for several simulated waste glass compositions has been determined using differential scanning calorimetry (Weber and Roberts, 1983). In general, the increase in stored energy with dose followed exponential behavior similar to that shown by the changes in volume; however, the dose for saturation of stored energy is considerably less than the dose required for saturation of volume changes, which suggests different mechanisms and associated defects. Primak and Roberts (1984) have postulated that this stored energy is associated with the breaking of glass network bonds and may be due to ionization damage from the α-particle. If this is the case, stored energy from ionization damage associated with β-decay could saturate in 30 yr. Stored energy data on neutron-irradiated waste glasses (Roberts *et al.*, 1976; Antonini *et al.*, 1980; Cousens and Myhra, 1983) are in good agreement with the results in Fig. 8. No data are available on stored energy release in γ- or electron-irradiated glasses to evaluate the role of ionization in the absence of significant displacive energy deposition.

The stored energy in actinide-doped simulated waste glasses is released over a broad temperature range from 100 to 600°C (Roberts *et al.*, 1976; Weber and Roberts, 1983). Since the specific heat of the nuclear waste glasses is of the order of 1 J $(g \cdot K)^{-1}$, the maximum temperature rise that could occur from the rapid release of this stored energy is only 50–125 K. Temperature excursions of this magnitude should

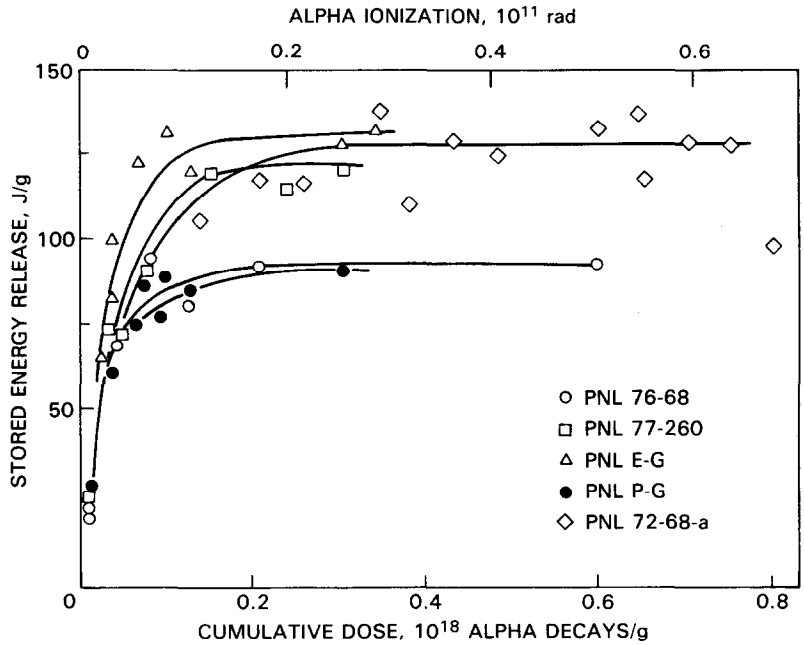

Fig. 8. Stored energy, measured by differential scanning calorimetry, as a function of dose in ^{244}Cm-doped simulated nuclear waste glasses. After Weber and Roberts (1983).

present no serious problems. Furthermore, the results of Roberts *et al.* (1976) indicate that the stored energy decreases almost linearly with increasing storage temperature. Thermal recovery of the stored energy in the PNL glasses (Fig. 8) was investigated by 7-day isochronal anneals (Weber and Roberts, 1983). The results show a single recovery stage that is similar for all the waste glass compositions, with full recovery occurring at 360°C (Fig. 9). These results are similar to those of Roberts *et al.* (1976) for the effects of storage temperature.

4.3. *Transmutations*

Nuclear transmutation is the formation of a new chemical element as a result of nuclear reactions or radioactive decay processes. The principal source of transmutations in nuclear waste is β-decay of the relatively abundant fission products cesium and strontium. Transmutation of these two elements is accompanied by changes in both ionic radius and valence. Cesium (1+) decays to barium (2+) with a decrease in ionic radius of 20%, and strontium (2+) decays to yttrium (3+), which in turn decays to zirconium (4+) with a final ionic radius decrease of 29%. In an accelerated study of cesium to barium transmutation in five glasses and two ceramics, Gray (1982) found no significant effect of the transmutations on microstructure, chemical durability or density.

4.4. *Helium accumulation*

Helium, which results from the capture of two electrons by an α-particle, must be accommodated interstitially or substitutionally, diffuse to internal defects, or be released at the glass surface. Based on a number of studies (Hall *et al.*, 1976; Turcotte, 1976; Malow and Andresen, 1979; Malow *et al.*, 1980) in which helium diffusion and release in nuclear waste glasses were measured, it can be concluded that the helium generated will accumulate in the glass, and only a small fraction can be expected to be released at ambient temperatures. Observed decreases in diffusion coefficients with increasing dose (Turcotte, 1976; Malow and Andresen, 1979) suggest trapping of helium at radiation-induced defects. Low-level helium concentrations (up to 100 atomic parts per million, appm) introduced both by (n, α) reactions under neutron irradiation and by accelerator implantation have resulted in bubble formation in simulated nuclear waste glasses after post-irradiation annealing at 600°C in one case (Dé *et al.*, 1976a) and 750°C in another (Malow and Andresen, 1979). When higher helium concentrations (up to 10^4 appm) are introduced by (n, α) reactions, bubble formation was observed at

ambient irradiation temperatures (< 100°C) by Dé *et al.* (1976a) and at slightly elevated irradiation temperatures (< 230°C) by Sato *et al.* (1988). The exact nature of the bubbles was not determined in either case, but they are assumed to be helium or helium/oxygen bubbles. In a more recent study, Inagaki *et al.* (1992) observed bubble formation in ^{238}Pu- and ^{244}Cm-doped glasses as a result of α-decay. The change in glass density determined by observed bubble size and abundance correlated well with the measured change in density.

4.5. *Microstructural changes*

The principal radiation-induced changes in the microstructures of nuclear waste glasses are phase changes, phase separation, microfracturing and bubble formation. Thermally-induced devitrification (Jantzen *et al.*, 1984; Spilman *et al.*, 1986) and phase separation (Tomozawa *et al.*, 1979) in HLW glasses are well known. Radiation-enhanced devitrification of nuclear waste glasses has not been investigated to date. Phase separation has been induced in simulated waste glasses by electron-irradiation (DeNatale and Howitt, 1984 and 1985). Crystalline phases that often form in waste glasses from thermal devitrification during cooling and storage (additionally, crystalline phases form in the glass during solidification from the melt) can undergo a radiation-induced crystalline-to-amorphous transformation. In a study of a Cm-doped waste glass containing crystallites of $Ca_3(Gd, Cm)_7(SiO_4)_5(PO_4)O_2$ (apatite structure) and $(Gd, Cm)_2Ti_2O_7$ (pyrochlore structure), the differential expansion (5–8%) associated with the crystalline-to-amorphous transformation of these phases resulted in significant microfracturing as a result of radiation-induced differential volume changes as illustrated in Fig. 10 (Weber *et al.*, 1979; Weber and Roberts, 1983). The behavior of these two particular phases is discussed in detail in Sections 5.2.1. and 5.2.6. This radiation-induced microcracking can significantly increase the surface area for radionuclide release.

As noted above, helium implantation in waste glasses can result in the formation of helium bubbles. Oxygen bubbles can also form and were first observed by Hall *et al.* (1976) in simulated nuclear waste glasses irradiated with electrons in a high-voltage electron microscope at 200°C to simulate the effects of β-irradiation. Since then, irradiation-induced oxygen bubble formation has been observed by others in a wide variety of glasses as a result of electron-beam irradiations (Todd *et al.*, 1960; Manara *et al.*, 1982, 1984; Sato *et al.*, 1983; DeNatale and Howitt, 1984, 1985, 1987; Arnold, 1985; DeNatale *et al.*, 1986; Heuer, 1987; Heuer *et al.*, 1986), ion-beam irradiations

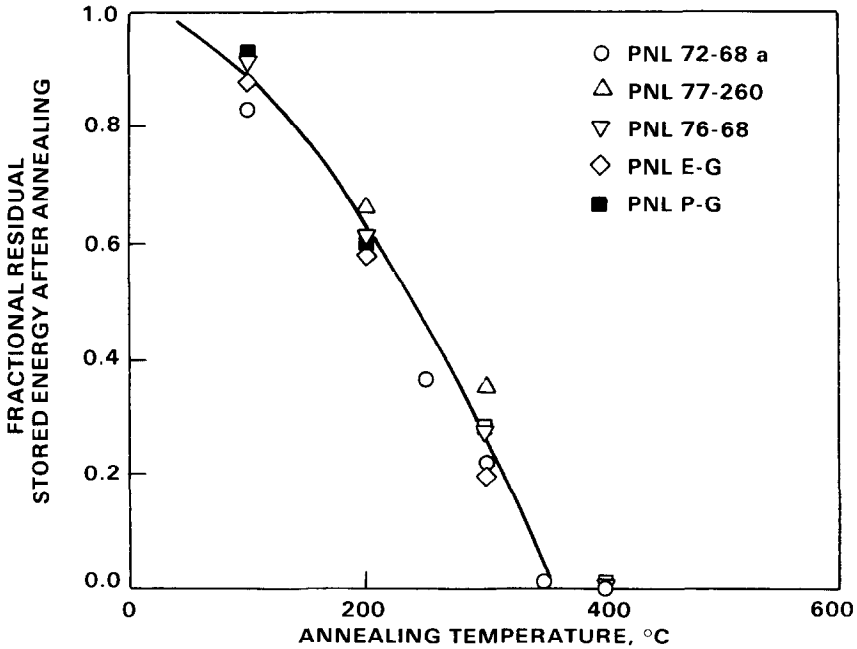

Fig. 9. Thermal recovery of stored energy in ^{244}Cm-doped simulated nuclear waste glasses. After Weber and Roberts (1983).

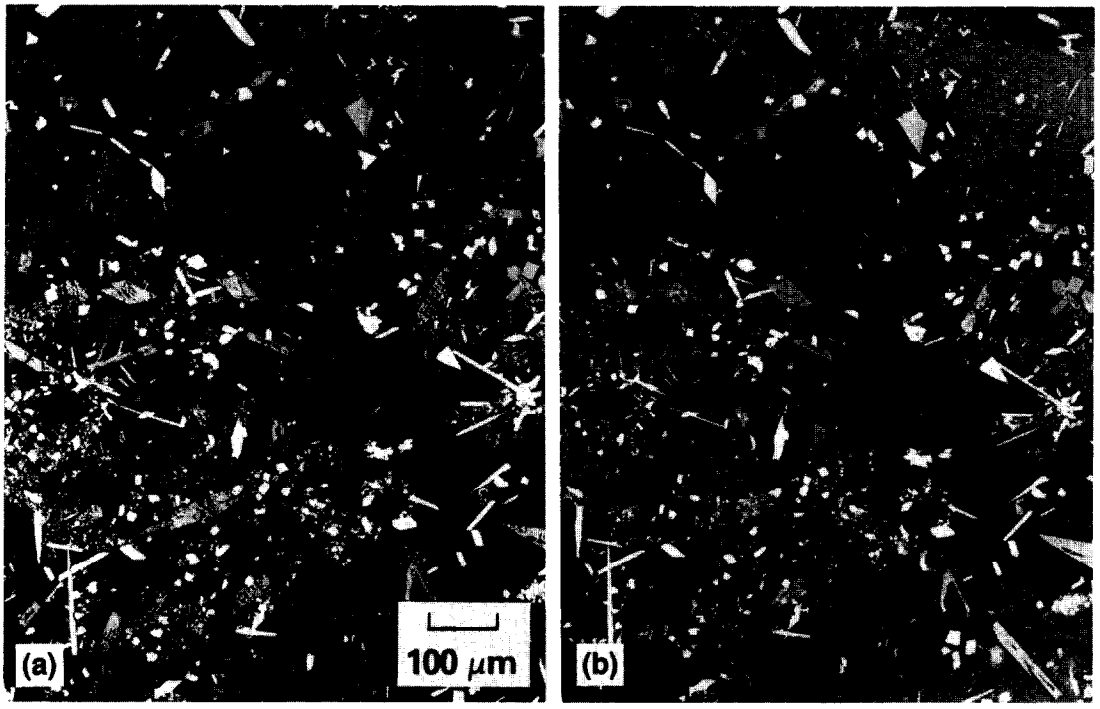

Fig. 10. Effect of radiation from alpha decay on microstructure in a HLW glass. (a) After 6×10^{15} α-decay events g^{-1}. (b) Microfracturing after 2.5×10^{17} α-decay events g^{-1}. After Weber *et al.* (1979).

(DeNatale *et al.*, 1986; DeNatale and Howitt, 1987; Heuer, 1987), and γ-irradiations (DeNatale and Howitt, 1985, 1987; Heuer, 1987; Howitt *et al.*, 1991). The presence of a gas phase in the bubbles has been confirmed in the studies by Hall *et al.* (1976) and Heuer *et al.* (1987). The formation of oxygen bubbles, which results from radiolytic decomposition, has been correlated with the ionization component of energy deposition and not the ballistic (atomic displacement) component (DeNatale *et al.*, 1986), in agreement with the results of Arnold (1985, 1988). Consequently, ionization effects from α-, β- and γ-radiation are more important to nuclear waste glass behavior than originally assumed. Although high-resolution microstructural characterization was not performed in the early studies of actinide-doped nuclear waste glasses, Weber (1988, 1991a) postulated that similar bubble formation from α-particles emitted in actinide-doped nuclear waste glasses may occur and could account for the volume expansions observed in Figs 4–6. Recent results by Inagaki *et al.* (1992) confirm that bubbles, probably of He, with radii of 200–300 nm are formed as a result of α-decay in a ^{244}Cm- and ^{238}Pu-doped simulated nuclear waste glass and are primarily responsible for the measured volume expansion.

4.6. *Radiolytic decomposition*

The early emphasis of radiation effects studies in nuclear waste glasses on displacement damage has led to some misconceptions concerning waste glass stability. Although not originally anticipated, it is now evident that complex borosilicate glasses, including those proposed for the storage of nuclear wastes, can decompose by an ionization-driven radiolytic process that produces molecular oxygen and may lead to oxygen bubble formation as described above. The initial observation of oxygen bubble formation by Hall *et al.* (1976) did not create much concern because the electron dose required to produce the bubbles was quite high, 10^{12}–10^{13} rad, exceeding the dose equivalent to a million years of storage. Nearly 10 yr later, DeNatale and Howitt (1985) reported that gamma irradiation of simulated nuclear waste glasses at significantly lower doses (10^9 rad) will result in bubble formation; this observation was of significant relevance to nuclear waste glass behavior. Subsequent γ-irradiation studies (DeNatale and Howitt, 1987; Heuer, 1987; Howitt *et al.*, 1991) have concluded that oxygen bubbles form (Fig. 11) in a wide variety of glasses at low doses. However, in another study (Tosten, 1989; Biber *et al.*, 1990) of one of the same

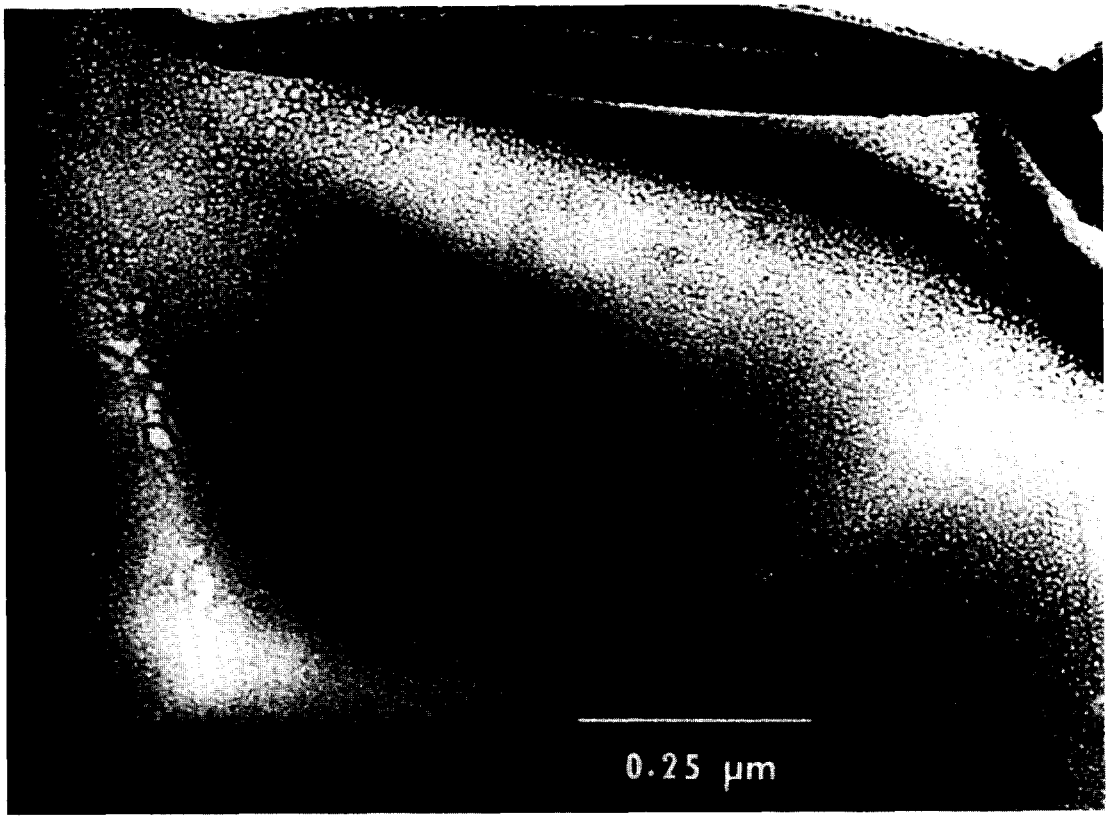

Fig. 11. Bubble formation in a simulated Savannah River Plant HLW glass gamma irradiated to 1.3×10^9 rad. Micrograph courtesy of J. P. Heuer and D. G. Howitt, University of California-Davis.

glass compositions, γ-irradiation-induced decomposition or bubble formation was not observed, even at an order of magnitude higher dose. These authors suggest that bubble formation in γ-irradiated glasses which were reported by others may be an artifact of sample preparation. Several quantitative studies have shown that the kinetics of the bubble formation process are consistent with the motion of alkali metal cations and not oxygen (DeNatale and Howitt, 1984; Laval and Westmacott, 1980). The formation of oxygen bubbles is apparently brought about by radiolytic decomposition of the ionic component of the glass, followed by the migration of the cations into the glass and the local precipitation of molecular oxygen (Howitt *et al.*, 1991). The bubbles observed in an actinide-doped simulated waste glass (Inagaki *et al.*, 1992) also may be produced by this mechanism, although the role of the helium (α-particles) and the composition of the bubbles (oxygen and/or helium) has not been established.

Irradiation studies of simulated waste glasses carried out by DeNatale and Howitt (1987) and Heuer (1987), utilizing γ-radiation, ion beams, and electron beams at similar temperatures, indicate a significant dose-rate effect for glass decomposition and subsequent bubble formation (Fig. 12). Decomposition under γ-irradiation occurs at much lower doses than for either ion- or electron-irradiations. The process for

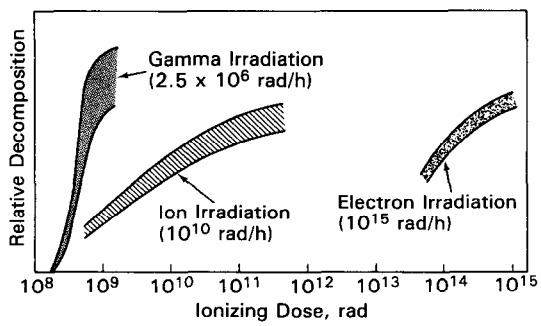

Fig. 12. Dose and dose rate dependence of ionization-induced bubble formation in simulated HLW glasses. Adapted from DeNatale and Howitt (1987) and Heuer (1987).

γ-induced decomposition under ambient conditions ($< 100°C$) has an onset at about 10^8 rad, saturates at 10^9 rad, and results in a uniform distribution of bubbles (Fig. 11) with an average diameter of 5–6 nm (Heuer, 1987). Under electron irradiation, bubble formation occurs over a broad temperature range with a maximum in the rate of formation at 250°C (DeNatale and Howitt, 1984; Heuer, 1987), as illustrated in Fig. 13. Similar behavior is reported by Manara *et al.* (1984) in electron-irradiated borosilicate glasses; however, the peak in bubble formation shifts with Na content. The temperature dependence of radiolytic decomposition and bubble formation under γ-irradiation has not been investigated (although DeNatale and Howitt (1985) reported enhanced bubble formation at 50°C), but given the strong dose-rate dependence in Fig. 12, a shift in the temperature dependence from that shown in Fig. 13 is expected.

The implications of these results may be more serious than other irradiation studies have suggested, as this radiolytic decomposition process, if operable, can be completed in relatively short time periods (< 10 yr) for actual nuclear waste glasses. In addition, the low-dose character of this effect underscores the need for a better understanding of the temperature dependence of this process, since the waste glasses will be exposed to elevated temperatures and temperature gradients during this time period. As noted above, two studies (Sato *et al.*, 1984; Manara *et al.*, 1984) have determined significant volume expansion (50%) from the size and density of observed bubbles. The swelling associated with this radiolytic process is sensitive to alkali content (Manara *et al.*, 1984) but cannot account for the decrease in the volume expansion with alkali content (Fig. 7). Concerns raised (Tosten, 1984; Bibler *et al.*, 1990) about whether radiolytic decomposition and bubble formation actually occur under γ-irradiation emphasize the need for a more fundamental understanding of this process in complex glasses.

4.7. *Mechanical properties*

In a recent study of a simulated nuclear waste glass doped with ^{238}Pu and ^{244}Cm, Inagaki *et al.* (1993) observed an exponential decrease in hardness and Young's modulus with dose, while the fracture toughness increased exponentially with dose. The maximum values of the relative changes reported for the hardness, Young's modulus, and fracture toughness in these glasses were -25%, -30% and $+45\%$, respectively. In the same study, the changes in hardness and Young's modulus completely recovered during annealing above 673 K with an activation energy of 0.28 eV; the recovery of the change in fracture toughness was initially more rapid, with an activation energy of 0.21 eV, then the rate of recovery slowed significantly, and complete recovery of the fracture toughness was never observed. The changes in fracture toughness are strongly correlated to the behavior of bubbles, which they observed previously in these

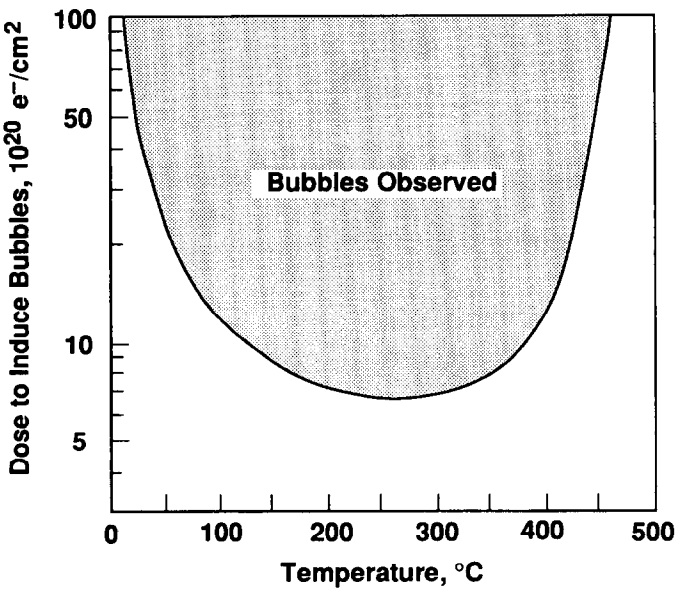

Fig. 13. Temperature dependence of the dose to induce bubble formation under electron irradiation in HLW glasses. Adapted from DeNatale and Howitt (1984) and Heuer (1987).

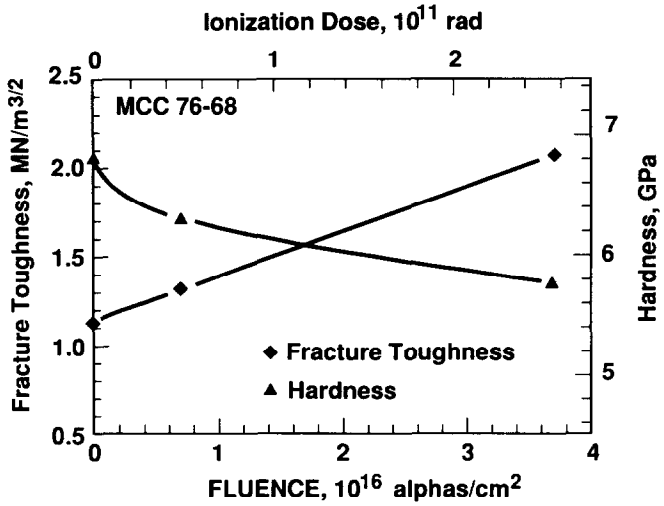

Fig. 14. Hardness and fracture toughness versus dose in an α-irradiated simulated HLW glass. After Weber and Matzke (1987).

glasses (Inagaki *et al.*, 1992). The bubbles, which can impede crack propagation, anneal with kinetics similar to the recovery of the fracture toughness.

A similar decrease in hardness (24%) was observed in an actinide-doped glass by Bonniaud *et al.* (1979). In a study of α-irradiated simulated waste glass (Weber and Matzke, 1987), the hardness decreased 15% and the fracture toughness increased 80% with dose (Fig. 14). In another study of α-irradiated waste glass (Routbort and Matzke, 1983), a 75% increase in fracture toughness was reported. These large increases in fracture toughness may also be associated with bubble formation; however, because the microstructural characterization was not completed, the presence and role of bubbles cannot be confirmed. Gamma-irradiation of a simulated nuclear waste glass to 6.6×10^8 rad indicates a slight decrease in elastic modulus and a slight increase in hardness and fracture toughness (Weber, 1988). In a study of a commercial borosilicate glass (Zdaniewski *et al.*, 1983), γ-radiation did not appreciably affect the strength or fracture toughness below 10^8 rad. The maximum doses in these studies are low; consequently, the effect of γ-radiation on mechanical properties is unknown for γ-doses equivalent to more than 1 yr of storage.

4.8. *Radionuclide release*

Radiation can affect the release rate of radionuclides from waste glasses by increasing the surface area for radionuclide release (microfracturing) and by changing the dissolution rate of the glass. The extent of the radiation-induced microfracturing will depend on differential volume changes, microstructure and mechanical properties. Presently, there are insufficient data and understanding currently available to predict the extent of radiation-induced microfracturing in waste glasses, except to note that it can be expected to occur, especially as a result of the radiation-induced differential expansion of the crystalline phases in the glass.

The dissolution rate of nuclear waste glasses may be affected by the radiation-induced changes in chemistry, microstructure and network bonding. As noted in several reviews (Turcotte, 1981; Burns *et al.*, 1982a,b; Weber and Roberts, 1983) and discussed in detail recently (Weber, 1988, 1991a), almost all data concerning the effects of α-decay on dissolution (leach) rates of waste glasses were determined prior to 1982 in short-term tests based solely on weight loss. The data obtained from these tests (Fig. 15) indicate no more than a factor of 3 increase in the short-term dissolution rates as a result of radiation effects from α-decay. It is now well-established that short-term tests based on weight loss can underestimate the radiation-induced increases in dissolution rate by a factor of 3–4 due to precipitation of alteration phases on the surface of the glass (Westsik and Harvey, 1981; Weber *et al.*, 1985a; Weber, 1988); consequently, based on this limited database, it has been suggested by Weber (1991a) that radiation effects are not expected to increase the nuclear waste glass dissolution rates by more than a factor of 10. Although this may overestimate (or even underestimate) the actual effects, it is the best assessment that can be drawn from the limited database and understanding that currently exists. This assessment is supported by a recent study by Eyal and Ewing (1993) of a Th-doped borosilicate glass, where the Th

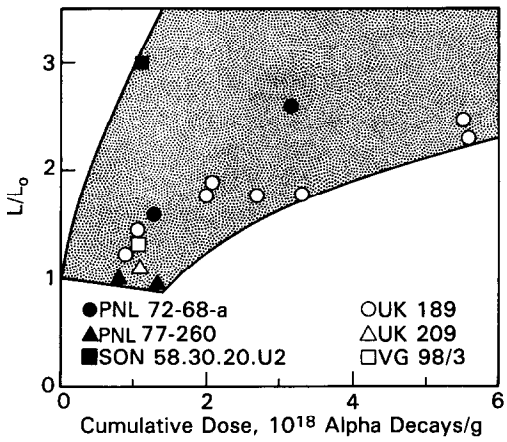

Fig. 15. Increased leaching (dissolution) factor, L/L_0, versus dose for short-term tests. After Weber (1988).

daughter product release rate was increased from 15 to 45% due to incongruent dissolution along the recoil tracks produced by the α-recoil nucleus.

Ion-irradiation (Manara *et al.*, 1982; Dran *et al.*, 1982; Primak, 1982) and neutron-irradiation (Cousens and Myhra, 1988) studies of several HLW glasses have shown irradiation-enhanced dissolution rates of up to a factor of 4. Another study (Arnold *et al.*, 1982) indicated no significant increase in dissolution rates. Ion irradiation, however, is known to introduce compositional variations (Arnold *et al.*, 1982), which affect the interpretation of the results. Gamma-irradiation of several HLW glasses up to doses of 10^{11} rad have lead to increased dissolution rates of up to a factor of 4 (Grover, 1973; Bibler, 1982). In another study (Bibler *et al.*, 1990), where radiolytic decomposition was confirmed not to occur, γ-irradiation to 3.1×10^{10} rad did not result in any measurable increase in the leach rate. The effect of radiolytic decomposition on dissolution rates remains unclear, because it has not been determined whether radiolytic decomposition occurred in the glasses for which increased dissolution rates have been measured.

In summary, depending on the type of corrosion model used for waste glass dissolution, the radiation-enhanced radionuclide release rates may be expected to increase in proportion to the increase in surface area (due to microfracturing). The actual release rate will depend on geochemical conditions (e.g. presence or absence of silica-saturated solutions). Additionally, in the absence of careful studies, a conservative factor of approximately 10 is estimated for the enhanced dissolution rate due to radiation-induced changes in the atomic structure of the glass (e.g. Eyal and Ewing, 1993). Any temperature dependence of the radiation effects could further affect this enhancement.

5. RADIATION EFFECTS IN CRYSTALLINE WASTE FORMS

5.1. *Multiphase ceramic waste forms*

As alternatives to nuclear waste glasses, several multi-phase, crystalline ceramic waste forms have been proposed that are tailored to produce specific crystalline phases as hosts for the different radionuclides. Generally, fission products (such as cesium and strontium) are confined to one or more crystalline phases, and the actinides (uranium, neptunium, plutonium, americium and curium) partition into other crystalline phases. Synroc and other related titanate-based ceramic waste forms have received the most attention (Ringwood *et al.*, 1979, 1981; Ringwood, 1982; Kesson *et al.*, 1983; Newkirk *et al.*, 1982). There has been more limited study of radiation effects in supercalcine, a silicate-based, tailored ceramic (McCarthy, 1977; McCarthy *et al.*, 1979) and glass-ceramics (Dé *et al.*, 1976a,b). There have been far fewer studies of radiation effects in the bulk crystalline ceramic waste forms as compared to glass waste forms. Details of the more extensive studies of radiation effects in component phases are presented in Section 5.2.

5.1.1. *Synroc.* Ringwood *et al.* (1980) have argued that Synroc is stable with respect to α-decay damage, based on an assessment of natural minerals of uranium and/or thorium-bearing perovskite and zirconolite, which are the actinide host phases of Synroc. Such data can provide only qualitative results, as natural and actinide-doped zirconolites do become amorphous. The rate of amorphization and subsequent changes in physical and chemical properties may vary with modifications in composition. Therefore, quantitative evaluation of Synroc as a waste form requires radiation-damage testing of actual or simulated waste forms.

In the early 1980s, a limited amount of accelerated irradiation-damage testing was performed on Synroc and its constituent phases by Reeve *et al.* (1981) and Woolfrey *et al.* (1982) using fast neutrons. Cold-pressed and sintered (cps) and hot pressed (hp) specimens of Synroc B and Synroc C, as well as cps specimens of their constituent minerals hollandite, perovskite and zirconolite, were irradiated in the fast-neutron flux of the HIFAR reactor at Lucas Heights, for different lengths of time. (Synroc B does not incorporate simulated fission products; Synroc C

does.) The largest dose reported on the Synroc specimens (10 wt% waste loading) was 2.7×10^{26} n m^{-2} ($E > 1$ MeV), which corresponds to 0.7 dpa or 8×10^{18} α-decays g^{-1} and represents an equivalent Synroc storage time of 6.5×10^5 yr. Volume, density, open porosity and unit cell parameter changes were measured. The volume expansion of Synroc specimens was generally larger than that of the separately irradiated specimens of the constituent phases. In addition, the results show that the volume expansion is much larger for the Synroc-B (cps) than for the Synroc-B (hp). The volume changes in Synroc-C are similar for both hp and cps specimens. The macroscopic volume expansion results for Synroc-C (hp) are included in Fig. 16 (the neutron dose has been converted to an equivalent α-decay dose). Based on these data, volume expansion at saturation cannot be predicted.

Accelerated testing of Synroc-C and its constituent phases has been completed using actinide-doping techniques at Harwell (Evans and Marples, 1985; Evans *et al.*, 1986). The radiation stability of hot-pressed Synroc specimens doped with 2 and 5 wt% ^{238}Pu was investigated. X-ray diffraction analysis indicated that the Pu-containing zirconolite and perovskite phases were X-ray diffraction amorphous after a bulk average dose corresponding to 2.8×10^{18} α-decay events g^{-1} (estimated to be 0.37 dpa in the zirconolite and perovskite phases), which is equivalent to a Synroc age of approximately 10^4 yr for a 10 wt% waste loading. The macroscopic volume expansion (Fig. 16) was determined from the change in density (Weber, 1990). The swelling exceeds 6% and shows only a slight indication of approaching a steady-state (saturation) value. The swelling of the Pu-doped Synroc-C occurs at about twice the rate as the equivalent neutron-irradiated Synroc-C. This may be due to the relatively simple assumptions made by Woolfrey *et al.* (1982) in estimating the equivalent α-decay dose for the measured neutron dose or may indicate that neutron irradiation does not produce the same radiation damage effects.

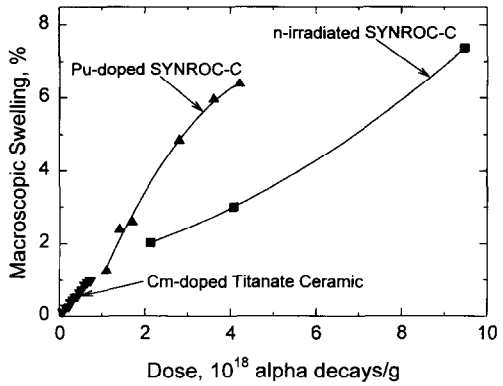

Fig. 16. Microscopic volume expansion in Pu-doped (Evans *et al.*, 1986) and neutron irradiated SYNROC-C (Reeve *et al.*, 1981; Woolfrey *et al.*, 1982), and a Cm-doped titanate ceramic (Mitamara *et al.*, 1990).

5.1.2. *Titanate ceramics*

The Japanese have investigated a titanate ceramic consisting of perovskite, zirconolite, hollandite, freudenbergite and loveringite for encapsulation of sodium-rich high-level waste. This titanate ceramic was doped with 0.69 wt% ^{244}Cm, and the effects of α-decay on density and dissolution rate were investigated (Mitamura *et al.*, 1990). The density decreased linearly with dose. The volume change was +1.0% after a dose of 0.7×10^{18} α-decays g^{-1} (Fig. 16), which was the maximum dose reached. The release rates measured for Cm and soluble non-radioactive elements (e.g. Na, Cs, Sr and Ca) showed a general trend of increase with increasing dose. The maximum dose reached was relatively low compared to those in other studies, corresponding to a storage time of 5000 yr.

Sandia National Laboratories investigated a titanate ceramic to immobilize acidic high-level nuclear waste. This titanate ceramic is a multi-phase assemblage that consists of rutile (TiO_2), an amorphous silicate phase, perovskite, zirconolite, hollandite and a U–Zr-rich phase believed to have a pyrochlore structure (Dosch *et al.*, 1984). Radiation effects from α-decay have been simulated by irradiating TEM specimens with Pb^+ ions (Dosch *et al.*, 1985). Multiple energies (40–250 keV) were used to produce a uniform damage profile. Irradiation at single energies of 240–250 keV were also performed. Examination by transmission electron microscopy of the irradiated specimens indicated considerable damage in all phases after a dose equivalent to 1×10^{19} α-decay events cm^{-3}. All phases remained crystalline except a phase with a chemistry typical of a pyrochlore, which became amorphous.

5.1.3. *Supercalcine.* The only radiation damage study that has been performed on a supercalcine formulation (SPC-2) was carried out at the Pacific Northwest Laboratory (Rusin *et al.*, 1979; Turcotte *et al.*, 1982). The SPC-2 formulation was doped with 2 wt% ^{244}Cm. Stored energy, X-ray diffraction analysis, and density measurements were made initially and at 3-month intervals, reaching a total bulk dose of 1.2×10^{18} α-decay events g^{-1}. Initial characterization

showed the supercalcine consisted of three major phases: fluorite, apatite and a tetragonal phase. Subsequent analysis suggested that curium predominantly partitioned into the apatite and the tetragonal phase.

Analysis by X-ray diffraction of the Cm-doped supercalcine, as a function of dose, showed a gradual transformation of the apatite from the crystalline to amorphous state, in agreement with the results of Weber *et al.* (1979) on the amorphization of apatite crystallites in a nuclear waste glass. An expansion in the unit cell of apatite was also observed with increasing dose; the increase in unit cell volume saturated at 2.5%. There was a slight increase in the intensity of the diffraction maxima associated with the tetragonal phase, but changes in the tetragonal unit cell could not be determined. The fluorite peak was used as a standard, as this phase did not appear to contain Cm and was unaffected by external radiation.

Stored energy and density measurements were also made as a function of dose for the Cm-doped supercalcine. The stored energy reached a maximum value of 42 J g^{-1} at a dose of 0.5×10^{18} α-decay events g^{-1} and decreased slightly with further increases in dose. Energy release was not complete at 600°C (the upper limit of the calorimeter used); therefore, additional energy release may occur at higher temperatures (> 600°C). The density decreased exponentially with dose, resulting in a volume expansion of 1.4% at a dose of 1.2×10^{18} α-decay events g^{-1}. The macroscopic swelling as a function of dose in SPC-2 is shown in Fig. 17. The volume expansion at saturation (1.4%) is partially attributed to the volume expansion in the apatite as a result of radiation-induced amorphization.

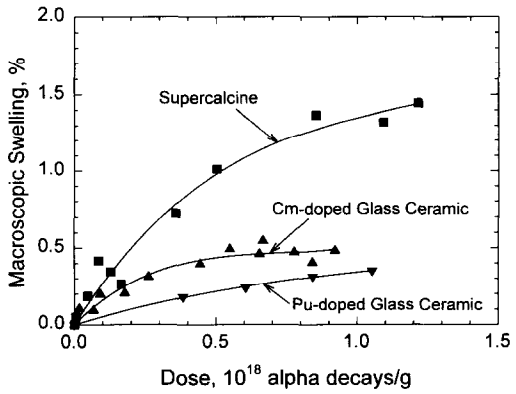

Fig. 17. Volume changes in Cm-doped supercalcine, celsian glass ceramic (Turcotte *et al.*, 1982), and Pu-doped celsian glass ceramic (Malow *et al.*, 1980).

5.1.4. *Glass-ceramics.* A glass-ceramic is a fine-grained mixture of glass and ceramic phase ideally derived from a homogeneous glass by heat-treating a glass precursor at the temperature of maximum nucleation rate for the ceramic phases(s), followed by a high-temperature treatment to yield a maximum growth rate. The celsian glass ceramic, developed at the Hahn-Meitner Institut and named for the predominant crystalline phase, is easy to fabricate, is homogeneously crystallized, and contains a variety of leach-resistant host phases for the radionuclides. Celsian glass-ceramic as a waste form has been studied for potential radiation effects both at the Pacific Northwest Laboratory (Turcotte *et al.*, 1982) in cooperation with the Hahn-Meitner Institut, and as part of a collaborative research program within the European Community (Malow *et al.*, 1980). In the study at PNL, the effects of radiation damage in ^{244}Cm-doped celsian glass-ceramic were investigated. The density was observed to decrease exponentially to saturation values at a dose of 0.9×10^{18} α-decay events g^{-1}. As shown in Fig. 17, the volume expansion at saturation was 0.5%. Stored energy also increased exponentially with dose to a value of 80 J g^{-1}. Data from the X-ray diffraction analysis revealed that a Cm-rich, rare-earth titanate phase with the pyrochlore structure underwent a small volume expansion with dose and eventually became X-ray diffraction amorphous at the same saturation dose of 0.9×10^{18} α-decay events g^{-1}. In the study by Malow *et al.* (1980), the celsian glass ceramic was doped with 2.5 wt% ^{238}Pu. The volume also expanded exponentially with dose, as shown in Fig. 17. Saturation is predicted at a dose of 1.6×10^{18} α-decay events g^{-1}, with a corresponding volume expansion of 0.5%, in good agreement with the PNL results. The stored energy was measured to be 43 ± 5 J g^{-1} after a dose of 1.1×10^{19} α-decay events g^{-1}. This is approximately half the value determined at PNL, but it is not known whether saturation was reached in this material. Changes in leach rates were measured for specimens stored at 23 and 170°C to a cumulative dose of 1.1×10^{18} α-decay events g^{-1}. The leach rate decreased by 4% in the specimen stored at 170°C. The fractional helium release was also determined to be 3% after storage at 170°C to a cumulative dose of 1.1×10^{18} α-decay events g^{-1}.

5.2. *Crystalline phases*

There have been a number of studies of individual synthetic phases and minerals that are structurally and/or chemically analogous to phases found in multiphase ceramic waste forms. These studies contri-

bute significantly to the understanding of radiation effects in the multiphase ceramic waste forms by providing a detailed understanding of the behavior of each component phase. The effects of radiation on the most important phases are summarized. Two of the phases to be discussed, pyrochlore and apatite, have also been observed as crystalline phases in nuclear waste glasses.

5.2.1. *Pyrochlores.* Pyrochlore (*Fd3m*, $Z=8$), $^{VIII}A_2{}^{VI}B_2{}^{IV}X_6{}^{IV}Y$ is a derivative of the fluorite structure type (Chakoumakos 1984, 1986) in which the A-site contains large cations (Na, Ca, U, Th, Y and lanthanides) and the B-site consists of smaller, higher valence cations (Nb, Ta, Ti, Zr, Fe^{3+}). The essential feature of the structure is sheets of corner-sharing, BX^6 octahedra parallel to the (111) plane which are arranged into three- and six-membered rings (the hexagonal tungsten bronze structure). Actinides may be accommodated in the A-site, and charge balance is maintained by cation deficiencies in the A-site and substitutions on the B-site. Rare-earth titanates with the pyrochlore structure have been observed as actinide-host phases in nuclear waste glasses (Weber *et al.*, 1979), in titanate ceramic waste forms (Dosch *et al.*, 1984), and in a glass ceramic waste form (Malow *et al.*, 1980; Turcotte *et al.*, 1982). In addition, the rare-earth titanates with the pyrochlore structure are chemically and structurally related to zirconolite, an important actinide host phase in Synroc and titanate ceramic waste forms.

In Cm-doped nuclear waste glass (Weber and Roberts, 1983), crystallites of the pyrochlore $(Gd, Cm)_2Ti_2O_7$ transformed from a crystalline to an amorphous state as a result of α-decay of the incorporated Cm. The volume expansion associated with the amorphous transformation of this pyrochlore phase and an apatite phase resulted in microfracturing of the simulated waste glass. Similarly, in a study of a Cm-doped celsian glass ceramic (Turcotte *et al.*, 1982), the originally crystalline pyrochlore phase, $(Nd_{0.85}Cm_{0.15})_2(Ti_{1.65}Zr_{0.35})O_7$, transformed to the amorphous state due to self-radiation damage from α-decay. The unit cell volume was estimated to expand 0.8% before amorphization was complete. Dosch *et al.* (1985) reported that the pyrochlore phase in a titanate ceramic waste transformed to an amorphous state as a result of irradiation with Pb^+ ions. More specific details of the amorphization process could not be obtained from the study of these multiphase waste forms.

The effect of α-decay on the pyrochlore phase $Gd_2Ti_2O_7$ doped with ^{244}Cm has been extensively

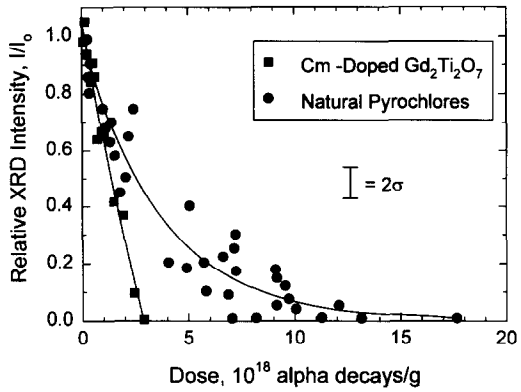

Fig. 18. Relative diffracted X-ray intensity as a function of cumulative dose for Cm-doped $Gd_2Ti_2O_7$ (Weber *et al.*, 1986) and for natural minerals of the pyrochlore group (Lumpkin and Ewing, 1988).

investigated (Weber *et al.*, 1985b, 1986). The decrease in diffracted X-ray intensity with increasing dose is shown in Fig. 18 for Cm-doped $Gd_2Ti_2O_7$ (Weber *et al.*, 1986) and for minerals of the pyrochlore group (Lumpkin and Ewing, 1988). The progression of the amorphization process in Cm-doped $Gd_2Ti_2O_7$ was also followed by transmission electron microscopy and selected area electron diffraction (Fig. 19). At a low dose of 0.6×10^{18} α-decays g^{-1} the material exhibits a strongly crystalline electron diffraction pattern and clearly resolvable individual defects and fission tracks. At increasing dose levels, the density of radiation-induced defects increases to the point that individual defect clusters are no longer readily distinguished and a radial ring of diffuse intensity associated with the presence of amorphous material is observed in the electron diffraction pattern. At higher doses, the material is nearly fully amorphous with some residual crystallinity evident in the electron diffraction pattern. At a dose of 3.1×10^{18} α-decay events g^{-1}, the material becomes fully amorphous with no evidence of any residual crystallinity.

The macroscopic swelling, $\Delta V_m/V_0$, of Cm-doped $Gd_2Ti_2O_7$ is shown in Fig. 20 as a function of dose, D, and follows an exponential relationship given by the expression:

$$\Delta V_m/V_0 = A_m[1-\exp(-B_mD)], \qquad (2)$$

where A_m is the swelling at saturation, and B_m is the amount of material damaged per α-decay event. The values of A_m and B_m have been determined to be 5.1% and 6.8×10^{-19} g, respectively (Weber *et al.*, 1985b, 1986).

Wald and Weber (1984) studied the radiation-induced changes in dissolution kinetics of Cm-doped

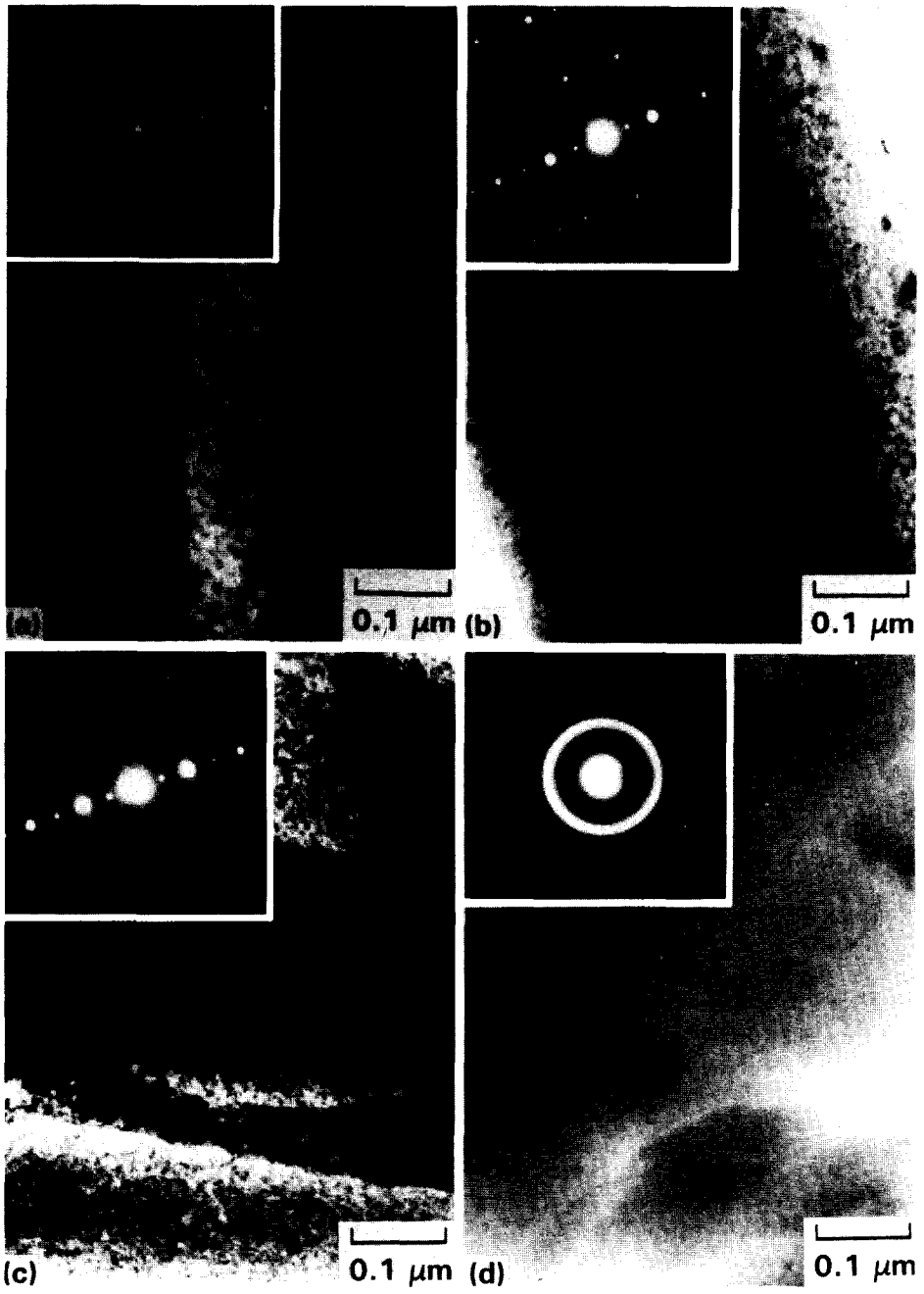

Fig. 19. Microstructural changes in Cm-doped $Gd_2Ti_2O_7$ at (a) 0.6×10^{18} α-decay events g^{-1}, (b) 1.0×10^{18} α-decay events g^{-1}, (c) 2.0×10^{18} α-decay events g^{-1}, and (d) 3.1×10^{18} α-decay events g^{-1} (Weber *et al.*, 1986).

$Gd_2Ti_2O_7$ by testing fully-damaged (amorphized specimens and a second set of specimens that had been fully recrystallized to the original structure by a 12 hr anneal at 1100°C). Specimens were immersed in distilled, deionized water at 90°C for 14 days. Weight loss measurements indicated an increase in dissolution rate of a factor of 2.5 as a result of the radiation-induced swelling and amorphization. More accurate

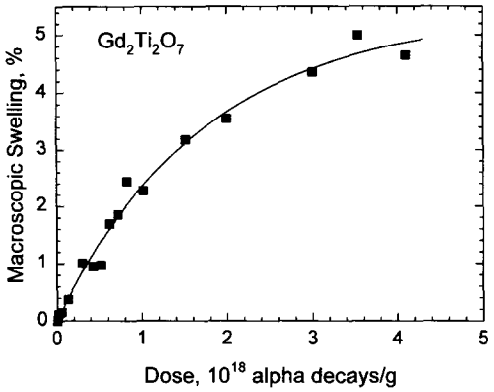

Fig. 20. Macroscopic swelling of Cm-doped $Gd_2Ti_2O_7$ as a function of cumulative dose. After Weber *et al.* (1985b).

radiochemical analysis indicated a radiation-induced increase of a factor of 20–50 in the dissolution rates of the non-network (TiO_6 octahedra form the network) Cm and Pu. The concentration of Ti in solution was below the detection limit of the inductively coupled plasma emission spectroscopy system, suggesting some dissolution resistance of the titania network. Analysis for non-network Gd was not performed. These results suggest that the dissolution may occur incongruently, selectively leaching the non-network ions. Similar behavior is observed for zirconolite (Wald and Weber, 1984). The increase in dissolution rate due to amorphization is probably due to the increase in the size of the network tunnels as the structure disorders and expands.

The fracture toughness in Cm-doped $Gd_2Ti_2O_7$ increased with cumulative dose to a broad maximum and then decreased slightly (Fig. 21). This is similar to the behavior of zirconolite (Clinard *et al.*, 1985a; Weber *et al.*, 1986) and apatite (Weber and Matzke,

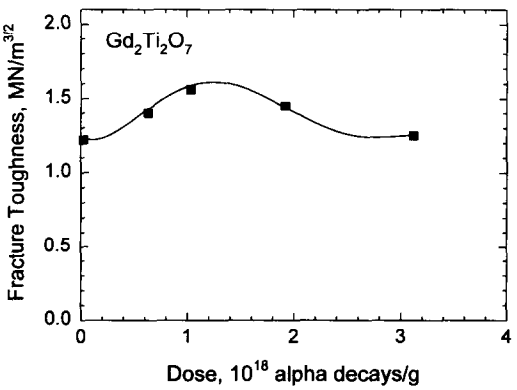

Fig. 21. Fracture toughness of Cm-doped $Gd_2Ti_2O_7$ as a function of cumulative dose. After Weber *et al.* (1986).

1986b). The increase in fracture toughness is attributed to the composite nature of the microstructure. At low to intermediate doses, the microstructure consists of amorphous tracks in a crystalline matrix, and this composite microstructure can inhibit crack propagation and increase the fracture toughness. As the amorphous phase becomes the dominant matrix at high doses with remnant crystallites, the fracture toughness decreases slightly as some of the internal stresses are relieved. This is supported by the observations of zirconolite that suggest a relaxation of disorder at high doses (Foltyn *et al.*, 1985) and the analysis of strain accumulation in natural pyrochlores (Lumpkin and Ewing, 1988).

Isochronal (12 h) annealing of fully amorphous Cm-doped $Gd_2Ti_2O_7$ shows a linear recovery of density with temperature up to the temperature where recrystallization begins (700°C). Recrystallization results in a sharp recovery of the density with a peak in the recovery rate at 750°C. Full recovery of the density and recrystallization of the original pyrochlore structure are essentially complete at 850°C. Thermal recovery studies of natural minerals of the pyrochlore group indicate that recrystallization is an exothermic reaction that peaks in the temperature range from 650 to 700°C and releases 120–200 J g^{-1} of stored energy (Lumpkin *et al.*, 1986). The temperature range is in reasonable agreement with the isochronal recovery behavior of Cm-doped $Gd_2Ti_2O_7$, and the stored energy released is similar in magnitude to that released during recrystallization of zirconolite (Weber *et al.*, 1986; Foltyn *et al.*, 1985) and apatite (Weber, 1983).

Systematic studies (Lumpkin and Ewing, 1985, 1986, 1988; Lumpkin *et al.*, 1986, 1988) have been completed of α-decay event damage of natural, isometric pyrochlore structure types. Minerals of the pyrochlore group are among the common rare element accessory minerals occurring in a wide range of igneous rocks: carbonatites, nepheline syenite pegmatites and granitic pegmatites. Actinides may be accommodated in the A-site, and in natural pyrochlores the substitution of uranium can be extensive (up to 30 wt%). Charge balance is maintained by cation deficiencies in the A-site and substitutions on the B-site (typically, Nb, Ta and Ti). Natural pyrochlores are classified on the basis of their major B-site cations: microlite (Ta > Nb, Ti < 33 mol%); pyrochlore (Nb ≥ Ta, Ti < 33 mol%); betafite (Ti ≥ 33 mol%) (Hogarth, 1977). Most of the detailed work on radiation damage effects has been completed on microlite, in which the compositions may reach values as high as 30 wt% UO_2 and 5 wt% ThO_2. Depending on the age of the sample, the total calculated dpa may be as high as 80. Careful analysis of samples from the

same deposit, e.g. the Harding pegmatite in New Mexico which is 1300 million years old, allows one to study radiation damage over a range of dpa (0.2–49) as a function of the uranium concentration (0.05–8.6 wt% UO_2). This provides a good analogue for long-term radiation damage effects in an actinide-bearing, crystalline waste form. In the remainder of this section, we summarize the results of such a study in which the periodic-to-aperiodic transition was characterized by X-ray diffraction (XRD) analysis, high-resolution transmission electron microscopy (HRTEM) and extended X-ray absorption spectroscopy (EXAFS) and X-ray absorption near edge spectroscopy (XANES) as a function of increasing α-decay event dose.

Figure 22 illustrates the change in the X-ray diffraction pattern of microlites as a function of increasing α-decay event dose. With increasing dose (#147, dpa = 0.2; #153, dpa = 49), the intensity of the diffraction maxima decreases and the peaks broaden, but not as quickly as in the actinide-doped material (Fig. 18). The positions of the diffraction maxima do not shift to lower values of 2Θ (as in the case of zircon when the unit cell volume increases) because, although unit cell expansion with increasing dose and the accumulation of defects is commonly observed, the

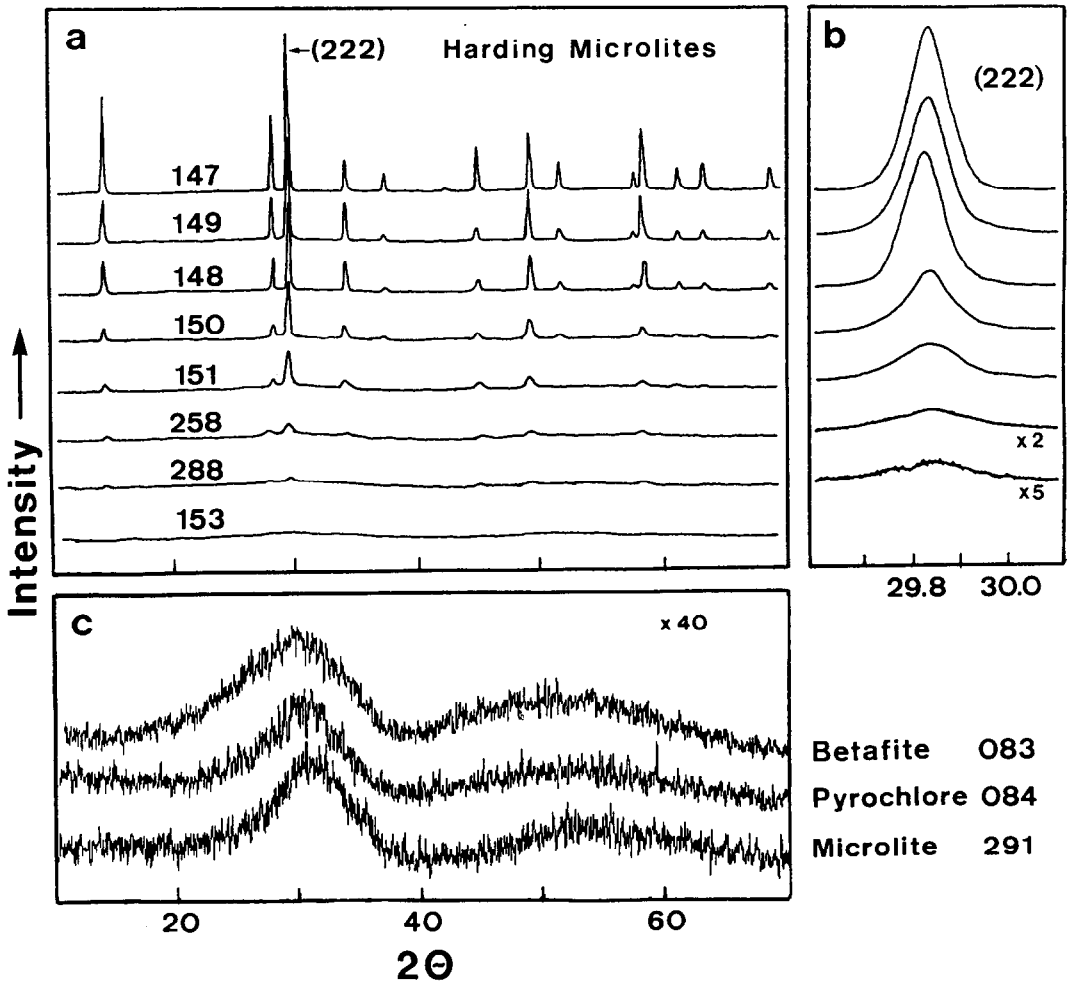

Fig. 22. X-ray powder diffraction patterns of pyrochlore group minerals. (a) Microlites from the Harding pegmatite, Taos County, New Mexico. D_c ($\tau_a = 100$ million yr) ranged from 0.014×10^{16} α-decay events mg^{-1} for sample #147 to 3×10^{16} α-decay events mg^{-1} for sample #153. (b) Peak profiles of the (222) diffraction maximum of the microlites. (c) Powder patterns of three fully metamict samples. $D_c = 5 \times 10^{16}$ α-decay events mg^{-1} for sample #083, 1×10^{16} α-decay events mg^{-1} for sample #084, and 1.5×10^{16} α-decay events mg^{-1} for sample #291. After Lumpkin and Ewing (1988).

increasing α-decay dose in natural pyrochlore is the result of the substitution of U for Ca and Na. The contraction of the unit cell due to the chemical substitution evidently compensates for the expansion of the unit cell due to radiation damage effects. Volume expansion has been well-documented in pyrochlores (Wald and Offerman, 1982) in which the composition remains constant. Debye–Scherrer patterns of microlite single crystals show, with increasing dose, loss of $K_{\alpha 1}$ and $K_{\alpha 2}$ peak splitting ($0.5–1.0 \times 10^{19}$ α-decay events g^{-1}), loss of back reflections ($1–5 \times 10^{19}$ α-decay events g^{-1}), and progressive loss of low angle peaks until none is discernible ($5–15 \times 10^{19}$ α-decay events g^{-1}). The Bragg diffraction maxima remain essentially symmetric throughout the transition from the crystalline to the metamict state. A detailed analysis (Karioris *et al.*, 1982) of the decrease in Bragg intensity can be used to estimate the amount of material damaged by each α-recoil (Lumpkin and Ewing, 1988). The calculated spherical diameter of an α-recoil track was estimated to be 4.6 nm, in good agreement with the value of 5.4 nm estimated by Clinard *et al.* (1985b) for Pu-doped zirconolite.

The X-ray line broadening was analysed using Williamson and Hall's technique (1953), which provides information on crystallite size and strain. The maximum strain reached is 0.003, halfway through the crystalline-to-metamict transition. Average crystallite dimensions decrease from approximately 450 nm to less than 15 nm just prior to the microlite becoming X-ray diffraction amorphous. This suggests that the early stage of damage accumulation is characterized by unit cell expansion and strain caused by isolated defects (predominantly due to α-particle damage). During the second stage, strain is reduced as the overlap of aperiodic regions (α-recoil tracks) increases. With the increase in the volume of the aperiodic domains, there is a reduction in the size of the crystallites that remain in the still crystalline regions. The slight rotation of these crystallites can contribute to the reduction in strain.

The results of the high-resolution transmission electron microscopy confirm the interpretation of the X-ray diffraction data (Fig. 23). High-resolution TEM images of highly crystalline samples recorded in the [110] orientation show variations in contrast resulting from the B_2X_6 framework and channels parallel to [110]. A typical image is shown in Figs 23(a,b). Most of the images (e.g. 23(c–g)) were taken in the (111) orientation, exhibiting 0.6 nm lattice fringes which probably result from the hexagonal tungsten bronze layer stacking parallel to (111). Some images also display 0.3 nm (222) lattice fringes. Effects of increasing U-content on the microstructure are illustrated by the series of HRTEM images in Fig. 23. The U-contents have been converted to a corrected dose assuming the mean life of an α-recoil track is of the order of 100 million years. The U-content and equivalent corrected dose (α-decay events mg^{-1}) for each image are given in the caption of Fig. 23. Three stages of damage are evident: (1) At an early stage of damage ($< 10^{18}$ α-decay events g^{-1}), lattice fringes are essentially continuous, but small variations in diffraction contrast suggest the presence of isolated defects. (2) At an intermediate stage of damage ($10^{18}–10^{19}$ α-decay events g^{-1}), lattice-fringe free areas indicate the increasing presence of aperiodic domains of α-recoil damage tracks. As the dose increases the proportion of aperiodic domains increases, and 'islands' of crystallinity decrease in size as the tracks increase in number and begin to overlap. (3) At the highest doses ($> 10^{19}$ α-decay events g^{-1}), no lattice fringes are apparent and the material is electron-diffraction amorphous. Electron diffraction maxima are absent, having been replaced by a diffuse, X-ray scattering halo.

Once long-range periodicity is lost, XRD and HRTEM techniques provide little insight into the results of further damage; however, spectroscopic techniques provide a powerful means of examining changes in the first and second coordination sphere geometries of the aperiodic material. In a series of studies, Greegor and colleagues (1984a,b, 1985a,b, 1986, 1987) applied EXAFS and XANES analysis to partially and fully-metamict members of $A_xB_yO_z$ oxides (e.g. AB_2O_6: euxenite, polycrase, priorite and blomstrandine; $A_2B_2O_7$: zirconolite; $A_{1-2}B_2O_6Y_{0-1}$ nH_2O; pyrochlore, microlite and betafite). Based on these results, which are summarized in Ewing *et al.* (1988), a good model of the structure of the metamict state is one in which there is: (1) a slight distortion of the nearest-neighbor coordination polyhedra; (2) a decrease in the coordination number and bond length in the primary coordination polyhedra; (3) a slight increase in the mean second nearest neighbor distances; (4) a loss of second nearest neighbor periodicity, probably due to the rotation of coordination polyhedra across shared corners and shared edges. The structure of Ta_2O_5, with its large cell volume and complex structure, is intermediate between the highly symmetric periodic pyrochlore structure and the aperiodic, metamict state; thus serving as a model for the aperiodic atomic arrangement of fully-damaged pyrochlore (Greegor *et al.*, 1987).

Lumpkin and Ewing (1988) have noted that if suites of pyrochlores (of different ages) are analyzed from single localities, the calculated dose for the crystalline-to-metamict transition increases with the age of the

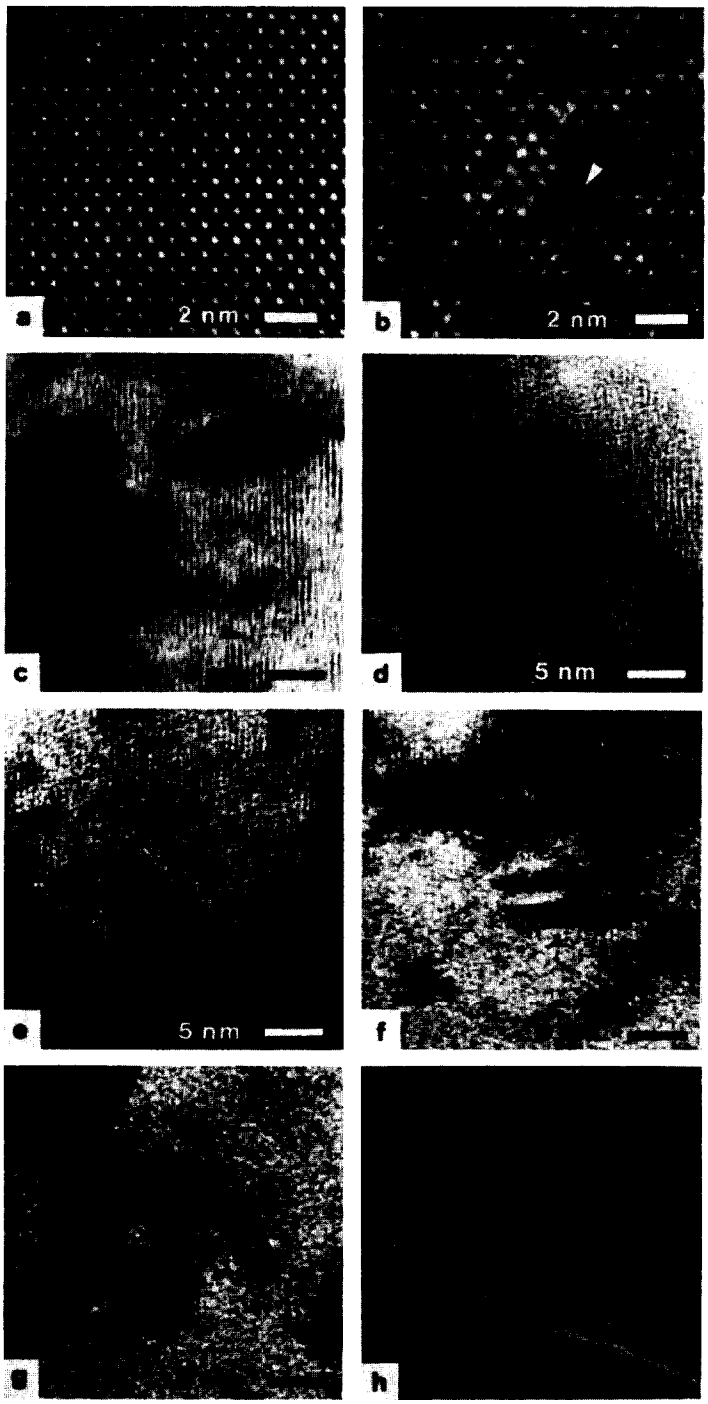

Fig. 23. HRTEM images of microlites from the Harding pegmatite arranged in order of increasing α-decay dose. (a) Sample #147, [110] image, $UO_2 = 0.05$, $D_c = 0.014 \times 10^{16}$ α-decay events mg^{-1}. (b) Sample #149, [110] image, $UO_2 = 0.9$, $D_c = 0.1 \times 10^{16}$ α-decay events mg^{-1}. (c–e) Sample #149, (111) lattice images. $UO_2 = 0.9$–1.5, $D_c = 0.1$–0.4×10^{16} α-decay events mg^{-1}. (f–g) Sample #288, (111) orientation. $UO_2 = 2.5$–2.9, $D_c = 0.7$–0.8×10^{16} α-decay events mg^{-1}. (h) Sample #288, fully-metamict, $UO_2 = 3.6$, $D_c = 1.2 \times 10^{16}$ α-decay events mg^{-1}. Arrows in (b) and (c) indicate possible α-recoil tracks (Lumpkin and Ewing, 1988).

geologic deposit (Fig. 24). This is clear evidence for the annealing of α-recoil damage over geologic time. The relationship between critical amorphization dose and geologic age was modeled assuming 'fading' of the α-recoil 'tracks' in a fashion similar to that used to describe fission fragment track fading. Critical parameters are the α-decay event dose, the age of the sample, the thermal history, and the mean life of an α-recoil track. The variation of dose as a function of age for natural pyrochlores can then be corrected by the consideration of recoil track annealing. Annealing under ambient conditions over long periods results in a higher *apparent* dose being required for amorphization. The actual dose versus time curves (Fig. 24) can be modeled by an exponential equation which considers the annealing to be described by the half-life of a recoil-track, τ_a, in the material (Lumpkin and Ewing, 1988). Figure 25 illustrates such a correction when the mean life of a track, τ_a, is assumed to be 100 million years. A similar analysis of data for zircon and zirconolite gave mean 'track' lives of 400 million years and 700 million years, respectively. This is in contrast to the mean lives determined by Eyal and coworkers using a differential etching technique to determine the mean life of damaged areas in monazite, UO_2, metamict betafite, thorite and metamict samarskite

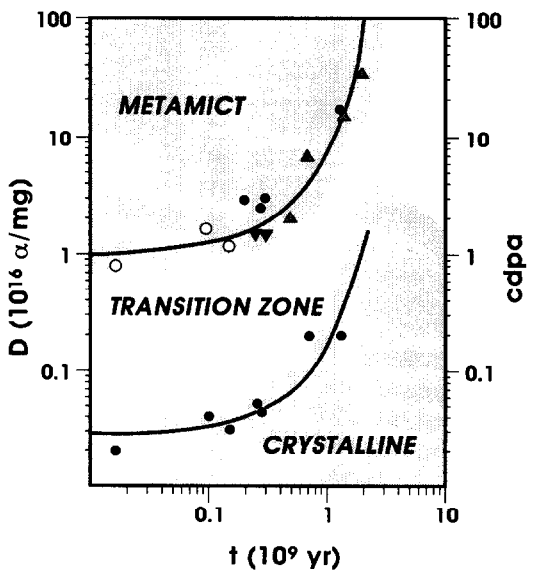

Fig. 24. Variation of dose as a function of age for natural pyrochlores. The upper curve and data represent the saturation dose estimated from slightly crystalline and metamict samples. The lower curve and data represent the onset of detectable α-decay damage defined by an XRD criterion of $I/I_0 = 0.8$–1.0. For a detailed explanation of the samples used and the symbols see Lumpkin and Ewing (1988).

(Eyal and Kaufman, 1982; Eyal and Fleischer, 1985; Eyal *et al.*, 1985, 1987; Lumpkin *et al.*, 1988). For phases which retain their crystallinity despite high α-decay event doses (> 10 dpa), the mean life of an α-recoil track was of the order of 10^4 yr. Thus, the natural samples provide clear evidence for annealing over geologic time under ambient conditions. The final state, crystalline or metamict, of the mineral depends on the mean life of the α-recoil track, a material dependent property.

One of the important issues with any waste form is the amount of stored energy associated with the radiation damage. For natural pyrochlores thermal recrystallization effects (measurement of the heat of recrystallization and identification of phases formed) have been determined on metamict members of the pyrochlore group which have received α-decay event doses of up to 4×10^{20} α-decay events g^{-1}. The heats of recrystallization range from 125 to 210 J g^{-1}. The temperature of the exotherm of recrystallization varies between 400 and 700°C; the exact temperature is determined by the sample composition (i.e. 400–600°C for pyrochlores and microlites; 650–700°C for betafites). Release of energy decreases as a function of the crystallinity (estimated on the basis of the intensity of X-ray diffraction maxima), with the fully-metamict samples approaching 200 J g^{-1}. Lower measured values (40–125 J g^{-1}) are the result of alteration of the pyrochlores. Other metamict, complex oxides with stoichiometries of ABO_4 and AB_2O_6 have lower heats of recrystallization (40–85 J g^{-1}) and are easily distinguished from pyrochlore group minerals. The recrystallization energies for the pyrochlore group minerals are consistently higher than those measured in synthetic, Pu-doped zirconolite (50 J g^{-1} at doses of 3×10^{16} α-decay events $mg^{-1} = 15 \times 10^{26}$ α-decay events m^{-3}), synthetic Cm-doped zirconolite (127 J g^{-1} at doses of 5×10^{18} α-decay events m^{-3}), and natural zirconolite (40–50 J g at doses of 2×10^{16} α-decay events $mg^{-1} = 1.0 \times 10^{26}$ α-decay events m^{-3}). Activation energies of recrystallization range between values of 0.29 and 0.97 eV, less than those measured for Pu-doped zirconolites (Foltyn *et al.*, 1985; Weber *et al.*, 1986).

5.2.2. *Zirconolite.* The waste form phase zirconolite (monoclinic $CaZrTi_2O_7$) is one of the three principal phases of Synroc, and zirconolite is one of the most extensively studied phases, as it is the primary actinide host. Monoclinic zirconolite is a fluorite-derivative structure closely related to pyrochlore. The (001) layers of the corner-sharing arrangement of TiO_6 octahedra are similar to the (111) layers in pyrochlore

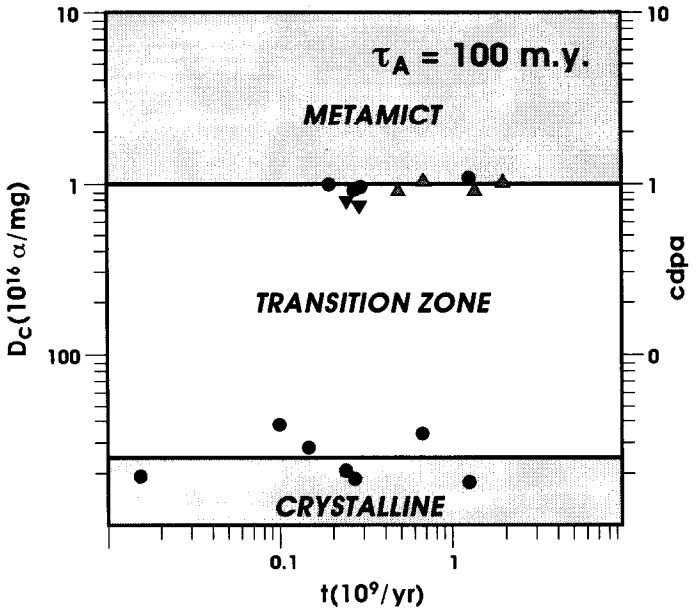

Fig. 25. Variation of dose as a function of age for natural pyrochlores after correcting for annealing of α-decay damage using a mean track life, τ_a, of 100 million yr. The upper line is the saturation dose and the lower line is the onset of α-decay damage detectable by XRD. The variable 'corrected displacements per atom' (cdpa) is equal to the dpa corrected for annealing (Lumpkin and Ewing, 1988).

and the (001) layers in the hexagonal tungsten bronzes. The A-site cations (Ca, Zr and actinides) are 'sandwiched' between the (001) sheets of B-site cations (corner-sharing TiO_6 octahedra). There can be several polytypes depending on the stacking arrangements of the sheets. In this section, we discuss the damage response as investigated by study of synthetic compositions doped with the short half-life actinides, ^{238}Pu (87.7 yr, α-decay to ^{234}U) and ^{244}Cm (18.1 yr, α-decay to ^{240}Pu), natural zirconolites damaged by α-decay of uranium and thorium, and finally ion-beam irradiated zirconolite.

5.2.2.1. ^{238}Pu-substituted zirconolite. A zirconolite ($CaPuTi_2O_7$) composition can be synthesized with the substitution of PuO_2 for ZrO_2. X-ray absorption spectroscopy demonstrated that the ^{238}Pu was incorporated into the A-site (Greegor *et al.*, 1988). The effect of this chemical substitution is to convert the zirconolite composition to an isometric, pyrochlore derivative structure (Clinard *et al.*, 1984). A major change in $CaPuTi_2O_7$ with increasing dose is the large decrease in density (Fig. 26). Storage at ambient temperature (approximately 350 K, due to self-heating) resulted in significant swelling, up to a saturation value of approximately 5.5 vol.% in material that had reached an α-decay dose of $2\text{–}3 \times 10^{25}$ α-decay events m^{-3} (for 200 days of storage time). Storage at 575 K results in less swelling, which required a longer time (300 days) to reach saturation. When this material was held at 875 K, swelling was minimal.

Transmission electron microscopy conducted after various storage times and temperatures (Clinard *et al.*, 1984) showed that with sufficient α-decay damage, Pu-zirconolite at 350 and 575 K converts from the crystalline to the aperiodic, metamict state. Shortly after the test material was fabricated, examination by transmission electron microscopy of the Pu-zirconolite at ambient temperature showed a typical crystalline diffraction pattern (Fig. 27). At intermediate states of damage, the microstructure consisted of a mixture of crystalline and aperiodic domains (Fig. 28). The observed microstructural heterogeneities are consistent with a random distribution of spherical damage tracks 5 nm in diameter, a microstructure that can be predicted from the shape of the corresponding swelling curve (Clinard, 1986). At high damage levels, electron diffraction patterns (Fig. 29) show full conversion from crystalline materials with sharp diffraction maxima to an inner correlation ring characteristic of the nearest neighbor interatomic spacing in an aperiodic structure.

Microhardness indentation studies indicated that as damage accumulated the zirconolite became softer (Fig. 33), yet fracture toughness increased (Fig. 34) (Clinard *et al.*, 1985a). The first of these changes is consistent with conversion to the metamict state, while

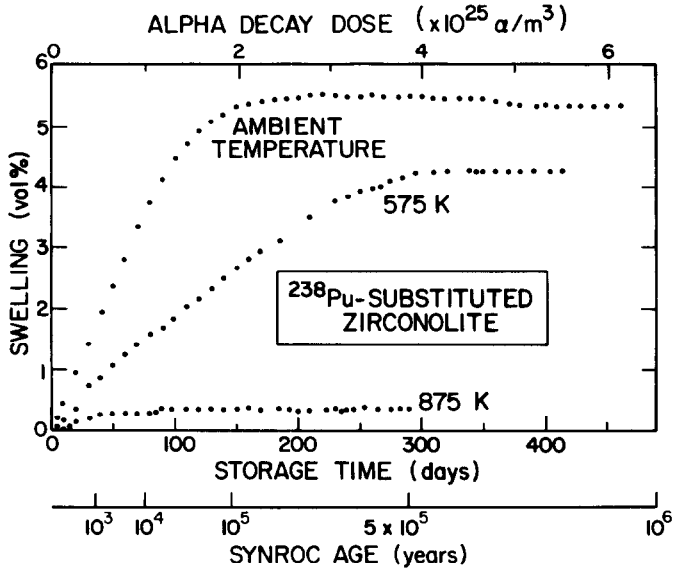

Fig. 26. Swelling of $CaPuTi_2O_7$ as a function of storage time, temperature and α-decay dose. Equivalent age for the SYNROC-C waste form containing 10 wt% commercial waste calcine is also shown (Clinard *et al.*, 1984).

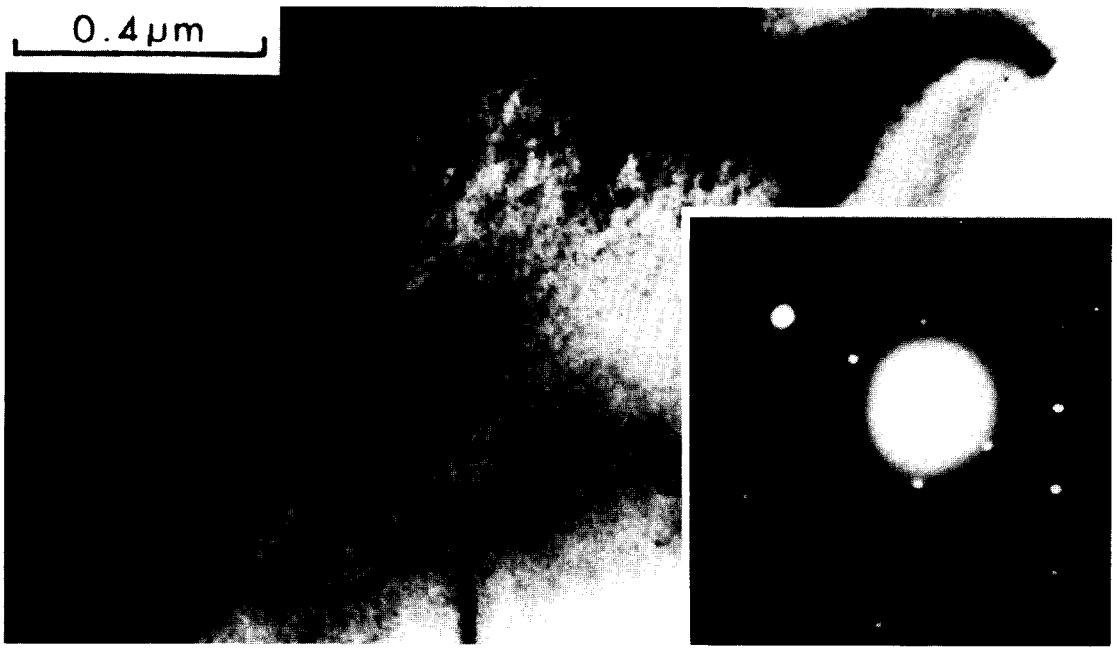

Fig. 27. Bright-field image and corresponding diffraction pattern from Pu-substituted zirconolite after 4 days storage near room temperature. The diffuse rings in the diffraction pattern are from the carbon substrate (Clinard *et al.*, 1984).

the latter was interpreted as resulting from the toughening effect of the two-phase microstructure (i.e. mixed periodic and aperiodic domains).

When the Pu-zirconolite which had been damaged at ambient temperature was heated to 875 K, the result was densification up to a value of 4 vol.% over a period of 400 days. Transmission electron microscopy confirmed that this recovery corresponded to recrystallization from the metamict state (Clinard *et al.*, 1985b). Differential scanning calorimetry measure-

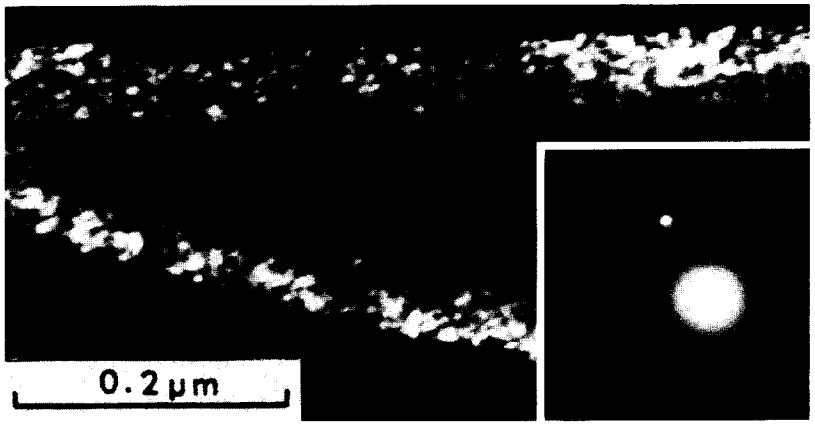

Fig. 28. Dark-field image and corresponding diffraction pattern from Pu-substituted zirconolite after 100 days storage near ambient temperature (Clinard *et al.*, 1984).

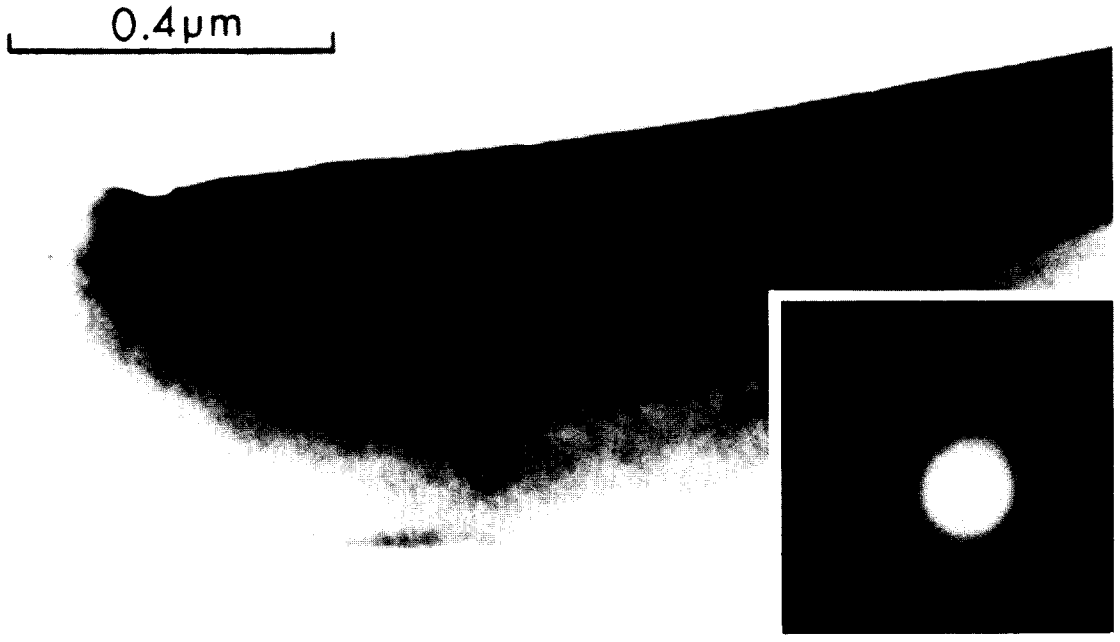

Fig. 29. Bright-field image and corresponding diffraction pattern from Pu-substituted zirconolite after 460 days near ambient temperature. Diffraction spots representative of crystalline material are no longer present (Clinard *et al.*, 1984).

ments (Foltyn *et al.*, 1985) showed that, as expected, recovery of metamict material to the crystalline state was an exothermic process. The amount of energy released initially increased with damage dose, but then peaked and subsequently decreased to about half the maximum value (Fig. 30). This suggests that redamage of previously-damaged material results in a reordering of the damage state to one of lower energy.

Modeling calculations (Fig. 31) were completed to determine the fraction of material that was undamaged, damaged by a single-track, and damaged by multiple overlap of tracks as a function of irradiation dose (Coghlan and Clinard, 1988). Comparison of Fig. 31 with Fig. 26 shows that swelling occurs under a constantly changing damage condition, not just with respect to the proportion of damaged and undamaged

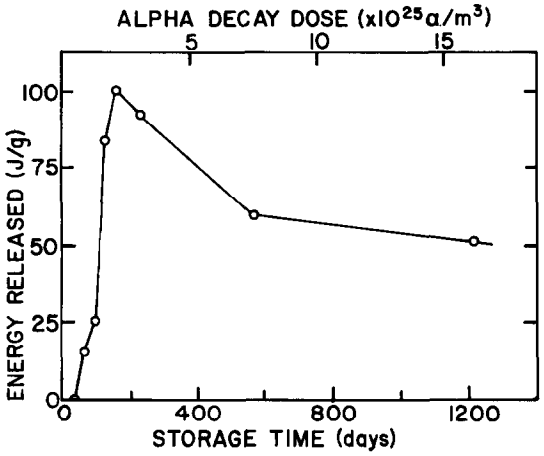

Fig. 30. Energy release from Pu-substituted zirconolite as a function of aging time and corresponding α-decay dose (Foltyn *et al.*, 1985).

material, but also with respect to the extent of redamaged material.

A comparison of stored energy and its corresponding damage state at different damage levels is shown in Table 2 (Coghlan and Clinard, 1988). The greatest amount of stored energy, 100 J g^{-1}, was measured in material that contained the largest fraction of single-track damaged material. At higher doses stored energy decreased (Table 2), although both the amount of redamaged material and the total amount damaged have increased. From these results, Coghlan and Clinard (1988) determined that the stored energy for the single track damaged condition is of the order of 200 J g^{-1}. Probable sources of the energy which is released on annealing of irradiation-damaged $CaPuTi_2O_7$ are: (1) the atomic disorder that is induced; (2) the accompanying strain that results from formation of aperiodic domains. An estimate was made of the maximum contribution from strain, 18%, (Klemens *et al.*, 1987); therefore, by difference, the decrease in stored energy can be primarily attributed to atomic-scale rearrangement of the aperiodic structure. The width of the inner correlation ring observed by TEM is another indication of the extent of disorder. Measurements of $CaPuTi_2O_7$ (Clinard, 1986) showed that this parameter varied with history of the test sample (Fig. 32). The greatest width of the inner correlation ring (diffuse scattering halo) resulted from material that was held for 460 days at 350 K. The extent of disorder decreased with irradiation; thus, it is not surprising that holding the material for 957 days caused a narrowing or sharpening of the correlation ring. Further sharpening was observed when the material was stored at 575 K for 430 days, or reheated to 875 K for a few days after being self-irradiated to the fully-redamaged aperiodic structure (625 days at 350 K). Thus, measurements of the inner correlation ring are consistent with the understanding of damage and redamage processes obtained by other techniques.

EXAFS/XANES studies completed on ^{238}Pu-substituted zirconolite held at 350 K for at least 500 days helped to identify details of the damage state (Greegor *et al.*, 1988). For comparison, measurements were made on essentially undamaged material (that is, substituted with ^{239}Pu with a half-life of 24,100 yr as compared to that of ^{238}Pu of 87.7 yr). In the heavily-damaged material, the Pu/O nearest neighbor bond length contracted by 0.003 nm, while expansion was observed for the more distant coordinating atoms, corresponding to a 6–7% overall volume expansion. This observation is close to the measured volume swelling of 5.5% (Fig. 26).

5.2.2.2. ^{244}Cm-doped zirconolite. Self-damage studies of zirconolite have also been carried out by doping with ^{244}Cm, an α-active isotope with a half-life of 18.1 yr. Weber *et al.* (1986) doped $CaZrTi_2O_7$ with 3 wt% ^{244}Cm and assessed changes in volume, microstructure, hardness, fracture toughness, leachability and recrystallization behavior. The Cm-doped zirconolite retained the monoclinic structure; whereas, the ^{238}Pu-doped zirconolite was isometric (although up to concentrations of 5 mol% PuO_2, the monoclinic, zirconolite structure was retained (Clinard *et al.*, 1984)). More importantly, the composition of the Cm-doped zirconolite was not greatly changed by the substitution; whereas, the Pu-substituted structure was significantly changed by replacement of ZrO_2 by PuO_2.

Swelling data at 350 K were obtained to near-saturation, and by use of an exponential relationship, a saturation swelling value of 6.0 vol.% was calculated for a dose of 2×10^{25} α-decay events m^{-3}. These results are in good agreement with those for the Pu-substituted material, which exhibited saturation swelling of 5.5 vol.% at nearly the same damage level (Clinard *et al.*, 1984). TEM images and diffraction patterns confirmed that Cm-doped zirconolite amorphized by the accumulation of damage tracks produced by the ^{240}Pu recoil ions that are emitted during α-decay of ^{244}Cm. A smaller amount of additional damage resulted from spontaneous fission of ^{244}Cm, which introduced a low density of fission tracks.

Changes in hardness and fracture toughness as a function of increasing α-decay event dose are shown in Figs 33 and 34 combined with the results for Pu-doped zirconolite. Both materials showed a decrease in hardness and an increase in fracture toughness; the

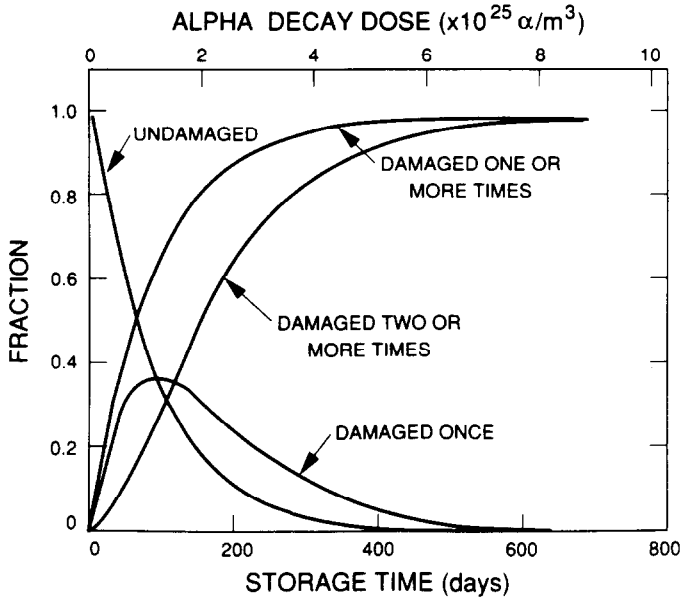

Fig. 31. Calculated fraction of undamaged, once-damaged, and multiply-damaged Pu-substituted zirconolite as a function of storage time and damage dose (Coghlan and Clinard, 1988).

former change is expected as a result of the radiation-induced transformation from a periodic to an aperiodic state, while the latter may result from the heterogeneous microstructure (Clinard *et al.*, 1985a).

Differential thermal analysis of the Cm-doped zirconolite after self-irradiation to 2.5×10^{25} α-decay events m^{-3} showed a strong exothermic reaction during recrystallization, with a sharp recovery stage of 114 J g^{-1} at 680–730°C. These values of stored energy and recovery temperature agree closely with those obtained from Pu-substituted zirconolite, although the latter material showed a halving of stored energy at higher radiation doses as a result of damage beyond the dose required for amorphization (Foltyn *et al.*, 1985). Measurements on the Cm-doped material showed that the temperature of the energy release peak increased with heating rate; this behavior allowed the calculation of an activation energy of recrystallation of 5.8 eV.

The dissolution (leaching) characteristics of the Cm-doped zirconolite were determined (Weber *et al.*, 1986) by testing fully-damaged (amorphized) specimens and a second set of specimens that had been fully recrystallized to the original structure by a 12 hr anneal at 1100°C. Samples were immersed in distilled, deionized water at 90°C for 14 days. The results, shown in Table 3, indicate a notable increase in leach rate with amorphization; especially significant is the factor of 10 increase for the α-decay product Pu. The high final pH is believed to limit the solubility of the Cm to the value shown. The low concentrations of Ti as compared to that of Ca suggest that the dissolution is incongruent, with the Ti ions (which are part of the TiO_6 octahedra comprising the network structure) being more resistant to leaching than the interlayer cations (e.g. Pu and Ca). The mechanism for the enhanced leaching of the radiation-induced amorphous state may be associated with the broken bonds and the increased free volume (a more open framework) of the amorphous state.

5.2.2.3. Ion beam-irradiated zirconolite. Radiation damage effects in zirconolite have also been investigated by bombardment with energetic heavy ions (Weber *et al.*, 1992). TEM of samples irradiated with 3 MeV Ar^+ ions showed damage build-up similar to that observed in material damaged by α-decay of ^{238}Pu or ^{244}Cm, namely, accumulation of small defects (alpha-recoil tracks) to the point where the material became globally disordered. Recent studies (White *et al.*, 1994) of the temperature dependence of amorphization in zirconolite have shown an increase in amorphization dose with temperature, in general agreement with the results of Clinard *et al.* (1984) for ^{238}Pu-substituted zirconolite.

Natural zirconolites have also been used in ion-beam irradiation simulations of α-decay event-induced amorphization (Ewing and Wang, 1992). Recrystallized samples (1130°C for 8 hr in air) were irradiated with 1.5 MeV Kr^+ ions using the HVEM-Tandem Facility at Argonne National Laboratory. The Kr^+

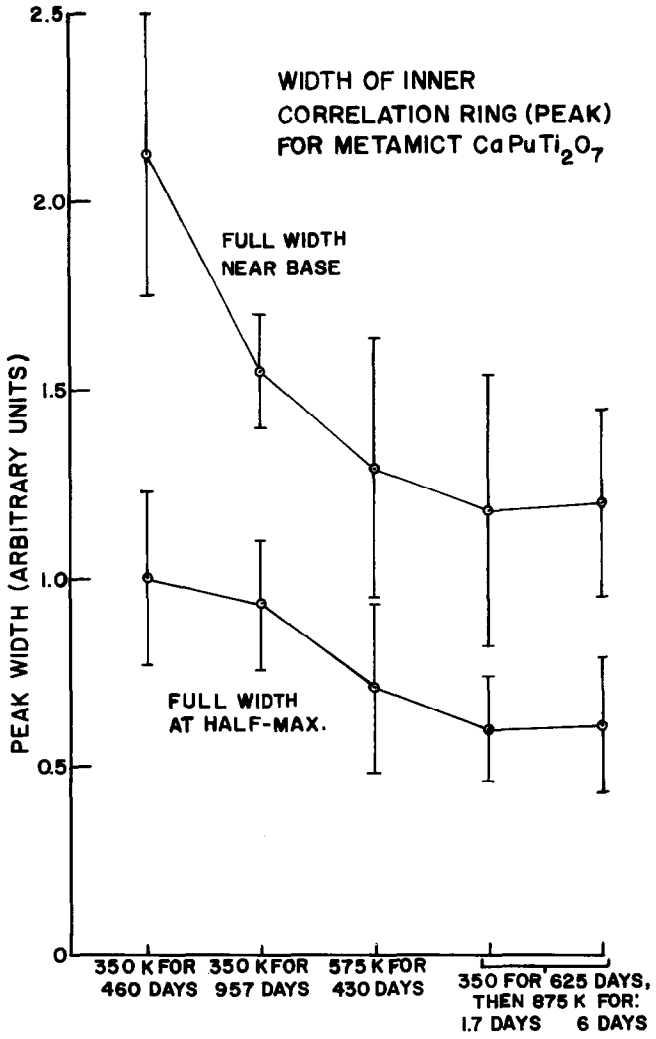

Fig. 32. Widths of inner correlation rings from electron diffraction patterns of metamict $CaPuTi_2O_7$ after conversion to intensity peaks. Values were determined at half-maximum and 10% of full height for five damage conditions (Clinard, 1986).

dose rate during the irradiation was 3.4×10^{11} ions $cm^{-2} s^{-1}$, which is a damage rate 2×10^{12} times higher than that which has occurred in the natural zirconolite due to decay of uranium. *In situ* transmission electron microscopy was completed during the ion irradiation. After a Kr^+ dose of 4×10^{14} ions cm^{-2} (= 0.3 dpa), the zirconolite grains were amorphized. The dpa level for ion beam induced amorphization is six times lower than that calculated for the natural α-decay induced process. Some of the α-decay event damage may have recovered by point defect migration over geologic periods of time. It is interesting to note that inclusions of thorianite, ThO_2, in the zirconolite did not become amorphous at equivalent doses. This is consistent with the already mentioned apparent radiation resistance of UO_2. The resistance of thorianite to amorphization compared to zirconolite is consistent with a model of damage accumulation in insulators in which the critical dose for amorphization is inversely proportional to the topologic and chemical complexity of the phase (Wang *et al.*, 1991). Thorianite is isometric with only one unique cation site. Zirconolite is monoclinic with three unique cation sites. Such criteria may be useful in evaluating the response of waste form ceramics to α-decay event damage.

Dose-dependence of damage in zirconolite has been studied by Headley *et al.* (1982) using Pb^+ ions of 40–240 keV at ambient temperature. Damage pro-

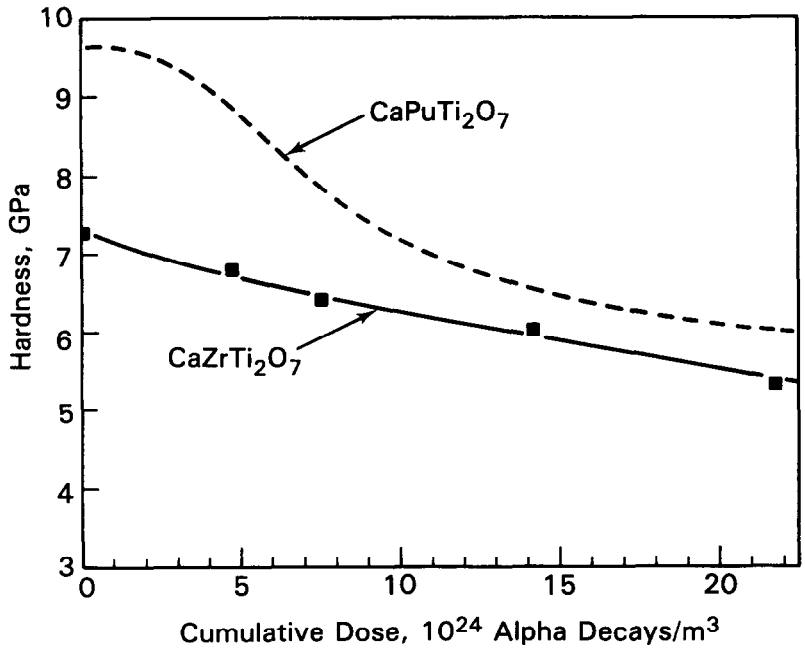

Fig. 33. Hardness of Cm-doped $CaZrTi_2O_7$ and Pu-substituted zirconolite as a function of cumulative dose (Weber *et al.*, 1986).

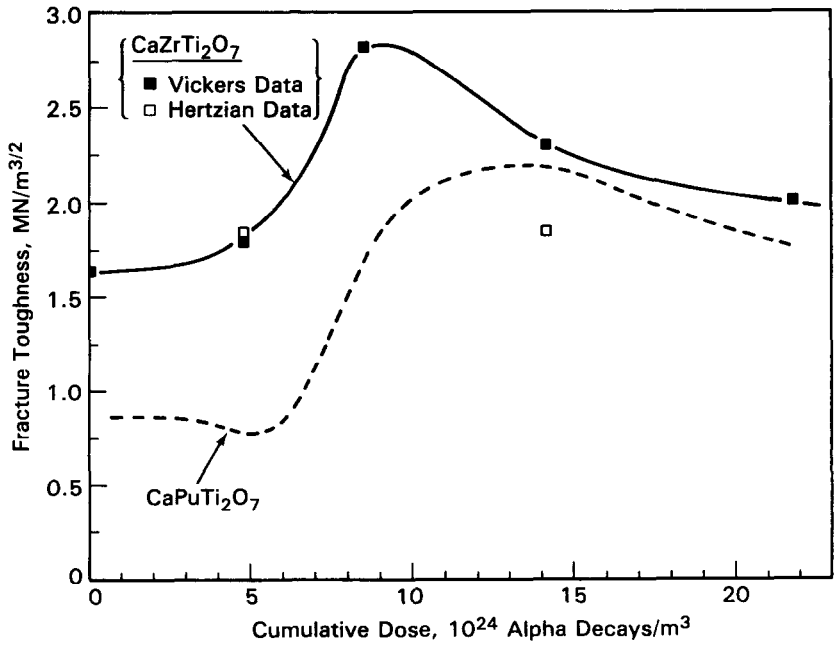

Fig. 34. Fracture toughness of Cm-doped $CaZrTi_2O_7$ and Pu-substituted zirconolite as a function of cumulative dose (Weber *et al.*, 1986).

Table 2. Damage level, stored energy and corresponding damage fractions for $CaPuTi_2O_7$ self-damaged near 300 K (Coughlan and Clinard, 1988)

Damage level (days)	Stored energy (kJ kg^{-1})	Amount undamaged (%)	Amount damaged once (%)	Amount redamaged (%)
154	100	18	32	50
224	92	10	23	67
558	59	0	2	98
1198	51	0	0	100

Table 3. Summary of 90°C, 14 days leach test data (Weber *et al.*, 1986)

Material	State	Normalized elemental mass loss (g m^{-2})				Percent weight loss	Final pH
		Ca	Ti	Cm	Pu		
$CaZrTi_2O_7$	Crystalline	0.72	<0.02	0.001	0.02	0.02	6.4
$CaZrTi_2O_7$	Amorphous	5.99	<0.02	0.001	0.22	0.05	7.3

ceeded in four stages: isolated tracks, track overlap, domination by aperiodic domains, and finally complete amorphization. Results were compared with those for natural zirconolite self-irradiated to various damage levels by α-decay over geologic times. Both the nature and extent of damage were similar, regardless of the large difference in damage rates. Later, Clinard *et al.* (1984) extended the comparison to include ^{238}Pu-substituted zirconolite and showed that damage at the intermediate rate characteristic of zirconolite was similar to that observed in natural and Pb^+ ion-bombarded material.

5.2.2.4. Natural zirconolite. Although zirconolite occurrences are rare, selected specimens have been the subject of extensive studies (Ewing *et al.*, 1982a; Ewing and Headley, 1983; Ewing, 1983; Oversby and Ringwood, 1981; Sinclair and Ringwood, 1981; Sinclair and Eggleton, 1982). Samples from Sri Lanka (550 million yr old) typically can have concentrations of UO_2 of 2 wt% and of ThO_2 of 20 wt%, thus reaching doses of 10^{16} α-decay events mg^{-1} ($=10^{26}$ α-decay events m^{-3}). This is a dose equivalent to nearly two displacements per atom.

X-ray diffraction analysis of fully-metamict zirconolite shows no diffraction maxima confirming that zirconolite is X-ray diffraction amorphous. Because of the paucity of samples which span a range of α-decay event doses, it is not possible to follow the change of diffraction maxima intensity and position with increasing α-decay event dose. A zirconolite annealed at 1130°C did give a diffraction pattern with sharp peaks which could be refined on the basis of a monoclinic unit cell (Lumpkin *et al.*, 1986b). Referring to the work of Wald and Offerman (1982) on a ^{244}Cm-doped zirconolite, the expansion of the unit cell was anisotropic with the greatest expansion perpendicular to the sheets of TiO_6 octahedra (Fig. 35) reaching a maximum value of 2.1% volume expansion at a dose of 10^{23} α-decay events m^{-3}.

High-resolution transmission electron microscopy showed no evidence for crystallinity (Lumpkin *et al.*, 1986b), and in approximately 10% of the grains examined there were subspherical microvoids ranging in diameter from 100 to 400 nm (Ewing and Headley, 1983). The microvoids are attributed to He-gas accumulation which is a result of the radioactive decay. Annealed samples (1100°C) recrystallized producing crystals up to 2000 nm in length. The crystallites were often twinned at the unit cell scale as a result of different stacking sequences of the TiO_6 sheets, thus resulting in laminar intergrowths of the various zirconolite polytypes (Lumpkin *et al.*, 1986b). The same texture of fine-scale twinning has been observed in synthetic zirconolite in Synroc C (White *et al.*, 1984) and synthetic zirconolite of $Ca_{0.6}Sm_{0.4}ZrNb_{0.4}Mg_{0.4}Ti_{1.2}O_7$ composition (White, 1984). The defects along the twin boundaries may become sites at which actinide elements are incorporated. In some instances (Lumpkin *et al.*, 1986b), there was evidence for the formation of crystals (5–100 nm) with *d*-spacings similar to those of the fluorite structure type. Lumpkin *et al.* (1986b) suggested that metamict zirconolite may recrystallize initially with a disordered, fluorite-type structure. Continued heating to higher temperatures (1000–1200°C) appears to favor the highly twinned, monoclinic zirconolite structure. Differential thermal analysis (30–1200°C) showed exothermic recrystallization at 780°C with a heat of recrystallization of

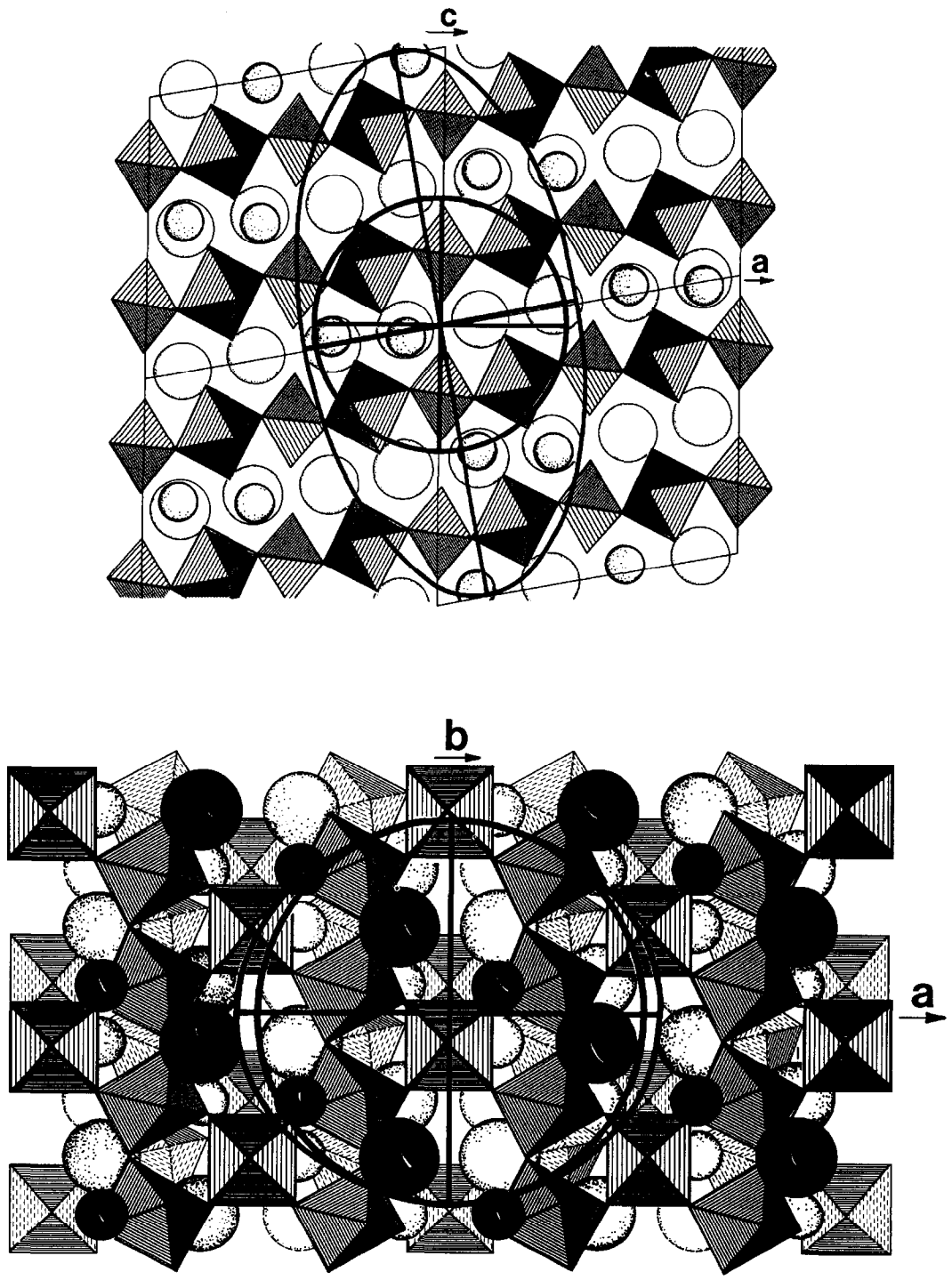

Fig. 35. Polyhedral representation of zirconolite ($CaZrTi_2O_7$) crystal structure. (Upper) (010) projection (four unit cells are outlined) with an ellipsoid superimposed to illustrate the relative expansion of the structure due to a dose of 10^{25} α-decay events m^{-3}. The octahedra represent TiO_6; the small spheres, Zr; the large spheres, Ca. (Lower) (001) projection (four unit cells shown as in upper diagram). The shading is darkest for the top layer, and lightens with increasing depth into the structure. No physical significance should be attached to the sphere sizes used. (Lumpkin *et al.*, 1986.)

50 J g^{-1} for a zirconolite with a total dose of $>10^{26}$ α-decay events m^{-3}. This is similar to the value obtained by Foltyn *et al.* (1985) for synthetic $CaPuTi_2O_7$ at nearly the same α-decay event dose of 10^{26} α-decay events m^{-3} after 1200 days. Although the measured energy release for the natural zirconolites and Pu-doped zirconolites of equivalent dose are nearly identical, both of these values are distinctly lower than the value (84 J g^{-1}) measured for Pu-doped zirconolite that had experienced a smaller dose (approximately 10^{25} α-decay events m^{-3}) (Foltyn, 1985) or for Cm-doped zirconolite (126 J g^{-1}) at a dose of 2.0×10^{25} α-decay events m^{-3} (Weber *et al.*, 1985a, 1986). Foltyn *et al.* (1985) have suggested that the decrease in released energy with increasing dose is due to a redamaging process that results in a reordering of atoms in the metamict state.

Detailed EXAFS and XANES studies have been completed on fully-aperiodic zirconolite (Lumpkin *et al.*, 1986b; Greegor *et al.*, 1984a; Farges *et al.*, 1993). These studies, in many cases on the same sample from Sri Lanka (#111.35), were on the Ca, Th, U, Zr and Ti EXAFS spectra, that is all of the major cations of zirconolite. Principal conclusions included: (1) The loss of long range atomic periodicity occurs by changes in the metal–oxygen–metal (M–O–M) angles across mainly edge-sharing coordination polyhedra. The tilting of nearest neighbor coordination polyhedra occurs without significant changes in the first and second neighbor distances. Thus, the second-neighbor coordination geometries for Ca, Ti and Zr may not be very different in metamict and crystalline zirconolite, despite the loss of long-range periodicity. This is illustrated in Fig. 36 which shows that a slight change (5°) in the mean Zr–O–M angle correlates with a relatively large variation (0.01 nm) in the Zr–M distance. Thus, variations in the mean M–O–M angle do not have to be large in order to have a significant effect on long-range periodicity and the medium-range order in this radiation-damaged phase. (2) Although there is some evidence for reduction in coordination number and an associated decrease in bond-length with increasing α-decay event dose (Greegor *et al.*, 1984), the short-range (nearest neighbor oxygen) environments of Zr^{4+}, Th^{4+}, Ca^{2+} and Ti^{4+} are little changed by increasing radiation damage. (3) The structural environments around Zr^{4+} and Th^{4+} in metamict zirconolite (7-coordinated and 8-coordinated, respectively) are clearly different from those measured in silicate and borosilicate glasses in which they are commonly 6-coordinated with oxygens. This suggests that there are fundamental structural differences in cation environments between radiation-induced aperiodic (metamict) phases and glasses quenched from melts (Sales and Boatner, 1990).

5.2.3. *Perovskite.* Perovskite, $CaTiO_3$, is a mineral that may assume a wide range of compositions as stable solid solutions. Perovskite is also a highly refractory phase that has been stable in near surface environments for billions of years. Thus, $CaTiO_3$ is an excellent candidate for immobilization of radioactive waste elements, particularly actinides, and is a major constituent phase in Synroc and other titanate ceramic waste forms. Perovskite is orthorhombic and consists of a three-dimensional network of corner-sharing TiO_6 octahedra with Ca occupying the large void space between the octahedra (the corner-sharing octahedra are located on the eight corners of a slightly distorted cube). The actinides, rare earths, and other large cations readily replace Ca in the structure, while smaller-sized cations replace titanium.

There are limited data on radiation effects in perovskite. Sinclair and Ringwood (1981) have studied natural perovskites of varying age and uranium and thorium contents. Natural perovskite samples that have received a dose of up to 2.6×10^{18} α-decay

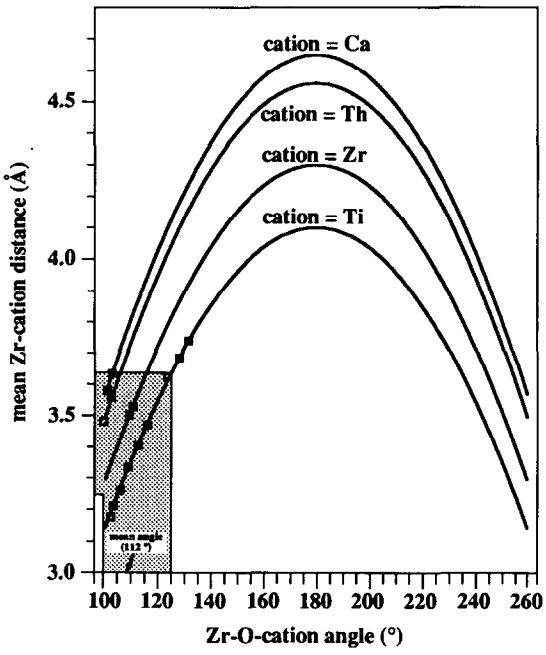

Fig. 36. Plot of mean Zr–metal distance (Å) versus Zr–O–M angle (°) for polyhedra of M-cations (M = Ti, Zr, Th, Ca) arranged in the edge-shared configuration in zirconolite. The stippled region shows the normal range of distance and angle values in crystalline zirconolite. (Farges *et al.*, 1993.)

events g^{-1} (equivalent to 20,000 years storage for Synroc) showed a high degree of atomic periodicity with no evidence of amorphization. The unit-cell volume expansion at this dose was 1.8% due to the accumulation of simple structural defects. Loparite is an isometric perovskite that contains large amounts of Ce and Nb and is also highly crystalline. The unit-cell volume expansion is 1.5–1.7% after a dose of $1–2 \times 10^{18}$ α-decay events g^{-1} (Ringwood *et al.*, 1980; Ringwood and Sinclair, 1981).

Cold-pressed and sintered specimens of synthetic $CaTiO_3$ have been neutron irradiated in the fast-neutron flux of the HIFAR reactor at Lucas Heights, for different lengths of time (Reeve *et al.*, 1981; Woolfrey *et al.*, 1982). The highest dose reported was 2.5×10^{26} n m^{-2} ($E > 1$ MeV), which represents an equivalent Synroc storage time of 5.8×10^5 yr and corresponds to 0.7 dpa or 8×10^{18} α-decay events g^{-1}. The volume expansion reached a value of 6% at the maximum dose achieved, but showed no indication of approaching a saturation value (Fig. 37). X-ray diffraction analysis indicated sharp diffraction maxima, suggesting strong resistance to amorphization, but shifts in specific peaks were not analyzed. Similar behavior has been observed in Pu-doped $CaTiO_3$ but at lower doses (Fig. 37).

While the above studies indicate that the perovskite structure is fairly resistant to radiation-induced amorphization, studies by Karioris *et al.* (1982) indicate that $CaTiO_3$ readily amorphizes under 3 MeV Ar^+ ion irradiation. Similarly, the perovskite-type compound $CmAlO_3$ has been reported to transform from a crystalline to a fully amorphous state after a dose of 1.4×10^{18} α-decay events g^{-1}, which was achieved in 7.5 days from the decay of ^{244}Cm (Mosley, 1971). The crystal structure $CmAlO_3$ was fully recovered after annealing at 1000°C for 30 min. Questions regarding the radiation stability of perovskite are being addressed in a new study of α-decay damage in Cm-doped perovskite. Preliminary results indicate a linear increase in volume with dose (0.75% at 5×10^{17} α-decay events g^{-1}), as well as an increased leach rate (Mitamura *et al.*, 1994).

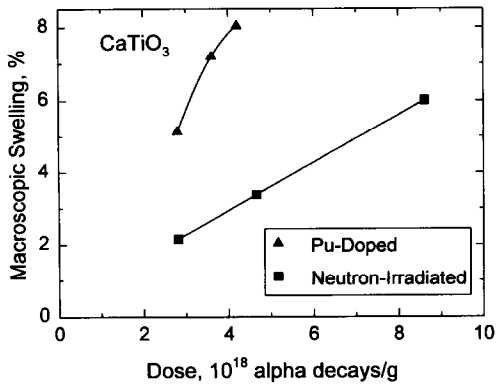

Fig. 37. Volume expansion of Pu-doped (Evans *et al.*, 1986) and fast neutron-irradiated (Woolfrey *et al.*, 1982) perovskite.

5.2.4. *Barium hollandite.* Barium hollandite, $BaAl_2Ti_6O_{16}$, is a major phase in several different Synroc formulations (Ringwood *et al.*, 1979, 1981; Ringwood, 1982; Newkirk *et al.*, 1982). The structure of barium hollandite consists of a framework of TiO_6 octahedra that are linked (edge-sharing and corner-sharing) to form square channels parallel to the *c*-axis. These channels can accommodate a wide variety of large cations, including fission products, such as Cs. Although hollandite will not contain actinides, it will experience irradiation from α-particles emitted in adjacent actinide-containing phases. The cumulative α-particle fluence incident on barium hollandite as a function of waste storage time is shown in Fig. 38.

Weber (1985) investigated the effect of α-particle irradiation on the structure of barium hollandite utilizing α-particles emitted isotropically from an effectively semi-infinite $^{238}PuO_2$ source. The energy spectra of the α-particles emitted from this source closely approximate that expected to be incident on the barium hollandite phase in Synroc. Irradiation with the α-particles resulted in a large expansion of the unit-cell volume that saturates at 2–2.5% and also induces a displacive transformation from the tetragonal structure to a lower symmetry monoclinic structure. The anisotropic unit-cell expansion is primarily along the *a*- and *b*-axes and causes a small increase of the angle β from 90° in the tetragonal structure to 91° in the deformed monoclinic structure. A similar tetragonal-to-monoclinic transformation has been observed as a result of heavy-ion and electron irradiations (Barry *et al.*, 1983). The anisotropy of the unit-cell expansion caused an increase in the size of the channels along the *c*-axis, which could significantly affect the ability of the barium hollandite structure to retain channel-site atoms, such as Cs, in an aqueous environment. The implied increase in dissolution rates of non-network atoms as a result of radiation-induced volume expansions has been previously described for both the pyrochlore and zirconolite structures (Wald and Weber, 1984) which also consist of a TiO_6 octahedra network.

Comparisons of the α-particle irradiation results of Weber (1985) with the fast-neutron irradiation results

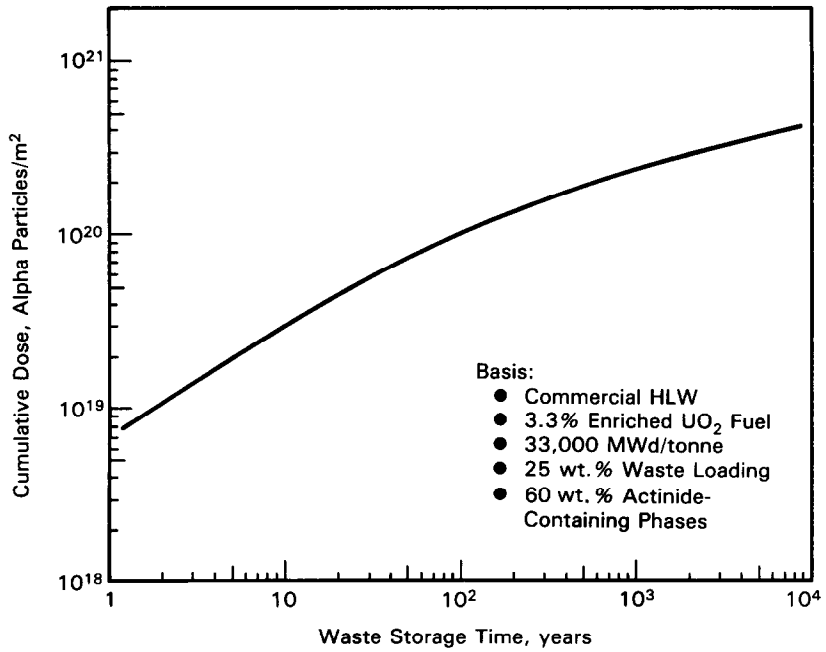

Fig. 38. Cumulative α-particle fluence incident on barium hollandite in SYNROC. After Weber (1985).

of Woolfrey *et al.* (1982) indicate a significant irradiation source dependence. Both studies were completed using specimens from the same batch preparation of hollandite. The volume changes under α-particle irradiation occur at an order of magnitude lower dose, calculated as displacements per atom, than the volume changes under fast-neutron irradiation (Fig. 39). This is significant since an order of magnitude in dose corresponds to two or three orders of magnitude in time. The α-particle irradiation primarily produces isolated interstitials and vacancies along the path of the α-particles that give rise to a large unit-cell expansion; whereas, the fast-neutron irradiation, according to Ball and Woolfrey (1983) produces planar interstitial clusters and isolated vacancies, with only a small increase in unit-cell volume.

While there was no evidence for amorphization in the α-irradiated barium hollandite, heavy-ion irradiation of barium hollandite has been reported to cause amorphization (Headley *et al.*, 1982; Karioris *et al.*, 1982). These results clearly demonstrate that the proper selection of irradiation source is important if an accurate simulation of waste form behavior is desired.

5.2.5. *Zircon.* Zircon ($ZrSiO_4$, $I4_1/amd$, $Z=4$) occurs in silica-rich tailored ceramics, and its structure type is the high-temperature form of the heavy rare earth phosphates (the low-temperature form has the monazite structure type). Pu can substitute for Zr, and radiation damage studies have been completed on ^{238}Pu-doped zircon up to concentrations of 8.1 mol% ^{238}Pu (Weber, 1990, 1991b). Additionally, zircon is a phase extensively used in U/Pb radiometric age-dating, as it may contain uranium in concentrations up to 5000 ppm. Early workers (Holland and Gottfried, 1955) investigated radiation damage effects in an effort to use the degree of damage as a measure of the age of the zircon. Theirs was the first study to quantitatively correlate the decrease in density, decrease in refractive index, and expansion of the unit cell parameters with increasing α-decay event dose. Based on their study of zircon, Holland and Gottfried proposed the first model of defect accumulation and damage in-growth for a complex ceramic. This early history of the study of radiation damage effects in metamict zircons is summarized by Ewing (1994).

There are data on radiation effects in natural zircons (irradiation time: 570 million yr (Murakami *et al.*, 1986, 1991; Woodhead *et al.*, 1991a,b)), Pu-doped zircon (irradiation time: 6.5 yr (Exarhos, 1984; Weber, 1990, 1991b)) and most recently ion-beam irradiated zircon (irradiation time: 30 min (Babsail *et al.*, 1991; Wang *et al.*, 1993; Weber *et al.*, 1994)). The damage rate for the ^{238}Pu-doped zircon is 6×10^{10} Bq g^{-1}, and the damage rate for natural zircons is $< 10^3$ Bq g^{-1}. This extraordinary data set with a dose rate range of

$>10^8$, allows one to investigate the efficacy of using accelerated techniques (actinide-doping and ion-beam irradiations) to simulate the long-term effects of α-decay event damage.

The study of natural zircons culminated with the very detailed analysis (Murakami *et al.*, 1991; Woodhead *et al.*, 1991a) of damage in-growth in suites of zircons from Sri Lanka (570 million yr old) which had experienced variable α-decay event doses due to variable U and Th contents (0.06×10^{15}–6.8×10^{15} α-decay events mg^{-1}). In addition to the decrease in density and refractive indices with α-decay event dose as determined by Holland and Gottfried in 1955, later workers applied detailed X-ray diffraction analysis (Murakami *et al.*, 1986, 1991), electron microprobe analysis (Murakami *et al.*, 1991; Chakoumakos *et al.*, 1987), high-resolution transmission electron microscopy (Murakami *et al.*, 1991; McLaren *et al.*, 1994), infrared spectroscopy (Woodhead *et al.*, 1991b), and X-ray adsorption spectroscopy (Farges and Calas, 1991; Farges, 1994) to the study of this radiation-induced transition to the aperiodic (metamict) state. Most recently, the decreases in harness (40%) and elastic moduli (60%) over the dose range of 0.15–0.65 dpa were determined in zoned zircons using a mechanical properties microprobe (Chakoumakos *et al.*, 1991), and increases in stored energy have been measured as a function of increasing α-decay event dose (Ellsworth *et al.*, 1994). The enthalpy of annealing at room temperature varies sigmoidally as a function of radiation dose and reaches a saturation plateau at doses of 5×10^{15} α-decay events mg^{-1}. The large magnitude of the enthalpy of annealing plateau, -59 kJ mol^{-1}, suggests that the damage to the structure is pervasive on the scale of nanometers.

Based on X-ray diffraction analysis and high-resolution transmission electron microscopy, Murakami *et al.* (1991) described three stages (Fig. 40) of damage in-growth. Stage-I ($<3 \times 10^{18}$ α-decay events g^{-1}) is characterized by sharp Bragg diffraction maxima with a minor contribution from the diffuse-scattering component. Electron diffraction patterns were sharp. Damage is dominated by the accumulation of isolated point defects which cause unit-cell expansion and distortion that account for most of the decrease in density. These defects may partially anneal over geologic time. Stage-II (3–8×10^{18} α-decay events g^{-1}) is characterized by significant decreases in the intensity of the Bragg diffraction maxima which become asymmetric due to increased contributions from the diffuse-scattering component. High-resolution transmission electron microscopy revealed that the microstructure consisted of distorted crystalline regions and amorphous 'tracks' caused by α-recoil nuclei. With increasing α-decay dose, damaged crystalline regions are converted into aperiodic regions, but with no further significant expansion of the unit cell in the remaining crystalline regions. Stage-III(>

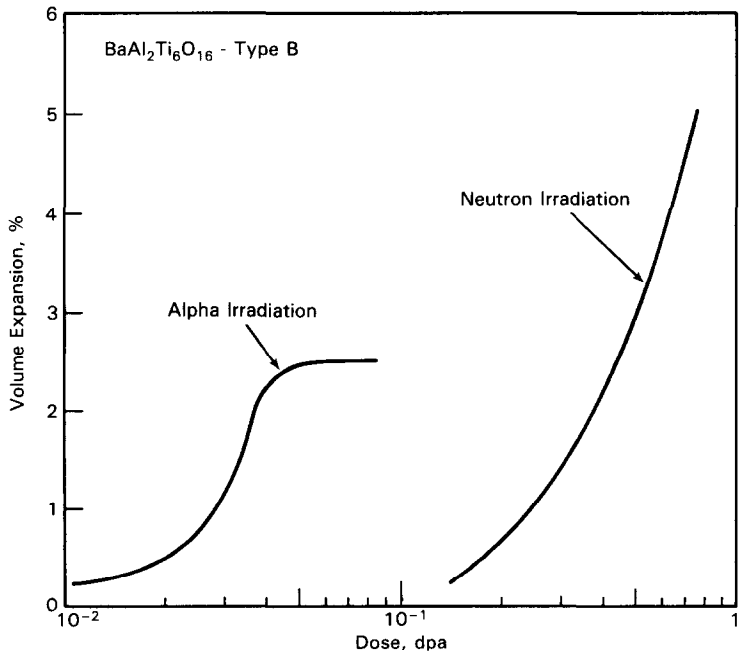

Fig. 39. Volume expansion in α-irradiated (Weber, 1985) and neutron-irradiated (Woolfrey *et al.*, 1982) barium hollandite.

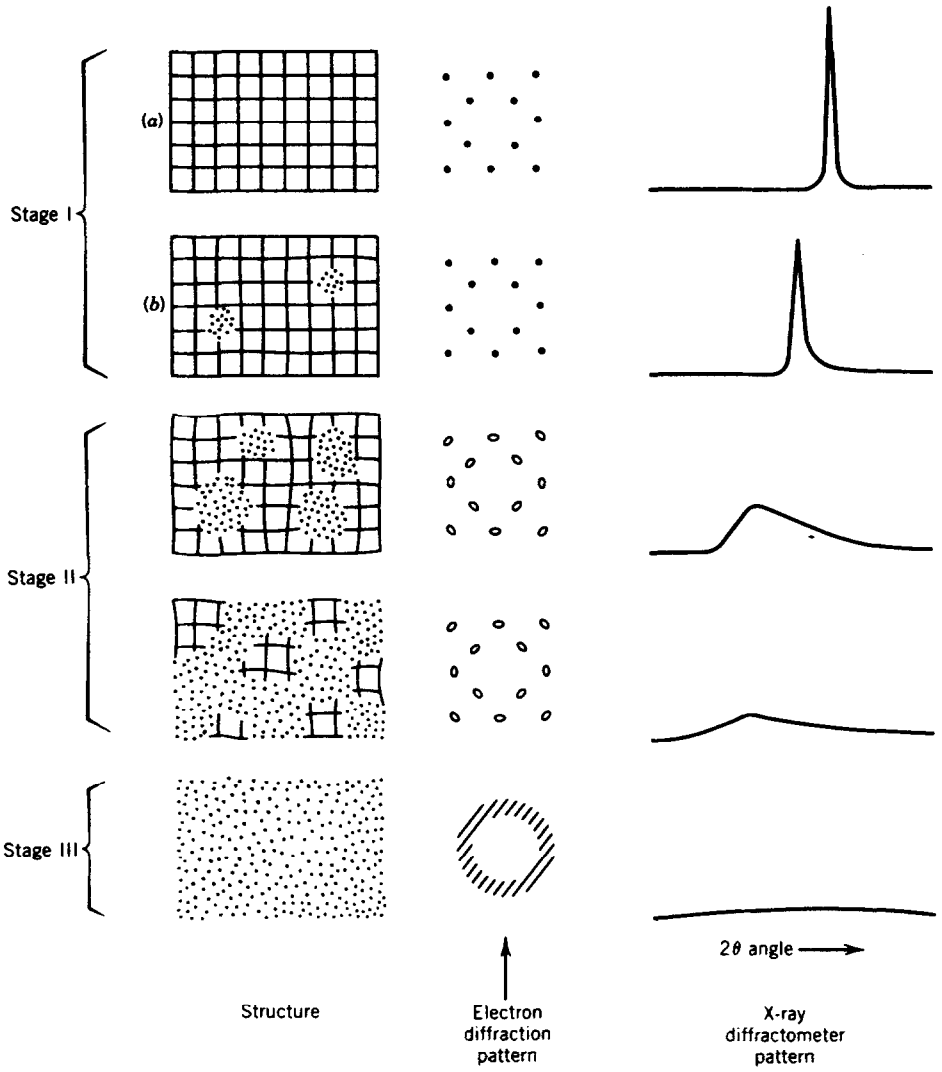

Fig. 40. Schematic representation of the change in X-ray diffraction pattern (right column), electron diffraction pattern (center column), and the structure (left column) with increasing α-decay event dose (top to bottom). After Murakami *et al.* (1991).

8×10^{18} α-decay events g^{-1}) consists of material which is entirely aperiodic as far as can be determined by X-ray or electron diffraction. Figure 40 is a schematic representation of the changes in X-ray diffraction and electron diffraction pattern that occur at each of the three stages. These stages of damage are illustrated in HRTEM micrographs over the range of 0.0025–0.50 dpa (Fig. 41).

Finally, there was no HRTEM or XRD evidence for the formation of ZrO_2 or SiO_2 as final products during the last stage of metamictization: however, recent work based on microcalorimetry (Ellsworth *et al.*, 1994), X-ray absorption spectroscopy (Farges, 1994) and SIMS and electron microscopy (McLaren *et al.*, 1994) has postulated the presence of zirconium- and silicon-rich domains which are less than 10 Å in size. These domains have been identified at higher temperatures by neutron diffraction experiments (Mursic *et al.*, 1992).

Based on modeled density changes, aperiodic regions continued to experience a change in structure as they were redamaged. During Stage-II of the process, the modeled density of aperiodic regions changed from 4.5 g cm^{-3} to 4.1 g cm^{-3}. The amorphization process is consistent with a model for the multiple overlap of displacement cascades (Carter and Webb, 1979; Webb and Carter, 1979, 1981), suggesting amorphization occurs as a result of defect accumu-

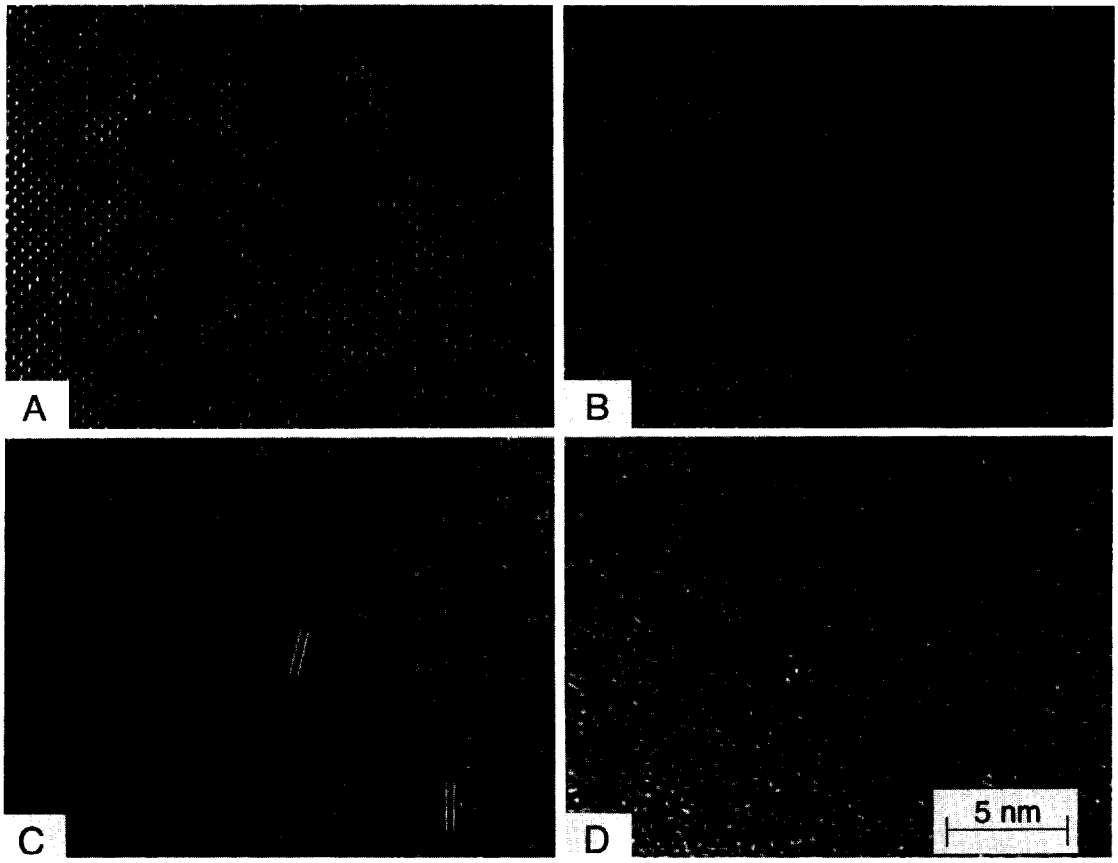

Fig. 41. HRTEM micrographs of self-radiation damage in natural zircons showing an increased degree of amorphization with increasing dose: (a) 0.0025 dpa, (b) 0.091 dpa, (c) 0.32 dpa, and (d) 0.50 dpa. The spacing marked in (c) is 0.33 nm [the (200) *d*-spacing]. The slight rotation of the remaining crystallites in the amorphous matrix in (c) is caused by local strain fields induced by amorphization. (Weber *et al.*, 1994.)

lation rather than directly within a single displacement cascade. Figure 42 compares the fraction of amorphous material (estimated from density and optical data) for Pu-doped and natural zircons (solid and dashed lines, respectively) to the calculated values for a double overlap model (i.e. the defect density for amorphization requires the overlap of three cascades as discussed below). Note the incubation dose (0.05 dpa) required for the natural zircon which reflects annealing of the isolated point defects. Comparison of the results for natural zircon with those for Pu-doped zircon (Weber, 1991b) showed that dose-rate variations (even as great as a factor of 10^8) had no substantial effect on the damage accumulation process.

Unit cell parameters and volume increased (Fig. 43) and density decreased more for the Pu-doped zircon than for natural zircon in the early stages of damage accumulation ($<3\times10^{18}$ α-decay events g^{-1}), suggesting that annealing of point defects in the early stages of the damage accumulation process occurs in natural zircon under ambient conditions. Evidence for annealing under ambient conditions was noted by Holland and Gottfried (1955) and the mean lifetime of an α-recoil track was estimated to be 400 million yr by Lumpkin and Ewing (1988). The annealing accounts for the distinct sigmoidal shape of the damage curves for natural zircon and the apparent incubation period before the onset of amorphization (see Fig. 42). Thus, radiation damage from α-decay events in zircon results in the simultaneous accumulation of simple structural defects and amorphous (or aperiodic) regions that exhibit loss of long-range order (Chakoumakos *et al.*, 1987; Murakami *et al.*, 1991; Farges and Callas, 1991). The amorphous regions eventually overlap to produce a completely amorphous state that may be structurally unique. The local amorphization process is believed to result from the spontaneous local collapse of the

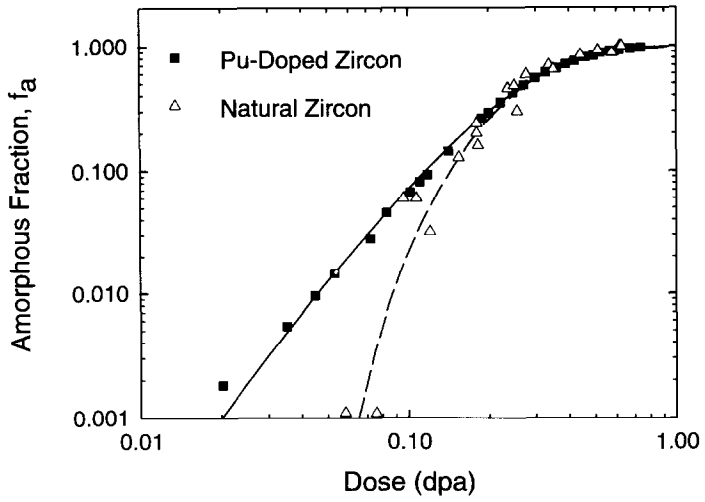

Fig. 42. Amorphous fraction, f_a, as a function of dose in Pu-doped and natural zircons. The solid curve for Pu-doped zircon is based on a fit of the double-overlap model (Webb and Carter, 1979, 1981) to the data of Weber (1990). The dashed curve for natural zircon is based on a fit of the double-overlap model, with an incubation dose (0.05 dpa), to the optical and density data of Holland and Gottfried (1955). After Weber *et al.* (1994).

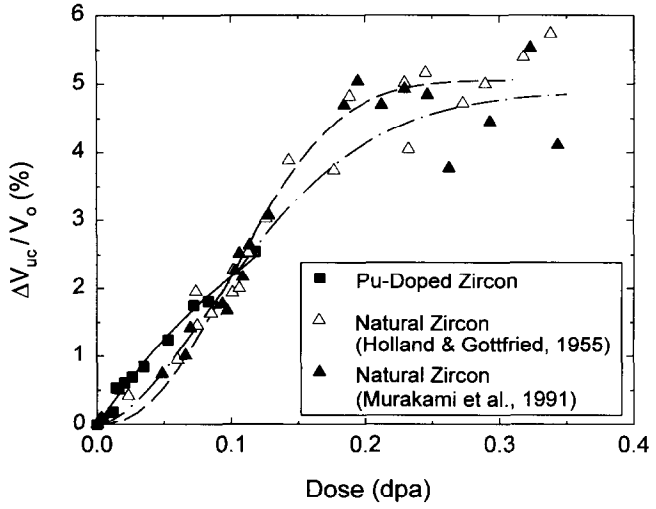

Fig. 43. Unit cell volume expansion, $\Delta V_{uc}/V_0$, as a function of dose in Pu-doped and natural zircons. The data of Weber (1990) for Pu-doped zircon fit a simple model (Nellis, 1977; Weber, 1981) for the accumulation of immobile defects, $\Delta V_{uc}/V_0 = A\{1-\exp[-BD]\}$. The data of Holland and Gottfried (1955) and Murakami *et al.* (1991) fit an empirical expression of the form $\Delta V_{uc}/V_0 - A\{1-\exp[-(BD)^n]\}$. After Weber *et al.* (1994).

crystal structure and disappearance of long-range order due to a local high-defect concentration; amorphization is triggered when the free energy of the high-defect region becomes equal to the free energy of the amorphous state. The local defect concentration necessary to trigger amorphization can occur directly in the displacement cascade (particle track) of a single heavy particle (recoil nucleus in α-decay) or from the overlapping cascades of individual light and heavy particles (α-particle and recoil nucleus).

Several models of both direct and multiple-overlap processes have been developed to describe amorphization in ion-irradiated semiconductors (Carter and Webb, 1979; Webb and Carter, 1979). These models have been used to gain some insight into the process for amorphization in zircon due to internal α-decay

events (Weber *et al.*, 1994). As shown previously (Weber, 1990, 1993) amorphization in Pu-doped and natural zircons is consistent with amorphization occurring by the catastrophic collapse of local structure through an increase in local defect concentration by the double overlap of displacement cascades. The fraction of amorphous phase, f_a, is given by the expression:

$$f_a = 1 - [(1 + RD + R^2D^2/2)\exp(-RD)], \quad (3)$$

for the double-overlap model (Carter and Webb, 1979; Webb and Carter, 1979), where R (with dpa as the unit of dose, D) is the average ratio of total atoms to displaced atoms within the cascades (tracks) produced by the α-decay event particles (α-decay events per unit volume or mass). The amorphous fractions have been determined previously for Pu-doped zircon from macroscopic swelling and unit-cell expansion data (Weber, 1990) and for natural zircons by Holland and Gottfried (1955) from both refractive indices and density data. The results and model fits are shown in Fig. 42. The amorphous fractions for Pu-doped and natural zircons exhibit very similar behaviors as functions of cumulative displacement dose, except for an offset at low dpa due to the incubation dose in natural zircon that is caused by the point-defect annealing over geologic time as discussed above. In the case of Pu-doped zircon, non-linear regression analysis yields a value of $R = 9.51$ dpa^{-1}. An incubation dose, D_0, must be assumed in the case of natural zircon for the double-overlap model to provide a reasonable fit to the results of Holland and Gottfried (1955). Non-linear regression analysis yields values of $R = 11.67$ dpa^{-1} and $D_0 = 0.05$ dpa for natural zircon. The value of R is in good agreement with the value determined for Pu-doped zircon, and the incubation dose is consistent with the incubation dose determined from both the XRD intensity data and the onset for expansion along the a-axis. Physically, the double-overlap model suggests that some limiting local defect concentration that corresponds to the overlap of three displacement cascades is required to trigger amorphization; this is consistent with the dependence of amorphous fraction on defect concentration reported earlier, with the observed effect of defect annealing, and with the observations of some intermetallic compounds.

If it is assumed that the crystalline fraction contains both isolated defects and disordered regions (recoil tracks) that give rise to the measured unit-cell expansion, then, due to the composite nature of the radiation-induced microstructure the total macroscopic swelling, $\Delta V_m/V_0$, of zircon can be expressed as:

$$\Delta V_m/V_0 = f_c \Delta V_{uc}/V_0 + f_a \Delta V_a/V_0, \quad (4)$$

where f_c is the mass fraction of crystalline phase, f_a is the mass fraction of amorphous phase, $\Delta V_{uc}/V_0$ is the average unit-cell volume change of the crystalline phase, and $\Delta V_a/V_0$ is the relative volume change associated with the amorphous phase (Weber, 1993). The unit-cell volume change, $\Delta V_{uc}/V_0$, is given by equation (6) with the fit parameters determined directly from experimental measurements (Fig. 43). It can be inferred that the volume change associated with amorphization, $\Delta V_a/V_0$, is constant and equal to the value of the macroscopic swelling at saturation, ($\Delta V_a/V_0 = 16.6\%$ for the Pu-doped zircon and $\Delta V_a/V_0 = 18.4\%$ for natural zircons). Consequently, as f_a is known and $f_c = 1 - f_a$, the total macroscopic swelling, $\Delta V_m/V_0$, can be calculated using equation (4) and is shown in Fig. 44, along with the experimental data on total macroscopic swelling and the calculated crystalline, $f_c \Delta V_{uc}/V_0$, and the amorphous, $f_a \Delta V_a/V_0$, components. The calculated macroscopic swelling, based on equation (4), provides an excellent fit to the experimental data. The dominance of the unit-cell expansion at low doses is clearly evident for both the Pu-doped and natural zircons.

Most recently, particle irradiations (2 MeV He^+ (Babsail *et al.*, 1991); 0.8 MeV Ne^+, 1.5 MeV Ar^+, 1.5 MeV Kr^+, 0.7 MeV Kr^+, 1.5 MeV Xe^+ (Wang *et al.*, 1993)) have been used to induce amorphization in zircon, and the results compared (the time scales in this comparison range from 0.5 hr to 570 million yr!) to the results of α-decay event damage (Weber *et al.*, 1994). High-resolution transmission electron microscopy confirms that the damage in-growth processes are similar for natural and ion-beam irradiated zircons (Fig. 45). The defects are produced in varying concentrations along each particle track, depending on mass and energy of the particle. Figure 46 shows the dependence of amorphization dose in zircon at room temperature with the average energy transferred to recoils per ion. These results show that the amorphization dose for the heavier ions (Kr^+ and Xe^+ dose rates of approximately 10^{-4}–10^{-3} dpa s^{-1}) is nearly identical to that determined from the 92 keV U^+ recoil emitted during α-decay in ^{238}Pu-doped zircon with a dose rate of 3×10^{-9} dpa s^{-1}. Thus, the amorphization process is nearly independent of the damage source (α-decay events versus heavy-ion beam irradiations) and is consistent with models based on the multiple overlap of particle tracks, indicating amorphization occurs as a result of a critical defect concentration.

Using *in situ* TEM to determine the critical amorphization dose of zircon irradiated by 1.5 MeV Kr^+ as

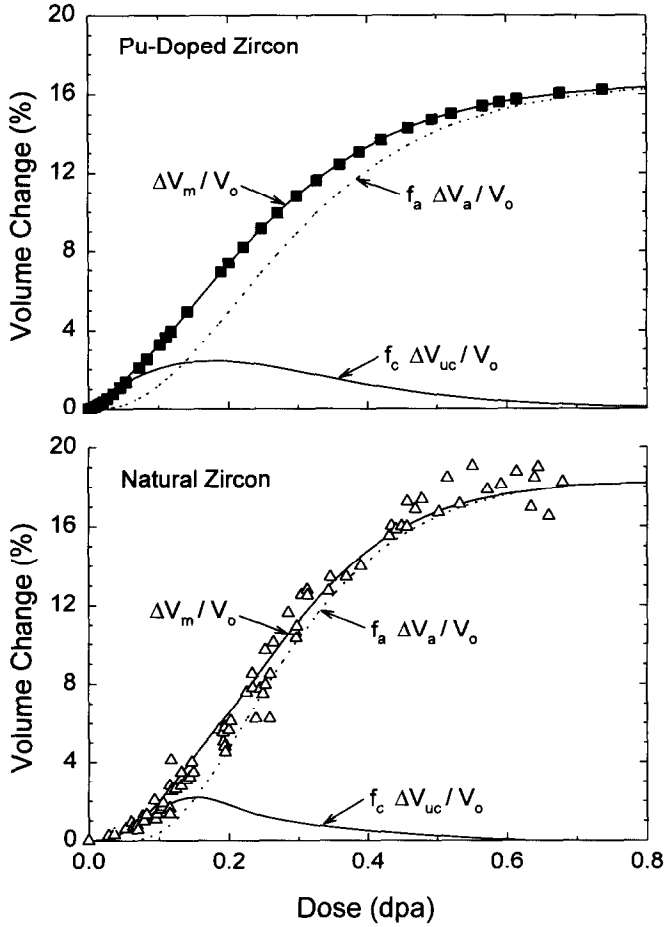

Fig. 44. Contributions of crystalline fraction volume change, $f_c\Delta V_{uc}/V_0$, and amorphous fraction volume change, $f_a\Delta V_a/V_0$, to the total macroscopic swelling, $\Delta V_m/V_0$, in Pu-doped and natural zircons based on a composite model of the radiation-induced swelling. The solid curve is the sum of $f_c\Delta V_{uc}/V_0$ and $f_a\Delta V_a/V_0$ and provides an excellent fit to the experimental data. After Weber *et al.* (1994).

a function of temperature provides an insight into the competing roles of defect recovery (annealing) and damage accumulation in a waste form ceramic (Fig. 47). The dose for complete amorphization in zircon increases with temperature in two stages. This increase in amorphization dose with temperature is believed to be due to a decrease in the average cascade size (intracascade defect density) or shrinkage of the amorphous regions (in overlapped cascades) as a result of the thermal annealing of irradiation-induced defects. The first stage (Stage-I), which occurs below 300 K, may be associated with the intracascade recombination of closely-spaced defects. As the temperature increases above 300 K, the Stage-I annealing process in zircon is complete (all Stage-I defects have recombined), and the dose for complete amorphization from the remaining (unannealed) defect structure within the cascade is constant, independent of temperature, from 300 to 473 K. Above 473 K, the dose for complete amorphization again increases with temperature in a second stage (Stage-II), which may be due to additional intracascade recombination from the thermal migration of remaining point defects or irradiation-enhanced epitaxial recrystallization (point defect annihilation at the crystalline–amorphous interface).

Because both the evolution of the amorphous state and the dose for complete amorphization in the 1.5 MeV Kr^+ irradiated zircon at room temperature are similar to that observed above for the Pu-doped and natural zircons, it is assumed that amorphization under heavy-ion irradiation is also due to the multiple

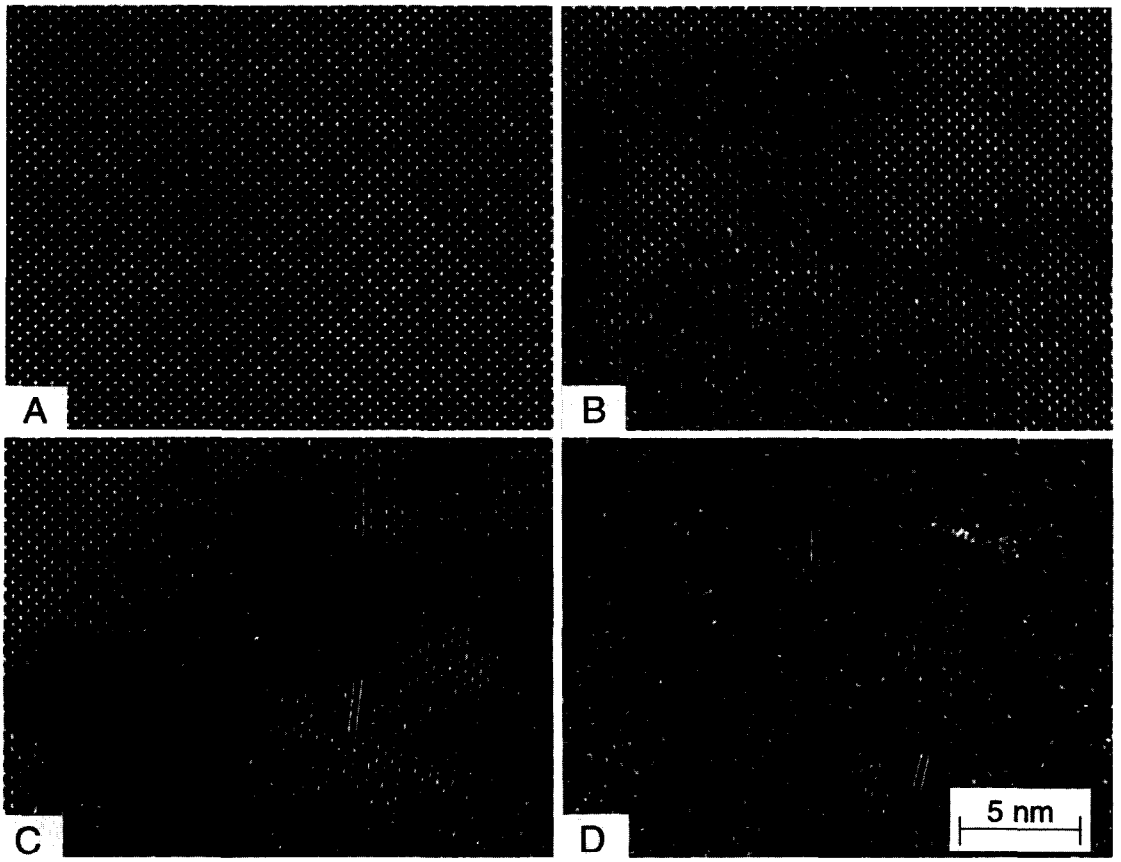

Fig. 45. HRTEM images of the crystalline-to-amorphous transformation in zircon irradiated with 1.5 MeV Kr^+ ions at 300 K: (a) unirradiated, (b) 0.057 dpa, (c) 0.17 dpa, and (d) 0.34 dpa. Complete amorphization is achieved at 0.55 dpa. The spacing marked in (c) and (d) is 0.33 nm [the (200) *d*-spacing]. Note the similarity of the images in (b), (c) and (d) to those of self-radiation damaged zircon in Figs 41(a), (b) and (c). (Weber *et al.*, 1994.)

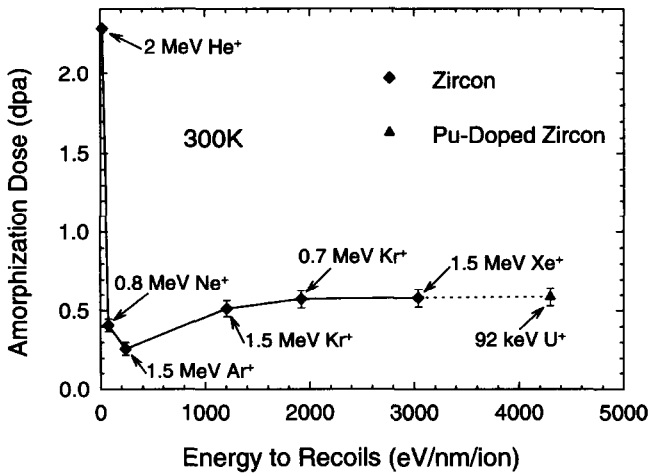

Fig. 46. The dependence of amorphization dose in zircon at room temperature on the average energy transferred to recoils per ion. The results show that the amorphization dose for the heavier ions (Kr^+ and Xe^+) is nearly identical with that determined for the 92 keV U^+ recoil emitted during α-decay of ^{238}Pu-doped zircon. (Weber *et al.*, 1994.)

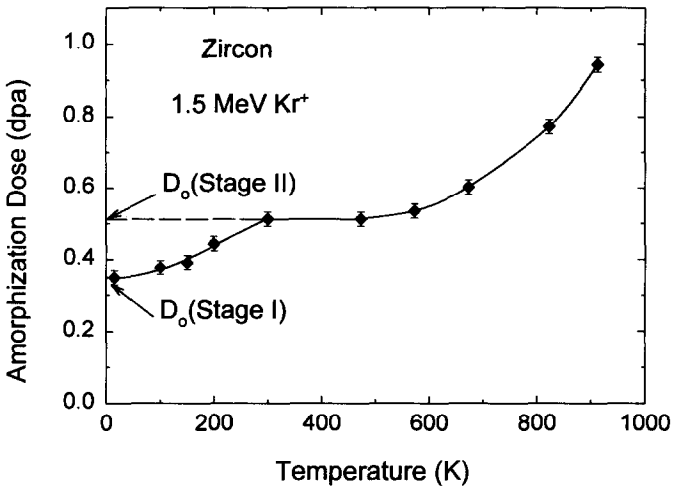

Fig. 47. Temperature dependence of the dose for complete amorphization under 1.5 MeV Kr^+ irradiation. The data show two stages associated with defect annealing that decrease the rate of amorphization. For Stage-I ($T < 300$ K), D_0 is estimated from a data fit to be 0.35 dpa. For Stage-II ($T > 473$ K), D_0 is estimated to be 0.51 dpa. (Weber *et al.*, 1994.)

overlap of cascades. The effects of temperature on amorphization can then be modeled by kinetic processes with activation energies, E_a, that decrease the average cascade size (or average defect density) and, consequently, the rate at which the fraction of material damaged directly by the cascades accumulates at constant flux. Weber *et al.* (1994) have determined the activation energy, E_a, associated with each annealing stage. The activation energy for Stage-I defect annealing is 0.02 ± 0.01 eV, and the activation energy determined for Stage-II defect annealing is 0.31 ± 0.03 eV. In addition to the activation energies, the critical temperature, T_c, above which complete amorphization does not occur due to the dominance of Stage-II defect annealing over damage production, can be determined. The critical temperature, T_c, for zircon under these irradiation conditions is estimated to be 1100 K. The critical temperature for complete amorphization in zircon for other ions and energies may be different, as has been observed for $Ca_2La_8(SiO_4)_6O_2$ (Weber and Wang, 1994). The low value of the activation energy for Stage-I suggests that this annealing stage in zircon is associated with an intracascade, close-pair recombination process at low temperatures that is active up to 300 K where annealing is apparently complete and above which it is assumed that all close pairs recombine instantaneously. This process, which is insufficient to prevent complete amorphization, reduces the number of defects that survive each cascade at temperatures above 300 K. The activation energy for Stage-II annealing in zircon is similar to activation energies reported in other materials for an irradiation-enhanced epitaxial recrystallization process associated with irradiation-enhanced defect mobility; however, because the amorphization process in zircon is apparently due to the accumulation of a critical defect concentration from cascade overlap, the Stage-II annealing could also be due to additional defect recombination and annealing from the mobility of one or more defects above 473 K. Although the exact nature of the second-stage annealing process is not yet known, it competes with the irradiation-induced amorphization process and dominates above T_c, thus preventing complete amorphization. The activation energy for the second annealing stage, 0.31 eV, is considerably less than the activation energy, 3.6 eV, for thermal track annealing (epitaxial thermal recrystallization) in zircon (Sandhu *et al.*, 1990) or the activation energies, 5.1 and 6.6 eV, for bulk thermal recrystallization of fully amorphous zircon (Weber *et al.*, 1994). This type of thermal annealing analysis is essential in the study of crystalline ceramic waste forms in order to determine their final damage state as a function of the thermal history of the waste form.

Because of the important implications in determining the U/Pb systematics of zircons for geologic age dating, there are data on the increased loss of nuclides as a function of increasing degree of damage (Pidgeon *et al.*, 1966; Ewing *et al.*, 1982b; Tole, 1985; Suzuki, 1987; Sinha *et al.*, 1992), as well as efforts to relate these data to nuclear waste containment (Gentry *et al.*, 1982; Ludwig *et al.*, 1984; Sinha *et al.*, 1991). In a study of a suite of natural zircons with varying contents of uranium and thorium, Ewing *et al.* (1982b) found that over a dose range of 10^{19}–10^{21} α-decay events g^{-1},

there was an increase of one order of magnitude in the wt% of zircon that is dissolved and an increase in the leach rate from 2.9×10^{-8} to 2.3×10^{-7} g cm^{-2} day^{-1}. For completely metamict zircons (dose $\geq 10^{22}$ α-decay events g^{-1}) the leach rate was as high as 1.8×10^{-6} g cm^{-2} day^{-1}. These results are consistent with the observation that loss of nuclides or increased solubility is, at least in part, related to the increasing level of radiation damage (Pidgeon *et al.*, 1966; Tole, 1985; Sinha *et al.*, 1992).

This unusually complete data set for damage effects in zircon provides a basis for confirming the use of accelerated damage processes (actinide-doping of synthetic phases and heavy-particle irradiations) to study the long-term behavior of ceramics in a radiation field. Similar studies should be possible for members of the pyrochlore group as these minerals occur abundantly in nature and can be synthesized with a wide variety of actinide-bearing compositions (Chakoumakos and Ewing, 1985).

5.2.6. *Apatite.* Several rare-earth silicates with the apatite structure have been observed or proposed as actinide host phases in a nuclear waste glass (Weber *et al.*, 1979), supercalcine (McCarthy, 1977; McCarthy *et al.*, 1979), a glass ceramic waste form (Dé *et al.*, 1976a,b), and a cement waste form (Jantzen and Glasser, 1979). The apatites in nuclear waste solids are rare-earth silicate isomorphs of natural apatite, $Ca_{10}(PO_4)_6(F, OH)_2$, and generally have the composition: $Ca_{4-x}RE_{6+x}(SiO_4)_{6-y}(PO_4)_yO_2$ (where RE = La, Ce, Pr, Nd, Pm, Sm, Eu and Gd). The actinides readily substitute for the rare earths in this hexagonal crystal structure when it is present in the waste form.

As noted above in the study of a Cm-doped nuclear waste glass (Weber *et al.*, 1979; Weber and Roberts, 1983), crystallites of $Ca_3(Gd, Cm)_7(SiO_4)_5(PO_4)O_2$ transformed from a crystalline to an amorphous state as a result of α-decay of the incorporated Cm. The volume expansion associated with the amorphous transformation resulted in microfracturing of the simulated waste glass. Similarly, in a study of Cm-doped supercalcine (Rusin *et al.*, 1979), the originally crystalline apatite phase, $Ca_2(Re, Cm)_8(SiO_4)_6O_2$, transformed to an amorphous state due to α-decay. The unit cell of this phase was estimated to expand 2.5% before the amorphization process was complete. More specific details of the amorphization process in these phases, structural data, and the effects of amorphization on the integrity of these apatite phases could not be obtained from the study of these multiphase waste forms. Several natural apatite minerals with significant amounts of rare earths and silica are known to have an appreciable thoria content. These minerals are reported to be partially or fully metamict (amorphous) due to self-radiation damage from the alpha decay of the Th (Lindberg and Ingram, 1964; Haaker and Ewing, 1981), but detailed structural data on the effects of radiation in these minerals have not been reported. Studies of fission track dating and annealing (Koul, 1979) and ion-beam-induced amorphization (Wang *et al.*, 1994) in naturally occurring apatites have also been reported.

In order to understand the effects of self-radiation damage from α-decay on apatite phases in nuclear waste forms, an extensive study of single-phase, ^{244}Cm-doped $Ca_2(Nd)_8(SiO_4)_6O_2$ has been carried out (Weber, 1982, 1983, 1993; Wald and Weber, 1984; Weber and Matzke, 1986a,b). Radiation damage from α-decay in this material results in the simultaneous accumulation of simple structural defects (i.e. vacancies and interstitials on both the cation and anion sublattices) and amorphous regions that exhibit loss of long-range order. The amorphous regions eventually overlap to produce a completely amorphous state (Fig. 48). Consequently, as the radiation damage process proceeds, the fraction of crystalline material, f_c, decreases and the fraction of amorphous material, f_a, increases. For this material, Weber (1993) has shown that amorphization primarily occurs directly in the cascades of the recoil nuclei emitted during α-decay of Cm and that the increase in amorphous fraction with dose, D, is given by the expression:

$$f_a = 1 - \exp(-B_a D), \tag{5}$$

where B_a, the mass of amorphous material produced per decay event, has been determined to be 4.42×10^{-19} g. The change in amorphous fraction with dose for Cm-doped $Ca_2Nd_8(SiO_4)_6O_2$ is shown in Fig. 49. The crystalline fraction, $f_c = 1 - f_a$, is consistent with the observed decrease in diffracted X-ray intensity (Weber, 1993).

The accumulation of structural defects in the crystalline fraction of material results in an increase in unit-cell volume with cumulative dose. The unit-cell volume expansion, $\Delta V_{uc}/V_0$, which is shown in Fig. 50, follows the characteristic exponential behavior predicted by models (Nellis, 1977; Weber *et al.*, 1991a) for the accumulation of isolated structural defects and is given by the expression:

$$\Delta V_{uc} = A_{uc}[1 - \exp(-B_{uc} D)], \tag{6}$$

where A_{uc} is the relative unit-cell volume expansion at saturation and B_{uc} is the rate constant (per unit dose) for the simultaneous recombination of structural defects during irradiation. The values for A_{uc} and B_{uc}

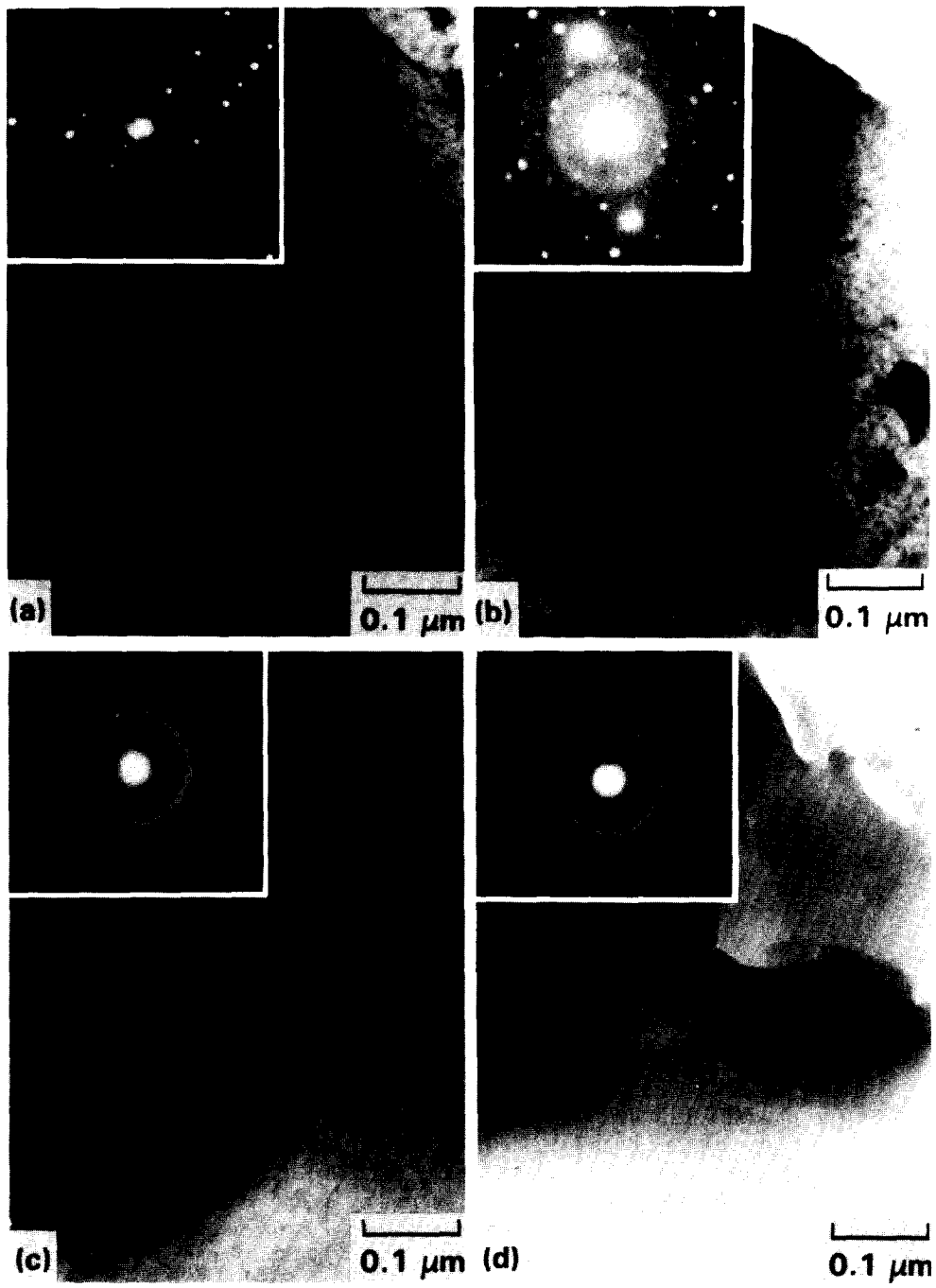

Fig. 48. Microstructural changes in Cm-doped $Ca_2Nd_8(SiO_4)_6O_2$ at (a) 0.76×10^{18}, (b) 1.32×10^{18}, (c) 2.02×10^{18}, and (d) 2.55×10^{18} α-decays g^{-1} (Weber, 1993).

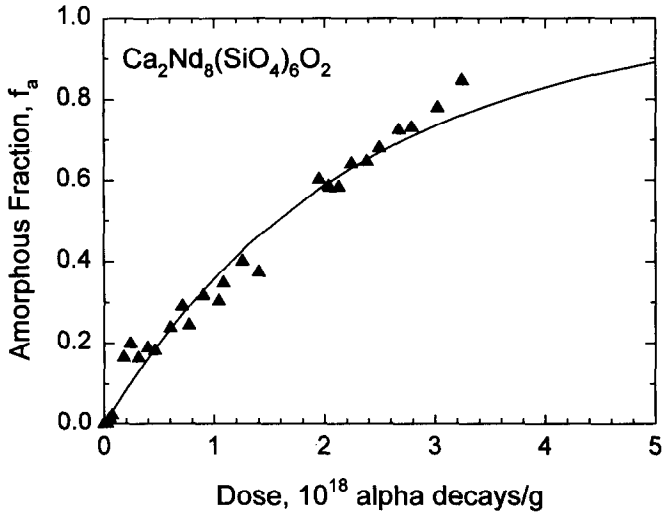

Fig. 49. Amorphous fraction, f_a, in Cm-doped $Ca_2Nd_8(SiO_4)_6O_2$ as a function of dose. After Weber (1993).

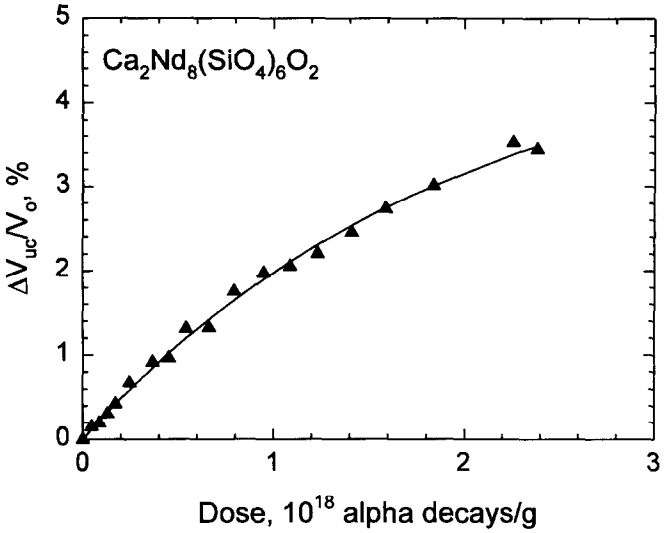

Fig. 50. Unit-cell volume expansion, $\Delta V_{uc}/V_0$, in Cm-doped $Ca_2Nd_8(SiO_4)_6O_2$ as a function of dose. After Weber (1993).

have been determined to be 4.95% and 5.08×10^{-19} g (Weber, 1993). The unit-cell expansion is anisotropic with the expansion of the unit cell along the a-axis about twice that along the c-axis. This anisotropic behavior is similar to that observed in ion-irradiated $Ca_2Nd_8(SiO_4)_6O_2$ and shown to be consistent with topological constraints on the changes in the polyhedral connectivity within this structure (Weber *et al.*, 1991).

The overall macroscopic swelling, $\Delta V_m/V_0$, which has contributions from the crystalline and amorphous fractions of material, is given by equation (4) (Weber, 1993). The overall macroscopic swelling determined experimentally from changes in immersion density is shown in Fig. 51 along with the predicted contributions from the crystalline and amorphous fractions. The solid curve is the sum of the crystalline and amorphous components (equation (4)) and provides an excellent fit to the data. The nearly equal contribution of the unit-cell expansion and amorphization process to the total macroscopic swelling at low doses is clearly shown as is the dominance of the amorphization process at high doses.

The normalized dissolution rate of Cm-doped $Ca_2Nd_8(SiO_4)_6O_2$ at 90°C in deionized water increased by about a factor of 10 as a result of

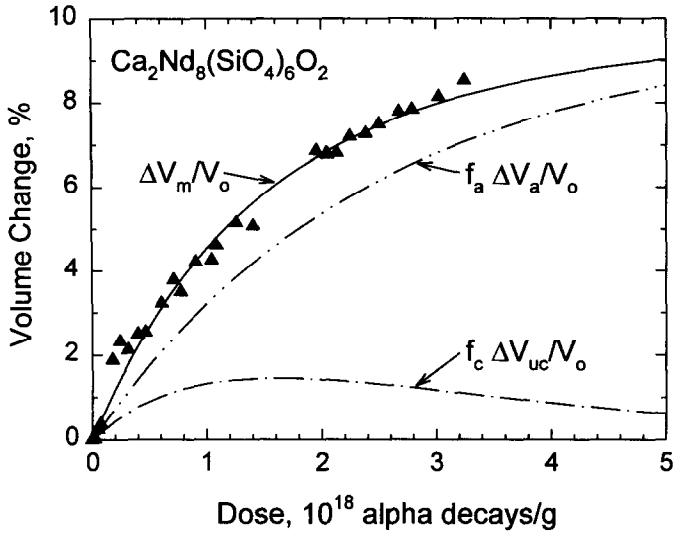

Fig. 51. Contributions of crystalline and amorphous components to the overall macroscopic swelling in Cm-doped $Ca_2Nd_8(SiO_4)_6O_2$ as a function of dose. After Weber (1993).

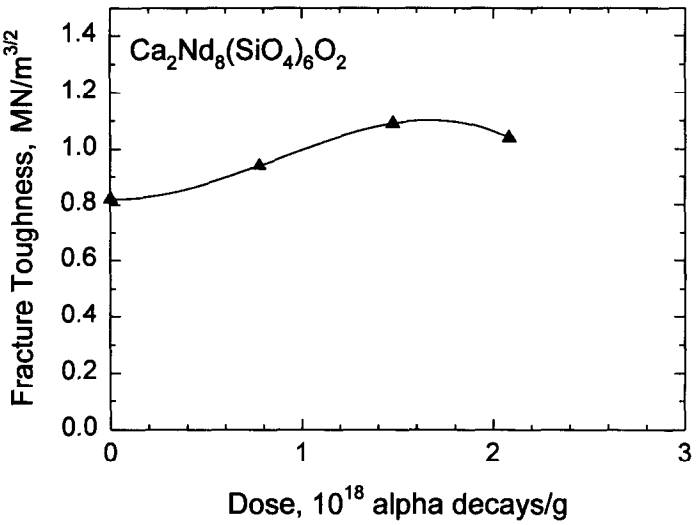

Fig. 52. Fracture toughness in Cm-doped $Ca_2Nd_8(SiO_4)_6O_2$ as a function of dose. After Weber and Matzke (1986b).

radiation-induced swelling and amorphization (Weber, 1983; Wald and Weber, 1984). The dissolution appears to occur congruently in this apatite phase. The mechanism for the enhanced dissolution of the amorphous phase is most likely associated with the high degree of disorder, broken bonds, and more open structure.

The fracture toughness in Cm-doped $Ca_2Nd_8(SiO_4)_6O_2$ increased with cumulative dose to a broad maximum and then decreases slightly (Fig. 52). This is similar to the behavior discussed above in pyrochlores and zirconolite (Clinard *et al.*, 1985; Weber *et al.*, 1986a). The increase in fracture toughness is attributed to the composite nature of the microstructure. At low to intermediate doses, the microstructure consists of amorphous tracks in a crystalline matrix, and this inhibits crack propagation and increases the fracture toughness. As the amorphous phase becomes the dominant matrix at high doses with remanent crystallites, the fracture toughness decreases slightly.

The activation energy for recrystallization from the fully amorphous state in Cm-doped $Ca_2Nd_8(SiO_4)_6O_2$ has been rigorously determined by Weber (1983) to be 3.1 ± 0.2 eV. Recrystallization of the

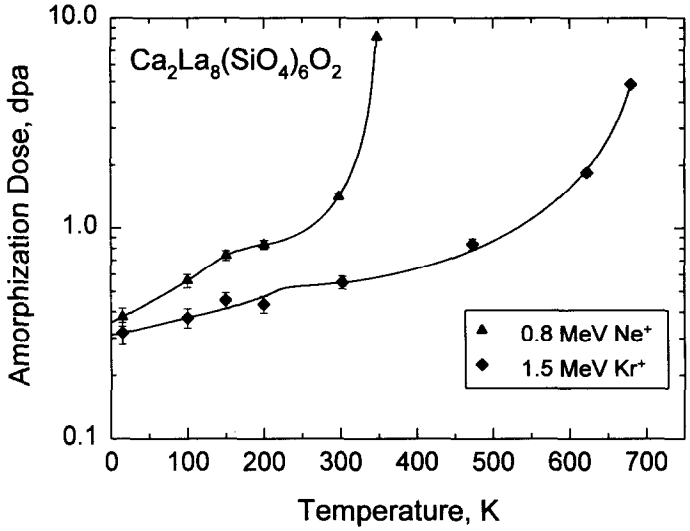

Fig. 53. Temperature dependence of the dose for complete amorphization in $Ca_2La_8(SiO_4)_6O_2$. After Weber and Wang (1994).

amorphous state occurs in a single exothermic recovery stage that releases 130 J g^{-1} of stored energy. Full recovery of the density and original apatite crystal structure occurs during this single-stage recrystallization process.

The temperature dependence of amorphization in single crystals of the apatite phase, $Ca_2La_8(SiO_4)_6O_2$, has been determined in recent ion-irradiation studies by Weber and Wang (1993, 1994). The dose for complete amorphization in $Ca_2La_8(SiO_4)_6O_2$ is independent of recoil-energy spectra at low temperatures (<15 K) and increases with temperature in two stages for both 0.8 MeV Ne^+ and 1.5 MeV Kr^+ irradiations (Fig. 53). The low-temperature stage (below 200 K) has an activation energy of 0.01 ± 0.003 eV and may be associated with close-pair recombination. The high-temperature stage (above 200 K) has an activation energy of 0.13 ± 0.02 eV and may be associated with irradiation-enhanced defect mobility. The critical temperature above which complete amorphization does not occur increased from 360 K for Ne^+ to 710 K for Kr^+. The amorphization dose below room temperature, 0.3–0.5 dpa for the heavier Kr^+ irradiations, is similar to the dose, 0.4 dpa, determined for full amorphization of Cm-doped $Ca_2Nd_8(SiO_4)_6O_2$ at room temperature. The dose for complete amorphization increases more rapidly for the lighter Ne^+ irradiations because of the larger fraction of recoverable defects and smaller cascades that are produced by the low-energy recoils.

5.2.7. *Monazite.* Monazite is unique, as it has been proposed as a single-phase ceramic to incorporate a wide variety of nuclear wastes, particularly those rich in actinides (Boatner *et al.*, 1980; Boatner and Sales, 1988). The mineral monazite is a mixed lanthanide orthophosphate, $LnPO_4$ (Ln = La, Ce, Nd, Gd, etc.), that often contains significant amounts of Th and U (up to 27 wt% combined). As a result, many natural monazites have been subjected to significant α-decay event damage over geologic time (some samples are up to 2 billion yr of age). In spite of the large radiation doses received by natural monazites, Ewing (1975) and Ewing and Haaker (1980) have noted that monazite is always found in the crystalline state. The apparent resistance of natural monazites to radiation-induced amorphization was an important factor in the initial proposal of monazite ceramics as potential candidates for the immobilization of nuclear wastes.

Karioris *et al.* (1981) have established that natural monazite (Ce, La, Y)PO_4 can be readily transformed to an amorphous state by irradiation with 3 MeV Ar^+ ions to moderate doses. Gowda (1982) determined that under 3 MeV Ar^+ ion irradiation the damage cross-section for amorphization was 0.54 ± 0.10 nm^2 for natural monazite and 0.56 ± 0.08 nm^2 for synthetic monazite, $CePO_4$. In natural monazite that was irradiated to a partially amorphous state (diffraction intensities were reduced by one-third), complete recovery of the fully crystalline state occurred after annealing at 300°C for 20 hr (Karioris *et al.*, 1981). The apparent stability of natural monazite is attributed to this relatively low temperature of recovery of the radiation damage. Differential scanning calorimetry (DSC) measurements of natural (Gowda, 1982) and synthetic (Gowda, 1982; Ehlert *et al.*, 1983)

monazites irradiated with 3 MeV Ar^+ ions have been performed. In natural monazite, the stored energy released during recrystallization was 33 J g^{-1}, the peak in the release rate occurred at 450°C, and the activation energy associated with the recovery process was estimated to be 2.77 eV. For synthetic monazite, $CePO_4$, the stored energy release was 30.5 ± 1.3 J g^{-1}, the temperature for maximum release was slightly lower at 370°C, and the activation energy was estimated to be 2.7 ± 0.3 eV.

Results by Sales *et al.* (1983) suggest that the leach rate of the host matrix of a synthetic monazite, $LaPO_4$, containing simulated waste remains low even after the material has been transformed to an amorphous state by irradiation with 250 keV Bi^+ ions. However, work by Eyal and Kaufman (1982) on natural monazite indicate that there is a preferential dissolution of the radionuclide daughter-products, ^{234}U, ^{230}Th and ^{228}Th, by factors of between 1.1 and 10 relative to the structurally incorporated parent isotopes ^{238}U and ^{232}Th. This isotopic fractionation is attributed to radiation damage in the tracks of the recoil nuclei emitted during α-decay of the parent isotopes. While there have been some concerns regarding these results (Boatner and Sales, 1988), the increases in dissolution rates are similar to those observed in other actinide-host phases.

5.2.8. *Sphene (=titanite).* Sphene, $CaTi(SiO_4)O$ (the proper mineral name is titanite) is a prominent phase in the sphene-glass ceramic. Sphene is an actinide-host (the structure will not accommodate Cs; but will accommodate minor concentrations of Sr), thus damage due to α-decay of actinides is an issue of concern.

Although there have been studies using heavy particle irradiations, 3 MeV Ar^+ and 280 keV Bi^{2+} (Vance *et al.*, 1984; Stevanovic *et al.*, 1989) and studies using γ-radiation, 200 keV electrons (Vance *et al.*, 1986), most work has focused on natural sphenes which contain U and Th (Vance and Metson, 1985; Hawthorne *et al.*, 1991). Up to doses of 2×10^{27} e m^{-2} there was no evidence of structural damage. The Ar^+ irradiation indicated that a fluence of 7×10^{18} α-decay events g^{-1} was required to produce complete metamictization. This is in good agreement with the value of 5×10^{18} α-decay events g^{-1} required to reach the metamict state in natural sphenes. Leaching experiments on damaged sphenes indicated that the increase in dissolution rate was no more than a factor of five; however, leaching experiments on Bi^{2+} implanted sphene and sphene-ceramics to doses of 6×10^{15} ions cm^{-2} resulted in an order of magnitude increase in the leach rate (Stevanovic *et al.*, 1989).

The study of natural sphenes by Hawthorne *et al.* (1991) was unusual in that a wide variety of techniques (electron microprobe analysis, powder X-ray diffraction, single-crystal X-ray diffraction, infrared spectroscopy, Mössbauer spectroscopy, magic-angle spinning nuclear magnetic resonance spectroscopy, high-resolution transmission electron microscopy, extended X-ray absorption spectroscopy and X-ray absorption near edge spectroscopy) were used to monitor structural changes with increasing α-decay event dose. The results substantiated the model for damage in-growth outlined by Murakami *et al.* (1991) and illustrated in Fig. 40. The work did suggest that the damage process is accompanied by the reduction of Fe^{3+} to Fe^{2+}, which resides mainly in the aperiodic domains. Valence changes of this type can have significant effects on the solubility of certain actinides (e.g. uranium and plutonium) particularly when they are partitioned into the aperiodic domains.

6. FUTURE RESEARCH NEEDS

The issues surrounding the permanent disposal of nuclear waste are both political and technological. The delays in winning public acceptance for current nuclear waste policy and technology threaten shutdown of current commercial nuclear power plants and hamper acceptance of new nuclear power reactors, both of which could play a vital role in the U.S. strategy to minimize human impact on global processes, such as CO_2 emissions. Thus, the successful demonstration that nuclear waste can be disposed of safely is an important step in the development of nuclear power. One of the critical barriers to radionuclide migration to the biosphere is the nuclear waste form; however, the physical and chemical properties of the waste form may change dramatically as a result of irradiation damage. Additionally, radiation–solid interactions might also affect important geochemical processes that are relied upon for nuclide retardation (e.g. sorption of radionuclides on clays, radiolysis of transporting fluids, radiolytic oxidation and corrosion of UO_2, and radiation damage in secondary phases which by their solubilities control radionuclide concentrations in the ground water). Unfortunately, due to the state of understanding and limited research in this area (Weber *et al.*, 1991b), the nature, dimensions, and implications of these radiation effects remain elusive, particularly with regard to how these effects impact regulatory criteria for radionuclide release.

More specifically, certain topics require immediate attention:

1. *The effect of ionizing radiation on borosilicate waste glasses*, particularly the possibility and impact of radiolytic decomposition and bubble formation, are neither well-understood or under current investigation. Studies are needed to determine the temperature and dose rate dependence of these phenomena and their impact on radionuclide release rates. A thorough understanding of the synergistic effects of ionizing and displacive radiation on waste glass behavior is needed. This should include the effects of radiolytic decomposition and microstructural evolution on increased surface area and leachability, which determine the release rate of radionuclides under unsaturated conditions. Also, there are only limited (and in most cases questionable) data on the effect of displacive events (e.g. α-recoil damage) on the leachability of borosilicate waste glasses.

2. *Computer simulation of displacement processes.* The final state of a radiation-damaged glass or ceramic is a result of the temperature-dependent balance between damage and annealing kinetics. The initial damage stage can only be ascertained by models of collision cascade formation (these events occur in periods of 10^{-10}–10^{-12} sec). Very little is known about the process of collision cascade formation in glasses and ceramics, as compared to the state of knowledge for metals. As an example, we have only very limited data on the displacement energies of cations in complex, multi-atom ceramics which are typical of nuclear waste form assemblages.

3. *Radiation-induced periodic-to-aperiodic transformations (amorphization).* Little is known of the mechanisms of crystalline-to-amorphous transformations, particularly in ceramics. There has been no systematic evaluation of the role of structure-type, bond-type, bond-strength and structural topology on this phenomenon. This knowledge is necessary for the efficient evaluation of crystalline ceramic waste phases and their response to different types and doses of radiation. This mechanistic understanding of the amorphization process is particularly important in extrapolating the long-term behavior of ceramics and glasses in a radiation field.

4. *Structure of the aperiodic state.* Preliminary research has demonstrated that there are many possible structures and topologies in aperiodic materials. These structural variations may reflect the mode of amorphization (e.g. radiation-induced, pressure-induced or quenched from a melt), and the aperiodic structure may change with increasing level of damage. These changes can have significant effects on the behavior (e.g. leach rate, devitrification and mechanical properties) of aperiodic phases, such as the borosilicate glass waste form.

Acknowledgements—The authors gratefully acknowledge the support that they have received from the Office of Basic Energy Sciences of the U.S. Department of Energy (WFC: contract #W-7405-ENG-36; RCE: grant #DE-FG03-93ER45498; WJW contract #DE-AC06-76RLO 1880). The BES support of basic, interdisciplinary research on radiation effects in minerals and ceramics has contributed greatly to the present understanding of radiation damage effects in nuclear waste forms. F. W. Clinard, Jr expresses his appreciation for the contributions of his coworkers in the Materials Science and Technology Division at Los Alamos National Laboratory; W. J. Weber acknowledges the contributions of his coworkers at the Pacific Northwest Laboratory; R. C. Ewing thanks his colleagues and students for their collaboration in the field of radiation damage effects in minerals and ceramics and the good times at El Patio. All errors of omission and interpretations of the data in the literature remain those of the authors. Finally, R. C. Ewing thanks his colleagues in the Department of Earth Sciences of Aarhus University for their support during his visit in 1994 during which most of the writing of this review was completed.

REFERENCES

Adelhelm C., Bauer C., Gahlert S. and Ondracek G. (1988) TiO_2—a ceramic matrix. In: *Radioactive Waste Forms for the Future*, Lutze W. and Ewing R. C. (Eds), pp. 393–426. North-Holland, Amsterdam.

Antonini M., Lanza F. and Manara A. (1979) Simulations of radiation damage in glasses. In: *Proceedings of International Symposium on Ceramics in Nuclear Waste Management*, Chikalla T. D. and Mendel J. E. (Eds), CONF-790420, p. 289. National Technical Information Service.

Antonini M., Camagni P., Lanza F. and Manara A. (1980) Atomic displacements and radiation damage in glasses incorporating HLW. In: *Scientific Basis for Nuclear Waste Management, Vol. 2*, Northrup, Jr C. J. M. (Ed.), pp. 127–133. Plenum Press, New York.

Arnold G. W., Northrup C. J. M. and Bibler N. E. (1982) Near-surface leaching studies of Pb-implanted Savannah River Plant waste glass. In: *Scientific Basis for Nuclear Waste Management-V*, Lutze W. (Ed.), pp. 357–368. North-Holland, New York.

Arnold G. W. (1985) Ion implantation damage processes in nuclear waste glass and other silicate glasses. In: *Scientific Basis for Nuclear Waste Management VIII*, Jantzen C. M., Stone J. A. and Ewing R. C. (Eds), pp. 617–622. Materials Research Society, Pittsburgh, Pennsylvania.

Arnold G. W. (1988) Ion-implantation-induced stress in glasses: Variation of damage mode efficiency with changes in glass structure. *Nucl. Instrum. Meth. Phys. Res.* **B32,** 504–507.

Ball C. J. and Woolfrey J. L. (1983) The effect of neutron irradiation on the structure of barium hollandite. *J. Nucl. Mater.* **118,** 159–164.

Babsail L., Hamelin N. and Townsend P. D. (1991) Helium-ion implanted waveguides in zircon. *Nucl. Instrum. Meth. Phys. Res.* **B59/60,** 1219–1222.

Banba T., Matsumoto S., Muraoka S., Yamada K., Saito M., Ishikawa H. and Sasaki N. (1994) Effects of alpha decay on the properties of actual nuclear waste glass. In: *Scientific Basis for Nuclear Waste Management XVIII*, Murakami T. and Ewing R. C. (Eds), Materials Research Society, Pittsburgh, PA (in press).

Barry J. C., Hutchison J. L. and Segall R. L. (1983) Ion-beam damage in hollandite. *J. Mater. Sci.* **18,** 1421–1425.

Beall G. W., Boatner L. A., Mullica D. F. and Milligan W. O. (1981) The structure of cerium orthophosphate, a synthetic analogue of monazite. *J. Inorganic Nucl. Chem.* **43,** 101–105.

Bibler N. E. and Kelley J. A. (1978) Effect of internal alpha radiation on borosilicate glass containing Savannah River Plant waste. Report No. DP-1482, Savannah River Laboratory, Aiken, SC.

Bibler N. E. (1982) Effects of alpha, gamma, and alpha-recoil radiation on borosilicate glass containing Savannah River Plant defense high-level nuclear waste. In: *Scientific Basis for Nuclear Waste Management*, Topp S. V. (Ed.), Materials Research Society Symposia Proceedings, Vol. 6, pp. 681–687. North-Holland, New York.

Bibler N. E., Tosten M. H. and Beam D. C. (1990) Recent results on the effect of gamma irradiation on the durability and microstructure of DWPF glass. In: *Proceedings of the High-Level Radioactive Waste Management Conference*, Vol. 2, pp. 1103–1109. American Nuclear Society.

Boatner L. A., Beall G. W., Abraham M. M., Finch C. B., Huray P. G. and Rappaz M. (1980) Monazite and other lanthanide orthophosphates as alternative actinide waste forms. In: *Scientific Basis for Nuclear Waste Management*, Northrup, Jr, C. J. M. (Ed.), Vol. 2, pp. 289–296. Plenum Press, New York.

Boatner L. A. and Sales B. C. (1988) Monazite. In: *Radioactive Waste Forms for the Future*, Lutze W. and Ewing R. C. (Eds), pp. 495–464. North-Holland, Amsterdam.

Bonniaud R. A., Jacquet Francillon N. R., Laude F. L. and Sombret C. G. (1979) Glasses as materials used in France for management of high-level wastes. In: *Ceramics in Nuclear Waste Management*, Chikalla T. D. and Mendel J. E. (Eds), CONF-790420, pp. 57–61. National Technical Information Service, Springfield, VA.

Burns W. G., Hughes A. E., Marples J. A. C., Nelson R. S. and Stoneham A. M. (1982a) Effects of radiation on the leach rates of vitrified radioactive waste. *J. Nucl. Mater.* **107,** 245–270.

Burns W. G., Hughes A. E., Marples J. A. C., Nelson R. S. and Stoneham A. M. (1982b) Effects of radiation damage and radiolysis on the leaching of vitrified waste. In: *Scientific Basis for Nuclear Waste Management-V*, Lutze W. (Ed.), pp. 339–348. North-Holland, New York.

Carter G. and Webb R. (1979) The accumulation of amorphousness as a function of irradiation fluence in a composite model of disorder production. *Radiation Effects Lett.* **43,** 19–24.

Chakoumakos B. C. (1984) Systematics of the pyrochlore structure type, ideal $A_2B_2X_6Y$. *J. Solid State Chem.* **53,** 120–129.

Chakoumakos B. C. and Ewing R. C. (1985) Crystal chemical constraints on the formation of actinide pyrochlores. In: *Scientific Basis for Nuclear Waste Management VIII*, Jantzen C. M., Stone J. A. and Ewing R. C. (Eds), Materials Research Society Proceeding, Vol. 44, pp. 641–646. Pittsburgh, Pennsylvania.

Chakoumakos B. C. (1986) Pyrochlore. In: *McGraw-Hill Yearbook of Science and Technology 1987*, Parker S. P. (Ed.), pp. 393–395. McGraw-Hill, New York.

Chakoumakos B. C., Murakami T., Lumpkin G. R. and Ewing R. C. (1987) Alpha-decay induced fracturing in zircon: the transition from the crystalline to the metamict state. *Science* **236,** 1556–1559.

Chakoumakos B. C., Oliver W. C., Lumpkin G. R. and Ewing R. C. (1991) Hardness and elastic modulus of zircon as a function of heavy-particle irradiation dose—I. *In situ* α-decay event damage. *Radiation Effects and Defects in Solids* **118,** 393–403.

Clinard F. W., Jr, Douglass D. L. and Woods R. (1970). Helium release from alpha-bombarded ThO_2. In: *Plutonium 1970 and Other Actinides*, Miner W. N. (Ed.), pp. 585–595. The Metallurgical Society, AIME.

Clinard F. W., Jr, Peterson D. E. and Rohr D. L. (1984a) Self-irradiation effects in ^{238}Pu-substituted zirconolite—I. Temperature dependence of damage. *J. Nucl. Mater.* **126,** 245–254.

Clinard F. W., Jr, Rohr D. L. and Roof R. B. (1984b) Structural damage in a self-irradiated zirconolite-based ceramic. *Nucl. Instrum. Meth. Phys. Res.* **B1,** 581–586.

Clinard F. W., Jr, Tucker D. S., Hurley G. F., Kise C. D., Rankin J. (1985a) Irradiation-induced reduction of microcracking in zirconolite. In: *Scientific Basis for Nuclear Waste Management VIII*, Jantzen C. M., Stone J. A. and Ewing R. C. (Eds), Materials Research Society Symposium Proceedings, Vol. 44, pp. 664–670. Materials Research Society, Pittsburgh.

Clinard F. W., Jr, Livak R. J., Hobbs L. W. and Rohr D. L. (1985b) Structural changes in ^{238}Pu-substituted zirconolite on recovery from the metamict state. In: *Scientific Basis for Nuclear Waste Management IX*, Werme L. O. (Ed.), Material Research Society Symposium Proceedings, Vol. 50, pp. 372–378. Materials Research Society, Pittsburgh.

Clinard F. W., Jr (1986) Review of self-irradiation effects in Pu-substituted zirconolite. *Ceram. Bull.* **65**(8), 1181–1187.

Clinard F. W., Jr, Foltyn E. M. and Ewing R. C. (1991) Stored energy in natural zirconolite and its synthetic counterpart after alpha recoil self-irradiation damage. *J. Nucl. Mater.* **185,** 202–207.

Coghlan W. A. and Clinard F. W., Jr (1988) Modeling of irradiation-induced amorphization in a titanate ceramic. *J. Less-Common Metals* **140,** 255–265.

Cousens D. R. and Myhra S. (1983) The effects of ionizing radiation on HLW glasses. *J. Non-Crystal. Solids* **54,** 345–365.

Day D. H., Hughes A. E., Leake J. W., Marples J. A. C., Marsh G. P., Rae J. and Wade B. O. (1985) The management of radioactive wastes. *Rep. Prog. Phys.* **48,** 101–169.

Dé A. K., Luckscheiter B, Lutze W., Malow G. and Schiewer E. (1976a) Development of glass ceramics for the incorporation of fission products. *Ceram. Bull.* **55,** 500–503.

Dé A. K., Luckscheiter B, Lutze W., Malow G., Schiewer E. and Tymochowicz S. (1976b) Fixation of fission products in glass ceramics. In: *Management of Radioactive Wastes from the Nuclear Fuel Cycle, Vol. II*, IAEA-SM-207, pp. 63–73. International Atomic Energy Agency, Vienna.

DeNatale J. F. and Howitt D. G. (1984) A mechanism for radiation damage in silicate glasses. *Nucl. Instrum. Meth. Phys. Res.* **B1,** 489–497.

DeNatale J. F. and Howitt D. G. (1985) The gamma-irradiation of nuclear waste glasses. *Radiation Effects* **91,** 89–96.

DeNatale J. F. and Howitt D. G. (1987) Importance of ionization damage to nuclear waste storage in glass. *Am. Ceram. Soc. Bull.* **66,** 1393–1396.

DeNatale J. F., Howitt D. G. and Arnold G. W. (1986) Radiation damage in silicate glass. *Radiation Effects* **98,** 63–70.

Dosch R. G., Headley T. J. and Hlava P. (1984) Crystalline titanate ceramic nuclear waste forms: processing and microstructure. *J. Am. Ceram. Soc.* **67,** 354–361.

Dosch R. G., Northrup C. J. and Headley T. J. (1985) Crystalline titanate ceramic nuclear waste forms: leaching and radiation damage. *J. Am. Ceram. Soc.* **68,** 330–337.

Dran J. C., Langevin Y., Maurette M., Petit J. C. and Vasent B. (1982) Leaching behavior of ion-implanted simulated HLW glasses and tentative prediction of their alpha-recoil aging. In: *Scientific Basis for Nuclear Waste Management*, Topp, S. V. (Ed.), pp. 651–659. North-Holland, New York.

Ehlert T. C., Gowda K. A., Karioris F. G. and Cartz L. (1983) Differential scanning calorimetry of heavy ion bombarded synthetic monazite. *Radiation Effects* **70,** 173–181.

Ellsworth S., Navrotsky A. and Ewing R. C. (1994) Energetics of radiation damage in natural zircon ($ZrSiO_4$). *Phys. Chem. Minerals* **21,** 140–149.

Evans J. P. and Marples J. A. C. (1985) The preparation of fully active Synroc and its radiation stability—Progress report, June, 1985. Report No. AERE-G3592, Harwell Laboratory, Harwell, UK.

Evans J. P., Boult K. A., Paige E. L. and Marples J. A. C. (1986) The preparation of fully active Synroc and its radiation stability—Progress report, July, 1986. Report No. AERE-G4010, Harwell Laboratory, Harwell, UK.

Ewing R. C. (1975) The crystal chemistry of complex niobium and tantalum oxides—IV. The metamict state. *Am. Mineral.* **60,** 728–733.

Ewing R. C. and Haaker R. F. (1980) The metamict state: implications for radiation damage in crystalline waste forms. *Nucl. Chem. Waste Mgmt* **1,** 51–57.

Ewing R. C., Haaker R. F., Headley T. J. and Hlava P. (1982a) Zirconolites from Sri Lanka, South Africa and Brazil. In: *Scientific Basis for Nuclear Waste Management, IV*, Materials Research Society Proceedings, Vol. 6, pp. 249–256, Topp S. V. (Ed.). North-Holland, New York.

Ewing R. C., Haaker R. F. and Lutze W. (1982b) Leachability of zircon as a function of alpha-dose. In: *Scientific Basis for Radioactive Waste Management—V*, Lutze W. (Ed.), pp. 389–397. North-Holland, New York.

Ewing R. C. and Headley T. J. (1983) Alpha-recoil damage in natural zirconolite ($CaZrTi_2O_7$). *J. Nucl. Mater.* **119,** 102–109.

Ewing R. C. (1983) Transition from the crystalline to the metamict state in zirkelite. Annual Meeting of the Geological Association of Canada and the Mineralogical Association of Canada, Victoria, p. A21.

Ewing, R. C., Chakoumakos B. C., Lumpkin G. R. and Murakami T. (1987) The metamict state. *Mater. Res. Soc. Bull.* **12,** 58–66.

Ewing R. C., Chakoumakos B. C., Lumpkin G. R., Murakami T., Greegor R. B. and Lytle F. W. (1988) Metamict minerals: natural analogues for radiation damage effects in ceramic nuclear waste forms. *Nucl. Instruments Meth. Phys. Res.* **B32,** 487–497.

Ewing R. C. (1988) Novel waste forms. In: *Radioactive Waste Forms for the Future*, Lutze W. and Ewing R. C. (Eds), pp. 589–634. North-Holland, Amsterdam.

Ewing R. C. (1992a) Preface. *J. Nucl. Mater.* **190,** vii–x.

Ewing R. C. (1992b) Special issue on Nuclear Waste Forms. *J. Nucl. Mater.* **190,** 1–347.

Ewing R. C. and Wang L. M. (1992) Amorphization of zirconolite: alpha-decay event damage versus krypton ion irradiation. *Nucl. Instruments Meth. Phys. Res.* **B65,** 319–323.

Ewing R. C. (1994) The metamict state: 1993—the Centennial. *Nucl. Instruments Meth. Phys. Res.* **B91,** 22–29.

Exarhos G. R. (1984) Induced swelling in radiation damaged $ZrSiO_4$. *Nucl. Instruments Meth. Phys. Res.* **B1,** 538–541.

Eyal Y. and Kaufman A. (1982) Alpha-recoil damage in monazite: preferential dissolution of radiogenic actinide isotopes. *Nucl. Technol.* **58,** 77–83.

Eyal Y. and Fleischer R. L. (1985) Preferential leaching and the age of radiation damage from alpha decay in minerals. *Geochimica Cosmochimica Acta* **49,** 1155–1164.

Eyal Y., Lumpkin G. R. and Ewing R. C. (1985) Alpha-recoil effect on the dissolution of betafite: rapid natural annealing of radiation damage within a metamict phase. In: *Scientific Basis for Nuclear Waste Management IX*, Werme L. O. (Ed.), pp. 379–386. Materials Research Society, Pittsburgh.

Eyal Y., Lumpkin G. R. and Ewing R. C. (1987) Natural annealing of alpha-recoil damage in metamict minerals of the thorite group. In: *Scientific Basis for Nuclear Waste Management X*, Bates J. K. and Seefeldt W. B. (Eds), pp. 635–643. Materials Research Society, Pittsburgh.

Eyal Y. and Ewing R. C. (1993) Impact of alpha-recoil damage on dissolution of thoriated glass. In: *Proceedings of the International Conference on Nuclear Waste Management and Environmental Remediation, Vol. 1, Low and Intermediate Level Radioactive Waste Management*, Alexandre D., Baker R., Kohout R. and Marek J. (Eds), Sponsored by the American Society of Mechanical Engineers, Prague, Czech Republic, 5–11 September, 191–196.

Farges F. and Calas G. (1991) Structural analysis of radiation damage in zircon and thorite: an X-ray absorption spectroscopic study. *Am. Mineral.* **76,** 60–73.

Farges F., Ewing R. C., Brown G. E., Jr (1993) The structure of aperiodic, metamict $(Ca,Th)ZrTiO_2O_7$ (zirconolite): an EXAFS study of the Zr, Th, and U sites. *J. Mater. Res.* **8,** 1983–1995.

Farges F. (1994) The structure of metamict zircon: a temperature-dependent EXAFS study. *Phys. Chem. Minerals* **20,** 504–514.

Feng X., Wronkiewicz D. J., Bates J. K., Brown N. R., Buck E. C., Gong M. and Ebert W. L. (1994) Glassy slags as novel waste forms for remediating mixed wastes with high metal contents. *Waste Mgmt '94* (in press).

Foltyn E. M., Clinard F. W., Jr, Rankin J. and Peterson D. E. (1985) Self-irradiation effects in ^{238}Pu-substituted zirconolite: II. Effect of damage microstructure on recovery. *J. Nucl. Mater.* **136,** 97–103.

Gentry R. V., Sworski T. J., McKown H. S., Smith D. H., Eby R. E. and Christie W. H. (1982) Differential lead retention in zircons: implications for nuclear waste containment. *Science* **216,** 296–297.

Gentry R. V. (1984) Lead retention in zircons. *Science* **223,** 835.

Gowda K. A. (1982) Heavy ion bombardment of zircon, monazite and other crystal structures. Ph.D. thesis, Department of Mechanical Engineering, Marquette University, Milwaukee, WI.

Gray W. J. (1982) Fission product transmutation effects on high-level radioactive waste forms. *Nature* **296,** 547–548.

Grover J. R. (1973) Glasses for the fixation of high-level radioactive wastes. In: *Management of Radioactive Wastes from Fuel Reprocessing* (Organisation for Economic Co-operation and Development, Paris), pp. 593–611.

Greegor R. B., Lytle F. W., Ewing R. C. and R. F. Haaker (1984a) Ti-site geometry in metamict, annealed and synthetic complex Ti-Nb-Ta oxides by X-ray absorption

spectroscopy. *Nucl. Instruments Meth. Phys. Res.* **B1,** 587–594.

Greegor R. B., Lytle F. W., Ewing R. C. and Haaker F. F. (1984b) EXAFS studies of metamict minerals. In: *Proc. 3rd Int. EXAFS Confs.*, Hodgson K. O., Hedman D. and Penner-Hahn J. E. (Eds), pp. 343–348. Springer, New York.

Greegor R. B., Lytle F. W., Chakoumakos B. C., Lumpkin G. R. and Ewing R. C. (1985a) An investigation of metamict and annealed natural pyrochlores by X-ray absorption spectroscopy. In: *Scientific Basis for Nuclear Waste Management VIII*, Jantzen C. M., Stone J. A. and Ewing R. C. (Eds), pp. 655–662. Materials Research Society, Pittsburgh.

Greegor R. B., Lytle F. W., Chakoumakos B. C., Lumpkin G. R. and Ewing R. C. (1985b) An investigation of uranium L-edges of metamict and annealed pyrochlore. In: *Scientific Basis for Nuclear Waste Management IX*, Werme L. O. (Ed.), pp. 387–392. Materials Research Society, Pittsburgh.

Greegor R. B., Lytle F. W., Chakoumakos B. C., Lumpkin G. R. and Ewing R. C. (1986) Structural investigation of metamict minerals using X-ray absorption spectroscopy. *Abstracts of the 14th General Meeting of the International Mineralogical Assoc.*, Stanford, CA, p. 114.

Greegor R. B., Lytle F. W., Chakoumakos B. C., Lumpkin G. R., Ewing R. C., Spiro C. and Wong J. (1987) An investigation of the Ta site in radiation damaged natural pyrochlores by X-ray absorption spectroscopy. In: *Scientific Basis for Nuclear Waste Management X*, Bates J. K. and Seefeldt W. B. (Eds), pp. 645–658. Materials Research Society, Pittsburgh.

Greegor R. B., Lytle F. W., Livak R. J. and Clinard J. W., Jr (1988) X-ray spectroscopic investigation of Pu-substituted zirconolite. *J. Nucl. Mater.* **152,** 270–277.

Haaker R. F. and Ewing R. C. (1981) Naturally occurring crystalline phases: analogues for radioactive waste forms. Report No. PNL-3505 (Pacific Northwest Laboratory, Richland, WA).

Hall A. R., Dalton J. T., Hudson B. and Marples J. A. C. (1976) Development and radiation stability of glasses for highly radioactive wastes. In: *Management of Radioactive Wastes from the Nuclear Fuel Cycle, Vol. II, IAEA-SM-207*, pp. 3–14. International Atomic Energy Agency, Vienna.

Harker A. B. (1988) Tailored ceramics. In: *Radioactive Waste Forms for the Future*, Lutze W. and Ewing R. C. (Eds), pp. 335–392. North-Holland, Amsterdam.

Hatch L. P. (1953) Ultimate disposal of radioactive wastes. *Am. Sci.* **441,** 410–421.

Hawthorne F. C., Groat L. A., Raudsepp M. and 16 authors (1991) Alpha-decay damage in titanite. *Am. Mineral.* **76,** 370–396.

Hayward P. J. (1988) Glass-ceramics. In: *Radioactive Waste Forms for the Future*, Lutze W. and Ewing R. C. (Eds), pp. 427–494. North-Holland, Amsterdam.

Headley T. J., Arnold G. W. and Northrup C. J. M. (1982) Dose-dependence of Pb-ion implantation damage in zirconolite, hollandite, and zircon. In: *Scientific Basis for Radioactive Waste Management V, Materials Research Society Proceedings*, Vol. 11, pp. 379–388, Lutze, W. (Ed.). North-Holland, New York.

Hench L. L., Clark D. E. and Campbell J. (1984) High level waste immobilization forms. *Nucl. Chem. Waste Mgmt* **5,** 149.

Heuer J. P. (1987) Gamma irradiation of nuclear waste glasses. M.S. thesis, Department of Mechanical Engineering, University of California, Davis.

Heuer J. P., Chan H. W., Howitt D. G. and DeNatale J. F. (1986) An accurate simulation of radiation damage in a nuclear waste repository. In: *Advances in Ceramics, Vol. 20, Nuclear Waste Management II*, Clark D. E., White W. B. and Machiels A. J. (Eds), pp. 175–180. The American Ceramic Society, Columbus, OH.

Hobbs L. W. and Pascucci M. R. (1980) Radiolysis and defect structure in electron-irradiated α-quartz. *J. Physique* **41,** C6-237-241.

Hogarth D. D. (1977) Classification and nomenclature of the pyrochlore group. *Am. Mineral.* **62,** 403–410.

Holland H. D. and Gottfried D. (1955) The effect of nuclear radiation on the structure of zircon. *Acta Crystall.* **8,** 291–300.

Howitt D. G., Chan H. W., DeNatale J. F. and Heuer J. P. (1991) Mechanism for the radiolytically induced decomposition of soda-silicate glasses. *J. Am. Ceram. Soc.* **74,** 1145–1147.

Illman D. L. (1993) Researchers take up environmental challenge at Hanford. *Chem. Engng News* **71**(25), 9–21.

Inagaki Y., Furuya H., Idemitsu K., Banba T., Matsumoto S. and Muraoka S. (1992) Microstructure of simulated high-level waste glass doped with short-lived actinides, ^{238}Pu and ^{244}Cm. In: *Scientific Basis for Nuclear Waste Management XV*, Sombret C. G. (Ed.), pp. 199–206. Materials Research Society, Pittsburgh, PA.

Inagaki Y., Furuya H., Ono Y., Idemitsu K., Banba T., Matsumoto S. and Muraoka S. (1993) Effect of α-decay on mechanical properties of simulated nuclear waste glass. In: *Scientific Basis for Nuclear Waste Management XVI*, Interrante C. G. and Pabalan R. T. (Eds), pp. 191–198. Materials Research Society, Pittsburgh, PA.

Janeczek K. and Ewing R. C. (1991) X-ray powder diffraction study of annealed uraninite. *J. Nucl. Mater.* **185,** 66–77.

Jantzen C. M. and Glasser F. P. (1979) Stabilization of nuclear waste constituents in portland cement. *Ceram. Bull.* **58,** 459–466.

Jantzen C. M., Bickford D. F. and Karraker D. G. (1984) Time-temperature-transformation kinetics in SRL waste glass. In: *Advances in Ceramics, Vol. 8, Nuclear Waste Management*, Wicks G. G. and Ross W. A. (Eds), pp. 30–38. The American Ceramic Society, Columbus, OH.

Jiang W., Wu X. and Roy D. M. (1993) Alkali-activated fly ash-slag cement based nuclear waste forms. In: *Scientific Basis for Nuclear Waste Management XVI*, Interrante C. G. and Pabalan R. T. (Eds) *Materials Research Society Symposium Proceedings*, Vol. 294, pp. 255–260. Materials Research Society, Pittsburgh.

Johnson L. H. and Shoesmith D. W. (1988) Spent fuel. In: *Radioactive Waste Forms for the Future*, Lutze W. and Ewing R. C. (Eds), pp. 635–698. North-Holland, Amsterdam.

Karioris F. G., Gowda K. A. and Cartz L. (1981) Heavy ion bombardment of monoclinic $ThSiO_4$, ThO_2, and monazite. *Radiation Effects Lett.* **58,** 1–3.

Karioris F. G., Appaji Gowda K., Cartz L. and Labbe J. C. (1982) Damage cross-sections of heavy ions in crystal structures. *J. Nucl. Mater.* **108–109,** 748–750.

Kesson S. E., Sinclair W. J. and Ringwood A. E. (1983) Solid solution limits in synroc zirconolite. *Nucl. Chem. Waste Mgmt* **4,** 259–265.

Klemens P. G., Clinard F. W., Jr and Livak R. J. (1987) Reduction of stored energy in a heavily irradiated ceramic. *J. Appl. Phys.* **62,** 2062–2064.

Koul S. L. (1979) On the fission track dating and annealing behaviour of accessory minerals (Andhra Pradesh, India). *Radiation Effects* **40,** 187–192.

Laval J. Y. and Westmacott K. H. (1980) Electron beam sensitivity and structure of the glassy phase of ceramics. In: *Electron Microscopy and Analysis, 1979*, Mulvey T. (Ed.) Conf. Series, No. 52, pp. 295–298. Institute of Physics, London.

Lindberg M. L. and Ingram B. (1964) Rare-earth silicate apatite from the Adirondack Mountains, New York. Prof. Paper 501-B, U.S. Geological Survey, 64–65.

Ludwig K. R., Zartman R. E. and Goldich S. S. (1984) Lead retention in zircons. *Science* **223,** 834.

Lumpkin G. R. and Ewing R. C. (1985) Natural pyrochlores: analogues for actinide host phases in radioactive waste forms. In: *Scientific Basis for Nuclear Waste Management VIII*, Jantzen C. M., Stone J. A. and Ewing R. C. (Eds), Materials Research Society Proceedings, Vol. 44, pp. 647–654. Materials Research Society, Pittsburgh.

Lumpkin G. R., Foltyn E. M. and Ewing R. C. (1986) Thermal recrystallization of alpha-recoil damaged minerals of the pyrochlore structure type. *J. Nucl. Mater.* **129,** 113–120.

Lumpkin G. R. and Ewing R. C. (1986) High-resolution transmission electron microscopy of microlite from the Harding pegmatite, Taos County, New Mexico. In: *Microbeam Analysis 1986*, Romig A. D., Jr and Chambers W. F. (Eds), pp. 145–147. San Francisco Press, San Francisco.

Lumpkin G. R., Chakoumakos B. C. and Ewing R. C. (1986a) Mineralogy and radiation effects of microlite from the Harding pegmatite, Taos County, New Mexico. *Am. Mineral.* **71,** 569–588.

Lumpkin G. R., Ewing R. C., Chakoumakos B. C., Greegor R. B., Lytle F. W., Foltyn E. M., Clinard F. W., Jr, Boatner L. A. and Abraham M. M. (1986b) Alpha-recoil damage in zirconolite ($CaZrTi_2O_7$). *J. Mater. Res.* **1,** 564–576.

Lumpkin G. R., Eyal Y. and Ewing R. C. (1988) Preferential leaching and natural annealing of alpha-recoil tracks in metamict betafite and samarskite. *J. Mater. Res.* **3,** 357–368.

Lumpkin G. R. and Ewing R. C. (1988) Alpha-decay damage in minerals of the pyrochlore group. *Phys. Chem. Minerals* **16,** 2–20.

Lutze W. and Ewing R. C. (1988) *Radioactive Waste Forms for the Future*. North-Holland, Amsterdam.

Lutze W. (1988) Silicate glasses. In: *Radioactive Waste Forms for the Future*, Lutze W. and Ewing R. C. (Eds), pp. 1–159. North-Holland, Amsterdam.

Malow G. and Andresen H. (1979) Helium formation from α-decay and its significance for radioactive waste glasses. In: *Scientific Basis for Nuclear Waste Management, Vol. 1*, McCarthy G. J. (Ed.), pp. 109–115. Plenum Press, New York.

Malow G., Marples J. A. C. and Sombret C. (1980) Thermal and radiation effects on properties of high level waste products. In: *Radioactive Waste Management and Disposal*, Simon R. and Orlowski S. (Eds), pp. 341–359. Harwood Academic Publishers, Chur, Switzerland.

Manara A., Antonini, M., Camagni P. and Gibson P. N. (1984) Radiation damage in silica-based glasses: point defects, microstructural changes, and possible implications on etching and leaching. *Nucl. Instruments Meth. Phys. Res.* **B1,** 475–480.

Manara A., Gibson P. N. and Antonini M. (1982) Structural effects of radiation damage in silica based glasses. In: *Scientific Basis for Nuclear Waste Management-V*, Lutze W. (Ed.), pp. 349–356. North-Holland, New York.

Matzke Hj. (1988a) Radiation damage effects in nuclear materials. *Nucl. Instruments Meth. Phys.* **B32,** 455–470.

Matzke Hj. (1988b) Concluding remarks to the workshop on radiation effects in nuclear waste materials. *Nucl. Instruments Meth. Phys. Res.* **B32,** 516–517.

McCarthy G. J. (1977) High-level waste ceramics: material considerations, process simulation, and product characterization. *Nucl. Technol.* **32,** 92–105.

McCarthy G. J., Pepin J. G., Pfoertsch D. E. and Clarke D. R. (1979) Crystal chemistry of the synthetic minerals in current supercalcine-ceramics. In: *Ceramics in Nuclear Waste Management*, Chikalla T. D. and Mendel J. E. (Eds), CONF-790420, pp. 315–320. National Technical Information Service, Springfield, VA.

McDaniel E. W. and Delzer D. B. (1988) FUETAP concrete. In: *Radioactive Waste Forms for the Future*, Lutze W. and Ewing R. C. (Eds), pp. 565–588. North-Holland, Amsterdam.

McLaren A. C., Fitzgerald J. D. and Williams I. S. (1994) The microstructure of zircon and its influence on the age determination from Pb/U isotopic ratios measured by ion microscope. *Geochimica Cosmochimica Acta* **54,** 993–1005.

Mitamura H., Matsumoto S., Miyazaki T., White T. J., Nukaga K., Togashi Y., Sagawa T., Tashiro S., Levins D. M. and Kikuchi A. (1990) Self-irradiation damage of a curium-doped titanate containing sodium-rich high-level waste. *J. Am. Ceram. Soc.* **73,** 3433–3441.

Mitamura H., Matsumoto S., Tusboi T., Vance E. R., Begg B. D. and Hart K. P. (1994) Alpha-decay damage in Cm-doped perovskite. In: *Scientific Basis for Nuclear Waste Management—XVIII*. Murakami T. and Ewing R. C. (Eds) (in press). Materials Research Society, Pittsburgh, PA.

Mosley W. C. (1971) Self-radiation damage in curium-244 oxide and aluminate. *J. Am. Ceram. Soc.* **54,** 474–479.

Mullica D. F., Grossie D. A. and Boatner L. A. (1985) Coordination geometry and structural determinations of $SmPO_4$, $EuPO_4$ and $GdPO_4$. *Inorganica Chimica Acta* **109,** 105–110.

Mullica D. F., Sappenfield E. L. and Boatner L. A. (1990) A structural investigation of several mixed lanthanide orthophosphates. *Inorganica Chimica Acta* **174,** 155–159.

Murakami T., Chakoumakos B. C. and Ewing R. C. (1986) X-ray powder diffraction analysis of alpha-event radiation damage in zircon ($ZrSiO_4$). In: *Advances in Ceramics: Nuclear Waste Management II, Vol. 20*, Clark D. E., White W. B. and Machiels J. (Eds), pp. 745–753. American Ceramic Society, Columbus, OH.

Murakami T., Chakoumakos B. C., Ewing R. C., Lumpkin G. R. and Weber W. J. (1991) Alpha-decay event damage in zircon. *Am. Mineral.* **76,** 1510–1532.

Mursic Z., Vogt T., Boysen H. and Frey F. (1992) Single-crystal neutron diffraction study of metamict zircon up to 2000K. *J. Appl. Crystal.* **25,** 519–523.

Nakae N., Iwata Y. and Kirhara T. (1979) Thermal recovery of defects in neutron irradiated UO_2. *J. Nucl. Mater.* **80,** 314–322.

National Academy of Sciences (1994) Management and Disposition of Excess Weapons Plutonium. National Academy Press, Washington, DC.

Nellis W. J. (1977) The effect of self-radiation on crystal volume. *Inorg. Nucl. Chem.* **13,** 393–398.

Newkirk H. W., Hoenig C. L., Ryerson F. J., Tewhey J. D., Smith G. S., Rossington C. S., Brackmann A. J. and

Ringwood A. E. (1982) Synroc technology for immobilizing U.S. defense waste. *Ceram. Bull.* **61,** 559–566.

Office of Technology Assessment (1991) Complex Cleanup The Environmental Legacy of Nuclear Weapons Production. OTA-O-484. Congress of the United States, Washington, DC.

Oversby V. M. and Ringwood A. E. (1981) Lead isotopic studies of zirconolite and perovskite and their implications for long range Synroc stability. *Radioactive Waste Mgmt* **1,** 289–308.

Oversby V. M., Van Konynenburg R. A., Glassley W. E. and Curtis P. G. (1994) Immobilization in ceramic waste forms of the residues from treatment of mixed wastes. In: *Scientific Basis for Nuclear Waste Management XVII, Materials Research Society Symposium Proceedings, Vol. 333,* pp. 285–292. Barkatt A. and Van Konynenburg R. A. (Eds). Materials Research Society, Pittsburgh.

Pabst A. (1952) The metamict state. *Am. Mineral.* **37,** 137–157.

Pidgeon R. T., O'Neil J. R. and Silver L. T. (1986) Uranium and lead isotopic stability in a metamict zircon under experimental hydrothermal conditions. *Science* **154,** 1538–1540.

Primak W. (1982) Radiation-enhanced saline leaching of silicate glasses. *Nucl. Sci. Engng* **80,** 689–699.

Primak W. and Roberts F. P. (1984) Stored energy in a radioactive waste borosilicate glass: its frequency factor and kinetics and its source. *Nucl. Sci. Engng* **86,** 191–205.

Quillin K. C., Duerden S. L. and Majumdar A. J. (1994) Accelerated ageing of blended OPC cements. In: *Scientific Basis for Nuclear Waste Management XVII,* Barkatt A. and Van Konynenburg R. A. (Eds), Materials Research Society Symposium Proceedings, Vol. 333, pp. 341–348. Materials Research Society, Pittsburgh.

Reeve K. D. and Woolfrey J. L. (1980). Accelerated irradiation testing of SYNROC using fast neutrons—I. First results on barium hollandite, perovskite, and undoped SYNROC B. *J. Aust. Ceram. Soc.* **16,** 10–15.

Reeve K. D., Levins D. M., Ramm E. J., Woolfrey J. L., Buykx W. J., Ryan R. K. and Chapman J. F. (1981) The development and testing of SYNROC for high-level radioactive waste fixation. In: *Proceedings of the Symposium on Waste Management '81,* Post R. G. (Ed.), pp. 249–266. Arizona Board of Regents, Tucson.

Reimann G. A. and Kong P. C. (1994) Iron-enriched basalt waste form improved with TiO_2 and ZrO_2. In: *Actinide Processing Methods and Materials.* Proceedings of an International Symposium of the 123rd Annual Meeting of the Minerals, Metals, and Materials Society, Mishra B. and Averill W. A. (Eds), pp. 275–288. Minerals, Metals, and Materials Society, Warrendale, PA.

Ringwood A. E., Kesson S. E., Ware N. G., Hibberson W. O. and Major A. (1979) The SYNROC process: a geochemical approach to nuclear waste immobilization. *Geochem. Jl* **13,** 141–165.

Ringwood A. E., Oversby V. M. and Sinclair W. (1980) The effects of radiation damage on SYNROC. In: *Scientific Basis for Nuclear Waste Management, Vol. 2,* Northrup, C. J. M., Jr (Ed.), pp. 273–280. Plenum Press, New York.

Ringwood A. E., Oversby V. M., Kesson S. E., Sinclair W., Ware N., Hibberson W. and Major A. (1981) Immobilization of high-level wastes in SYNROC: a current appraisal. *Nucl. Chem. Waste Mgmt* **2,** 287–305.

Ringwood A. E. (1982) Immobilization of radioactive wastes in SYNROC. *Am. Sci.* **70,** 201–207.

Ringwood A. E. (1985) Disposal of high-level nuclear wastes: a geological perspective. *Mineral. Mag.* **49,** 159–176.

Ringwood A. E., Kesson S. E., Reeve K. D., Levins D. M. and Ramm E. J. (1988) Synroc. In: *Radioactive Waste Forms for the Future,* Lutze W. and Ewing R. C. (Eds), pp. 233–334. North-Holland, Amsterdam.

Roberts F. P., Jenks G. H. and Bopp C. D. (1976) Radiation effects in solidified high-level wastes—Part 1, stored energy. Report No. BNWL-1944. Pacific Northwest Laboratory, Richland, WA.

Routbort J. L. and Matzke Hj. (1983) The effects of composition and radiation on the fracture of a nuclear waste glass. *Mater. Sci. Engng* **58,** 229–237.

Roy R. (1979) Science underlying radioactive waste management: status and needs. In: *Scientific Basis for Nuclear Waste Management, Vol. 1,* McCarthy G. J. (Ed.), pp. 1–20. Plenum Press, New York.

Rusin J. M., Gray W. J. and Wald J. W. (1979) Multibarrier waste forms—Part II; characterization and evaluation. Report No. PNL-2668-2. Pacific Northwest Laboratory, Richland, WA.

Sales B. C., White C. W. and Boatner L. A. (1983) A comparison of the corrosion characteristics of synthetic monazite and borosilicate glass containing simulated nuclear waste glass. *Nucl. Chem. Waste Mgmt* **4,** 281–289.

Sales B. C. and Boatner L. A. (1990) Different structures of amorphous solids. *Oak Ridge Natl Lab. Rev.* **23**(4), 19–29.

Sandhu A. S., Lakhwant S., Ramola R. C., Singh S. and Virk H. S. (1990) Annealing kinetics of heavy ion radiation damage in crystalline minerals. *Nucl. Instrum. Meth. Phys. Res.* **B46,** 122–124.

Sato S., Asakura K. and Furuya H. (1983) Microstructure of high-level radioactive waste-glass heavily irradiated in a high-voltage electron microscope. *Nucl. Chem. Waste Mgmt* **4,** 147–151.

Sato S., Furuya H., Asakura K., Ohta K. and Tamai T. (1984) Radiation effect of simulated waste glass irradiated with ion, electron and γ-ray. *Nucl. Instrum. Meth. Phys. Res.* **B1,** 534–537.

Sata S., Furuya H., Kozaka T., Inagaki Y. and Tamai T. (1988) Volumetric change of simulated radioactive waste glasses irradiated by the $^{10}B(n,\alpha)^{7}Li$ reaction as simulation of actinide irradiation. *J. Nucl. Mater.* **152,** 265–269.

Shelby J. E. (1980) Effect of radiation on the physical properties of borosilicate glasses. *J. Appl. Phys.* **51,** 2561–2565.

Sinclair W. and Ringwood A. E. (1981) Alpha-recoil damage in natural zirconolite and perovskite. *Geochem. Jl* **15,** 229–243.

Sinclair W. and Eggleton R. A. (1982) Structure refinement of zirkelite from Kaiserstuhl, West Germany. *Am. Mineral.* **67,** 615–620.

Sinha A. K., Student J. and Essex R. Zircons and fluids: an experimental investigation with applications for radioactive waste disposal. Report from Virginia Polytechnic Institute & State University #13951-4.

Sinha A. K., Wayne D. M. and Hewitt D. A. (1992) The hydrothermal stability of zircon: preliminary experimental and isotopic studies. *Geochimica Cosmochimica Acta* **56,** 3551–3560.

Spilman D. B. Hench L. L. and Clark D. E. (1986) Devitrification and subsequent effects on the leach behavior of a simulated borosilicate nuclear waste glass. *Nucl. Chem. Waste Mgmt* **6,** 107–119.

Stevanovic D. V., Thompson D. A. and Vance E. R. (1989) Rutherford backscattering investigation of radiation

damage effects on the leaching of sphene and sphene-based glass-ceramics. *J. Nucl. Mater.* **161,** 169–174.
Sunder S., Shoesmith D. W., Christensen H. and Miller N. H. (1992) Oxidation of UO_2 fuel by the products of gamma radiolysis of water. *J. Nucl. Mater.* **190,** 78–86.
Suzuki K. (1987) Discordant distribution of U and Pb in zircon of Naegi granite: a possible indication of Rn migration through radiation damage. *Geochem. Jl* **21,** 173–182.
Todd B. J., Linweaver J. L. and Kerr J. T. (1960) Outgassing caused by electron bombardment of glass. *J. Appl. Phys.* **31,** 51–55.
Tole M. P. (1985) The kinetics of dissolution of zircon ($ZrSiO_4$). *Geochimica Cosmochimica Acta* **49,** 453–458.
Tomozawa M., Singer G. M., Oka Y. and Warden J. T. (1979) Phase separation in nuclear waste glasses. In: *Ceramics in Nuclear Waste Management*, Chikalla T. D. and Mendel J. E. (Eds), CONF-79042, pp. 193–197. National Technical Information Service, Springfield, VA.
Tosten M. H. (1989) TEM examination of irradiated waste glass. Report No. WSRC-RP-89-584. Westinghouse Savannah River Co., Aiken, SC.
Turcotte R. P. (1976) Radiation effects in solidified high-level wastes—part 2, helium behavior. Report No. BNWL-2051. Pacific Northwest Laboratory, Richland, WA.
Turcotte R. P. (1981) Radiation effects in high-level radioactive waste forms. *Radioactive Waste Mgmt* **2,** 169–177.
Turcotte R. P., Wald J. W., Roberts F. P., Rusin J. M. and Lutze W. (1982) Radiation damage in nuclear waste ceramics. *J. Am. Ceram. Soc.* **65,** 589–593.
Van Konynenburg R. A. and Guinan M. W. (1983) Radiation effects in Synroc-D. *Nucl. Technol.* **60,** 206–217.
Vance E. R., Karioris F. G., Cartz L. and Wong M. S. (1984) Radiation effects on sphene and sphene-based glass-ceramics. In: *Advances in Ceramics, Vol. 8*, Wicks G. G. and Ross W. A. (Eds), pp. 62–70. American Ceramic Society, Columbus, OH.
Vance E. R. and Metson J. B. (1985) Radiation damage in natural titanites. *Phys. Chem. Minerals* **12,** 255–260.
Vance E. R., Cann C. D. and Richardson P. G. (1986) Electron irradiation-induced amorphism of some silicates. *Radiation Effects* **98,** 71–81.
Wald J. W. and Offermann P. (1982) A study of radiation effects in curium-doped $Gd_2Ti_2O_7$ (pyrochlore and $CaZrTi_2O_7$ (zirconolite). In: *Scientific Basis for Nuclear Waste Management XII*, Lutze W. (Ed.), pp. 369–378. Elsevier Science, New York.
Wald J. W. and Weber W. J. (1984) Effects of self-radiation damage on the leachability of actinide-host phases. In: *Advances in Ceramics, Vol. 8, Nuclear Waste Management*, Wicks G. G. and Ross W. A. (Eds), pp. 71–75. The American Ceramic Society, Columbus, OH.
Wang L. M., Eby R. K., Janeczek J. and Ewing R. C. (1991) *In situ* study of ion-beam-induced amorphization of complex silicate structures. *Nucl. Instruments Meth. Phys. Res.* **B59/60,** 395–400.
Wang L. M., Ewing R. C., Weber W. J. and Eby R. K. (1993) Temperature and ion-mass dependence of amorphization dose for ion beam irradiated zircon ($ZrSiO_4$). In: *Beam-Solid Interactions: Fundamentals and Applications*, Nastasi M., Harriott L. R., Herbots N. and Averback R. S. (Eds), Proceedings of the Materials Research Society. Vol. 279, pp. 451–456. Pittsburgh, PA.
Wang L. M., Cameron M., Weber W. J., Cowley K. D. and Ewing R. C. (1994) *In situ* TEM observation of radiation induced amorphization of crystals with apatite structure. Hydroxyapatite and Related Materials, P. Brown and B. Constantz (Eds), CRC Press, pp. 243–249.
Webb R. P. and Carter G. (1979) Difficulties in deducing disordering mechanisms from experimental studies of disorder-ion fluence functions in ion irradiation of semiconductors. *Radiation Effect* **42,** 159–168.
Webb R. P. and Carter G. (1981) The effects of annealing upon the accumulation of amorphousness in a composite model of disorder production. *Radiation Effects* **59,** 69–76.
Weber W. J., Turcotte R. P., Bunnell L. R., Roberts F. P. and Westsik J. H. (1979) Radiation effects in vitreous and devitrified simulated waste glass. In: *Ceramics in Nuclear Waste Management*, Chikalla T. D. and Mendel J. E. (Eds), CONF-790420, pp. 294–299. National Technical Information Service, Springfield, VAA.
Weber W. J. (1981) Ingrowth of lattice defects in alpha irradiated UO_2 single crystals. *J. Nucl. Mater.* **98,** 206–215.
Weber W. J., Wald J. W. and Gray W. J. (1981) Radiation effects in crystalline high-level nuclear waste solids. In: *Scientific Basis for Nuclear Waste Management, Vol. 3*, Moore J. G. (Ed), pp. 441–448. Plenum Press, New York.
Weber W. J. (1982) Radiation damage in rare-earth silicate with the apatite structure. *J. Am. Ceram. Soc.* **65,** 544–548.
Weber W. J., Turcotte R. P. and Roberts F. P. (1982) Radiation damage from alpha decay in ceramic nuclear waste forms. *Radioactive Waste Mgmt* **2**(3), 295–319.
Weber W. J. and Turcotte R. P. (1982) Materials characterization center second workshop on irradiation effects in nuclear waste forms: summary report. Report No. PNL-4121. Pacific Northwest Laboratory, Richland, WA.
Weber W. J. (1983) Radiation-induced swelling and amorphization in $Ca_2Nd_8(SiO_4)_6O_2$. *Radiation Effects* **77,** 295–308.
Weber W. J. and Roberts F. P. (1983) A review of radiation effects in solid nuclear waste forms. *Nucl. Technol.* **60,** 178–198.
Weber W. J., Pederson L. R., Gray W. J. and McVay G. L. (1984) Radiation effects on nuclear waste storage materials. *Nucl. Instruments Meth. Phys. Res.* **B229,** 527–533.
Weber W. J., Wald J. W. and Matzke Hj. (1985a) Self-radiation damage in actinide host phases of nuclear waste forms. In: *Scientific Basis for Nuclear Waste Management VIII, Vol. 8*, Jantzen C. M., Stone J. A. and Ewing R. C. (Eds), pp. 679–686. Materials Research Society, Pittsburgh.
Weber W. J., Wald J. W. and Matzke Hj. (1985b) Self-radiation damage in $Gd_2Ti_2O_7$. *Mater. Lett.* **3,** 173–180.
Weber W. J. (1985) Effects of alpha irradiation on barium hollandite and nickel-iron spinel. In: *Scientific Basis for Nuclear Waste Management VIII*, Jantzen C. M., Stone J. A. and Ewing R. C. (Eds), pp. 671–678. Materials Research Society, Pittsburgh, PA.
Weber W. J., Wald J. W. and Matzke Hj. (1986) Effects of self-irradiation damage in Cm-doped $Gd_2Ti_2O_7$ and $CaZrTi_2O_7$. *J. Nucl. Mater.* **138,** 196–209.
Weber W. J. and Matzke Hj. (1986a) Radiation effects in actinide host phases. *Radiation Effects* **98,** 93–99.
Weber W. J. and Matzke Hj. (1986b) Effects of radiation in microstructure and fracture properties in $Ca_2Nd_8(SiO_4)_6O_2$. *Mater. Lett.* **5,** 9–16.
Weber W. J. and Matzke Hj. (1987) Fracture toughness in nuclear waste glasses and ceramics: environmental and radiation effects. *Europ. Appl. Res. Rep.* **7,** 1221–1234.
Weber W. J. (1988) Radiation effects in nuclear waste glasses. *Nucl. Instruments Meth. Phys. Res.* **B32,** 471–479.
Weber W. J. (1990) Radiation-induced defects and amorphization in zircon. *J. Mater. Res.* **5,** 2687–2697.

Weber W. J. (1991a) The effect of radiation on nuclear waste forms. *J. Minerals, Metals Mater. Soc.* **43,** 35–39.

Weber W.J. (1991b) Self-radiation damage and recovery in Pu-doped zircon. *Radiation Effects Defects Solids* **115,** 341–349.

Weber W. J., Eby R. K. and Ewing R. C. (1991a) Accumulation of structural defects in ion-irradiated $Ca_2(Nd)_8(SiO_4)_6O_2$. *J. Mater. Res.* **6,** 1334–1345.

Weber W. J., Mansur L. K., Clinard F. W., Jr and Parkin D. M. (1991b) Radiation effects on materials in high-radiation environments: a workshop summary. *J. Nucl. Mater.* **184,** 1–21.

Weber W. J., Hess N. J. and Maupin G. D. (1992) Amorphization in $Gd_2Ti_2O_7$ and $CaZrTi_2O_7$ irradiated with 3 MeV argon ions. *Nucl. Instruments Meth. Phys. Res.* **B65,** 102–106.

Weber W. J. (1993) Alpha-decay induced amorphization in complex silicate structures. *J. Am. Ceram. Soc.* **76,** 1729–1738.

Weber W. J. and Wang L. M. (1993) Ion-beam amorphization of $Ca_2La_8(SiO_4)_6O_2$ single crystals. In: *Beam–Solid Interactions: Fundamentals and Applications*, Nastasi M., Harriott L. R., Herbots N. and Averback R. S. (Eds), pp. 523–528. Materials Research Society, Pittsburgh, PA

Weber W. J. and Wang L. M. (1994) Effect of temperature and recoil-energy spectra on irradiation-induced amorphization in $Ca_2La_8(SiO_4)_6O_2$. *Nucl. Instruments Meth. Phys. Res.* **B91,** 22–29.

Weber W. J., Ewing R. C. and Wang L. M. (1994) The radiation-induced crystalline-to-amorphous transition in zircon. *J. Mater. Res.* **9**(3), 688–698.

Westsik J. H. and Harvey C. O. (1981) High-temperature leaching of a simulated high-level waste glass. Report No. PNL-3172. Pacific Northwest Laboratory, Richland, WA.

White T. J., Segall R. O., Hutchison J. L. and Barry J. C. (1984) Polytypic behaviour of zirconolite. *Proc. Roy. Soc. Lond. Ser.* **A392,** 343–358.

White T. J. (1984) The microstructure and microchemistry of synthetic zirconolite, zirkelite and related phases. *Am. Mineral.* **69,** 1156–1172.

White T. J., Ewing R. C., Wang L. M., Forrester J. S. and Montross C. (1994) Temperature dependence of amorphization for zirconolite and perovskite irradiated with 1 MeV krypton ions. In: *Scientific Basis for Nuclear Waste Management—XVIII*, Murakami T. and Ewing R. C. (Eds) (in press). Materials Research Society, Pittsburgh, PA.

Williamson G. K. and Hall W. H. (1953) X-ray line broadening from filed aluminum and wolfram. *Acta Metall.* **1,** 22–31.

Woodhead J. A., Rossman G. R. and Silver L. T. (1991a) The metamictization of zircon: radiation dose-dependent structural characteristics. *Am. Mineral.* **76,** 74–82.

Woodhead J. A., Rossman G. R. and Silver L. T. (1991b) The metamictization of zircon: radiation dose-dependent structural characteristics. *Am. Mineral.* **76,** 74–82.

Woolfrey J. L., Reeve K. D. and Cassidy D. J. (1982) Accelerated irradiation testing of SYNROC and its constituent minerals using fast neutrons. *J. Nucl. Mater.* **108–109,** 739–747.

Wronkiewicz D. J. (1993) Effects of radionuclide decay on waste glass behavior—a critical review. Report No. ANL-93/45. Argonne National Laboratory, Argonne, IL.

Zdaniewski W. A., Easler T. E. and Bradt R. C. (1983) Gamma radiation effects on the strength of a borosilicate glass. *J. Am. Ceram. Soc.* **66,** 311–313.